LBL-15896
c.2

Lawrence Berkeley Laboratory
UNIVERSITY OF CALIFORNIA

Materials & Molecular Research Division

ORIGIN OF SWELLING IN GASEOUS REDUCTION OF IRON BEARING ORES

M. Chang
(Ph.D. Thesis)

March 1983

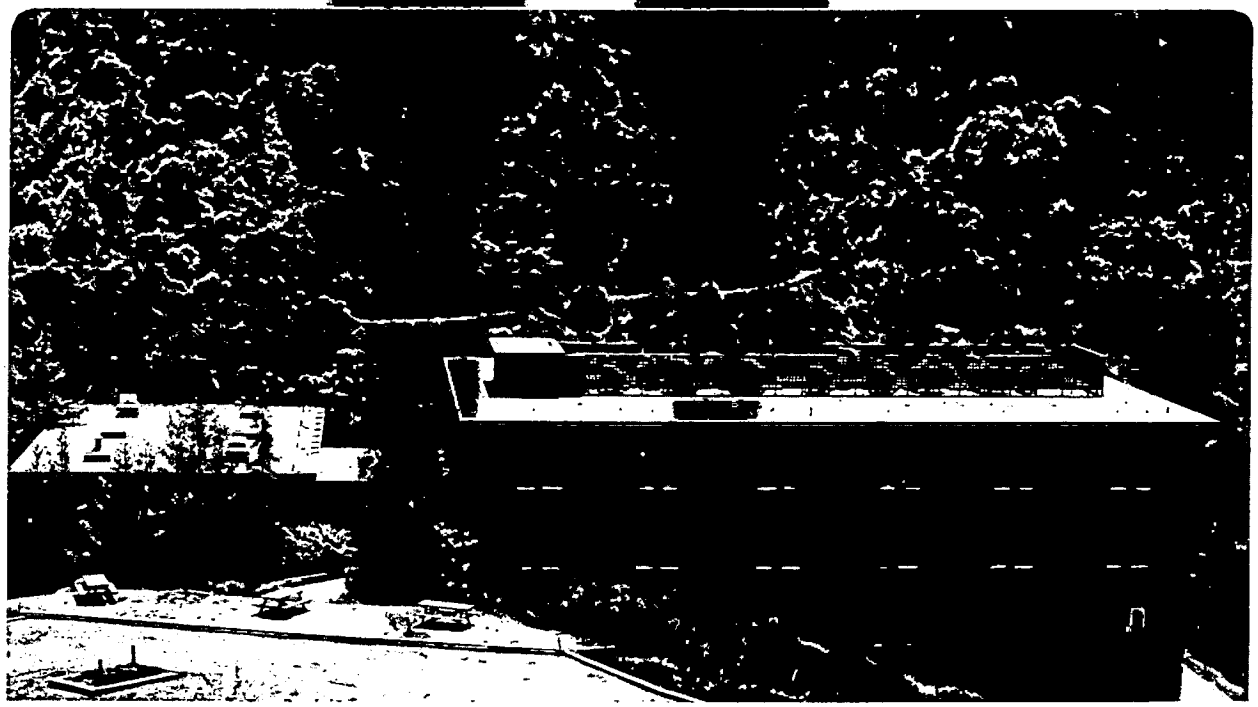

Prepared for the U.S. Department of Energy under Contract DE-AC03-76SF00098

LBL-15896
c.2

DISCLAIMER

ORIGIN OF SWELLING IN GASEOUS REDUCTION OF IRON BEARING ORES

Mei Chang
Ph.D. Thesis

Materials Science and Mineral Engineering
Department of Materials and Molecular Research Division
Lawrence Berkeley Laboratory
University of California
Berkeley, CA 94720

This work was supported by the Division of Materials Sciences, Office of Basic Energy Sciences of the U.S. Department of Energy under Contract No. DE-AC03-76SF00098.

ORIGIN OF SWELLING IN GASEOUS REDUCTION OF IRON BEARING ORES

Mei Chang

Degree: Doctor of Philosophy in Engineering

Major: Materials Science and Mineral Engineering

ABSTRACT

Abnormal swelling due to profuse metal whisker formation was found during $CO-CO_2$ reduction of iron bearing ores. Dense, polycrystalline cobalt ferrite was reduced at 900°C to explore the basic mechanism of the whisker formation. Various effects on the whisker formation, such as reaction conditions, initial oxide phase, and impurity species, have been clarified.

Previous models mostly emphasized the initiation stage of the whisker formation and argued about the distribution of impurities on the oxide surface. Controversy arose when it was found that MgO enhanced the metal nucleation rate but did not enhance the swelling. A significant effect of gas pressure on the whisker diameter was observed in the present experiments, that cannot be explained in terms of previous models.

The analysis emphasizes the whisker diameter during whisker growth, and proposes a new model to explain the whisker development: the steady state whisker diameter is determined by the balance of the fluxes removing oxygen from the oxide-gas interface and from the

metal-oxide interface. The faster the oxide consumption at the gas-oxide interface or the slower the metal-oxide interface flux, the thinner the whisker.

The oxide-gas interface reaction rate is directly controlled by the gas pressure and the gas composition. The oxygen removal from the metal-oxide interface is completed by coupling the oxygen diffusion along the metal-oxide interface with a catalytic reaction at the metal-oxide-gas triple junction. Impurities may drastically retard the triple junction reaction, and enhance whisker formation. The ability of different impurity species to cause whisker formation depends on how long these impurities can remain on the surface.

Evidence for fast metal-oxide interface oxygen diffusion is provided for the reduction of wustite. The mechanism of the catalytic reaction at the triple junction and the role of impurities in the mechanism are discussed.

ORIGIN OF SWELLING IN GASEOUS REDUCTION OF IRON BEARING ORES

Mei Chang
Ph.D. Thesis

Materials Science and Mineral Engineering
Department of Materials and Molecular Research Division
Lawrence Berkeley Laboratory
University of California
Berkeley, CA 94720

ABSTRACT

Abnormal swelling due to profuse metal whisker formation was found during $CO-CO_2$ reduction of iron bearing ores. Dense, polycrystalline cobalt ferrite was reduced at 900°C to explore the basic mechanism of the whisker formation. Various effects on the whisker formation, such as reaction conditions, initial oxide phase, and impurity species, have been clarified.

Previous models mostly emphasized the initiation stage of the whisker formation and argued about the distribution of impurities on the oxide surface. Controversy arose when it was found that MgO enhanced the metal nucleation rate but did not enhance the swelling. A significant effect of gas pressure on the whisker diameter was observed in the present experiments, that cannot be explained in terms of previous models.

The analysis emphasizes the whisker diameter during whisker growth, and proposes a new model to explain the whisker development: the steady state whisker diameter is determined by the balance of the

fluxes removing oxygen from the oxide-gas interface and from the metal-oxide interface. The faster the oxide consumption at the gas-oxide interface or the slower the metal-oxide interface flux, the thinner the whisker.

The oxide-gas interface reaction rate is directly controlled by the gas pressure and the gas composition. The oxygen removal from the mtal-oxide interface is completed by coupling the oxygen diffusion along the metal-oxide interface with a catalytic reaction at the metal-oxide-gas triple junction. Impurities may drastically retard the triple junction reaction, and enhance whisker formation. The ability of different impurity species to cause whisker formation depends on how long these impurities can remain on the surface.

Evidence for fast metal-oxide interface oxygen diffusion is provided for the reduction of wustite. The mechanism of the catalytic reaction at the triple junction and the role of impurities in the mechanism are discussed.

TABLE OF CONTENTS

I. INTRODUCTION

Gaseous reduction of oxide ores is an essential step in the iron-making process. Pronounced swelling of the iron ore pellets sometimes occurs during the reduction step, causing considerable difficulties. There are two types of swelling;[1] one is called "normal swelling" which causes a volume expansion of only about 20 percent and has been identified to be a consequence of phase transformation of hematite to magnetite;[2] the other one is called "abnormal swelling" or "catastrophic swelling" which can cause a volume change as high as 300 percent.[3] Normal swelling will not result in any difficulties in the operation of the blast furnance, but abnormal swelling will lead to severe problems. It is therefore necessary to understand the source and the mechanisms of abnormal swelling.

The abnormal swelling always occurs as a result of the transformation of wüstite to metallic iron, and metallographic examinations have clearly shown that there are abundant thin, long metallic iron filaments in the catastrophically swelled pellets.[3-8] We call these thin, long filaments "whiskers". The basic mechanism of the formation of such a specific morphology will be explored in this thesis.

1. Background:

The reduction process of iron ore in a blast furnace is a typical example of a gas-solid reaction leading to a porous solid product. The overall chemical reaction can be written as:

$$CO_{(g)} + Fe_xO_{(s)} \longrightarrow CO_{2(g)} + x\ Fe_{(s)} \qquad (1)$$

where x depends on the initial composition of iron ore (for hematite x=2/3, for magnetite x=3/4, and for wüstite x=1). The solid product, iron, is usually very porous and does not densely cover the solid reactant, iron oxide. The gases, CO and CO_2, can easily penetrate through the porous product layer by gas phase diffusion which is usually much faster than solid state diffusion. A chemical reaction occurs on the iron oxide surface, removing oxygen from the oxide lattice near or at the surface. It is a characteristic of gas-solid reaction having porous solid product that chemical reactions can occur on the reactant solid surface.

Since the chemical reaction removes only oxygen, some material transfer mechanisms might have to be coupled with the reaction, such as iron diffusion from the oxide surface to the metal and oxygen diffusion to the free oxide surface. The paths and the rate of transport of these species can be greatly affected by lattice and surface structure, and by the presence of impurities.

The phase diagram of Fe-O system is shown in Figure 1.[33-35] There are several oxidation states: the highest one is hematite Fe_2O_3, then magnetite Fe_3O_4, and the lowest one is wüstite FeO. When the temperature is above 570°C, the phase coexistent with metallic iron is wüstite. Therefore, thermodynamically, metallic iron should always appear on the surface of wüstite during reduction above 570°C. Iron ores, hematite or magnetite, will go through phase transformations producing wüstite when reduced. In the temperature range where

swelling is observed, roughly between 800°C and 1100°C, the rates of the phase transformations leading to wüstite are fast enough to form a continuous FeO layer on the oxide surface.[9,10] The chemical reaction on the oxide surface then can be described more precisely as:

$$CO_{(g)} + Fe_{1-\delta}O_{(s)} \longrightarrow CO_{2(g)} + (1-\delta)\ Fe_{(s)} \qquad (2)$$

where δ is the nonstoichiometric deviation of wüstite which can be as high as 0.1-0.2, depending on the oxygen partial pressure (refer to Figure 1b).[11]

After the oxygen on the oxide surface has been removed by chemical reaction, the generated excess iron ions have to diffuse away to the metal product phase to keep a fresh oxide surface, either by oxide surface or by oxide lattice transport. Wagner[24,25] proposed a mechanism of the reduction of a metal deficient oxide or sulphide, such as FeO, CoO, Ag_2S etc. The reducing gas, CO or H_2, removes an oxygen simultaneously destroying a nearby vacancy, and releases free electrons into the conduction band, or reduces trivalent ferric ions in the oxide lattice to divalent ferrous ions. In Kröger-Vink notation,[26] this reaction is simply written as:

$$CO_{(g)} + O_O + V''_{Fe} \longrightarrow CO_{2(g)} + 2\ e' \qquad (3)$$

or

$$CO_{(g)} + O_O + V''_{Fe} + 2\ Fe^{\bullet}_{Fe} \longrightarrow CO_{2(g)} + 2\ Fe_{Fe} \qquad (4)$$

The excess ferrous ions on the oxide surface then diffuse into the oxide bulk to decrease the metal deficit in the oxide, or diffuse through the oxide lattice to the metal sink where ferrous ions combine with free electrons to deposit metallic iron. Fast solid state of diffusion of a iron in wüstite has been demonstrated. It was observed that the thickness of a wüstite layer which was grown on metallic iron would shrink without iron appearing on the outer wüstite surface during reduction at 900°C.[24] It is generally accepted that iron diffusion through the wüstite lattice is the dominant path, rather than the diffusion on the wüstite surface.

At the beginning of reduction, no metallic iron appears and the excess ferrous ions can only diffuse into the oxide bulk where they accumulate. The continuously accumulated ferrous ion will gradually force the nonstoichiometry of the oxide across the metallic iron-wüstite phase boundary, and the supersaturation of ferrous ion will initiate the metallic iron nucleation process. If the supersaturation exceeds a critical degree, metallic iron will appear. The supply of ferrous ions from the reaction surface and from the supersaturated oxide will keep the metallic iron growing. There is usually a time delay of metal appearance, the so-called "incubation time," during reduction of those metal deficient oxides. An oxygen chemical potential exceeding the metallic iron-wüstite equilibrium value was detected in the fluidized bed reduction of iron ore.[12] This implies that there can be a high barrier to the nucleation of metallic iron and a rather high critical degree of supersaturation would be needed to initiate metal phase.

The critical degree of supersaturation is a local property; it depends on the local atomic structure and on impurities that might vary drastically with position in a practical reduction situation. Quantitative treatment of the metal phase initiation stage would therefore appear almost impossible.

Once metallic iron is formed on the wüstite surface, the influence of the metal on the reaction mechanism has to be taken into consideration: there are several choices of materials transport routes and surface chemical reactions, as schematically shown in Figure 2. Oxygen removal reactions with a gas reactant maybe occur on the metal surface and at metal-oxide-gas triple junction. The oxygen in the oxide under the metal may diffuse out via 1) metal lattice, 2) metal-oxide interface, 3) oxide lattice paths, with accompanying electron counterdiffusion. For each of the routes, there is a coupled surface reaction; the fastest combination of surface reaction and diffusion path then is the most likely mechanism. Clarification of these mechanisms would be beneficial to understand the development of a specific product morphology.

2. Previous Work:

In the last decade, a variety of effects on iron ore abnormal swelling behavior have been reported. They include nearly all the aspects of operatioal variables, such as metallurgical structure and composition of iron ore; species and contents of impurities or additives in iron ore; size of iron ore pellet; nature, composition,

composition program, and flow rate of reducing gas; reaction temperature and heat treatment temperature program.

The metallurigical structure of iron ore depends on the firing temperature in the pelletizing operation; at a firing temperature of 1300°C in air magnetite is completely oxidized to hematite, at a firing temperature of 1100°C fine hematite plates grow into the larger magnetite grain. Several authors found that abnormal swelling only seems to occur in pellets with such intergrowth structure.[4,14,15] But, it also has been found that the abnormal swelling occurs on completely oxidized pellets, i.e. hematite.[7,13,16] A pre-reduction step which transforms hematite and magnetite into wüstite before metallic iron appears can suppress the abnormal swelling.[8,17] But prior formation of the wüstite phase does not exclude the possibility of iron whisker formation. El Kasabgy and Lu[18] demonstrated that wüstite mixed with calcium oxide can be reduced to form whiskers. The starting phase and the metallurgical structure per se thus have no direct relation to the whisker formation and to the abnormal swelling. They would influence surface impurity concentration which will be shown later to be decisive in the whisker formation.

Impurities have a dramatic effect on the whisker formation. Iron whiskers may grow on reagent grade ferric oxide as well as on natural iron ore,[5] but the swelling does not occur in pure iron oxide reduction. Alkali metal oxides,[3,5,7,14,20] calcium oxide,[4,6,8,20] and zinc oxide[19] were suggested as the cause of the abnormal swelling. Bleifuss[6] found no tendency of abnormal swelling for a

2 percent addition of MnO and MgO. Ores containing much silica and alumina, such as North America magnetite concentrates, do not exhibit any abnormal swelling.[19] Recently de Haas et al.[21] noticed that a small amount of sulphur, as low as a few ppm of SO_2, can initiate intense whisker formation. Among the impurities, CaO and MgO have been the most frequently studied; the reason why the former can easily cause the whisker formation but the latter not, will be discussed later.

Nearly all the observed abnormal swelling occurred in a $CO-CO_2$ atmosphere. Reduction in H_2-H_2O atmosphere generally will not cause any abnormal swelling; only at very low gas flow rates did iron ore pellets swell to some extent during reduction, as reported by vom Ende.[3]

The reduction rate, which is controlled by total gas pressure and gas composition, has great influence on the swelling behavior. Vom Ende et al.[3] concluded that the faster the reaction rate, the more severe the abnormal swelling. Lu[22] recognized that the individual grains in a pellet may be reduced by a naturally "programmed" gas composition which might be quite different from the composition in the main gas stream. Thus, the gas composition program may affect the swelling behavior of pellets having different sizes. It was observed by Linder and Tanning[19] that the smaller the pellet size, the larger the swelling after reduction to metal.

All the reported abnormal swelling occurred in the temperature range of 800°C to 1100°C, and the heaviest swelling occurred around

900°C. No abnormal swelling was observed below 700°C, probably due to inadequate diffusivity of iron ions at lower temperature.

Pre-reduction heat temperature in air sometimes can suppress the abnormal swelling.[7,8,17] If calcium is the major impurity, the abnormal swelling decreases with increasing temperature of heat treatment.[4] But for sodium carbonate as an additive, Lu[19] reported that the swelling increases with increasing temperature of heat treatment.

3. Mechanism Review:

There are two factors affecting the extent of swelling: 1) the nucleated density of the whiskers, 2) the diameter of the whiskers. Since the total amount of reduced metallic iron is a constant, a lower number density whiskers and a thinner whisker diameter will result in longer whiskers and thus a larger extent of swelling. The nucleated density of whiskers is determined by the nucleation process, that is, by how metallic iron nuclei are distributed on wüstite surface, while the whisker diameter is controlled by the radial growth process.

Nearly all the proposed mechanisms of whisker formation have focused on the initiation stage of metallic iron. They consider the distribution of metallic iron--how this is affected by heat treatments which can redistribute the impurities in the iron ore--, and they argue about the role of impurities--whether they enhance or depress the nucleation of metallic iron, form a second phase on the wüstite surface, or affect the critical degree of supersaturation of iron and

iron diffusivity in wüstite--. It seems that nobody has paid attention to how the whisker keeps its diameter very thin so that whiskers between grains cause the oxide grains to repel each other and so that tangling whiskers cause pellets to swell.

Bleifuss[6] suggested calcium oxide might inhibit the nucleation of metallic iron and the unreducible calcium ion would be accumulated on the wüstite surface forming a layer of calciferrous oxide. Once metallic iron appears somewhere, the calciferrous oxide layer would restrict the lateral expansion of the metallic iron phase, and result in whisker formation. This model can not account for the dependence of whisker diameter on the chemical composition in the gas phase, as we will show later.

Lu[19,27] adopted Bleifuss' opinion on the impurity role in the nucleation of metallic iron. He identified the calciferrous oxide phase as a calcium enriched wüstite. The nonhomogeneous distribution of impurities on the wüstite surface was suggested as the major cause of whisker formation. Metallic iron would be nucleated preferentially at the wüstite surface with less calcium. A high temperature heat treatment would homogenize the distribution of impurities on the oxide surface, and would increase the density of the metal nucleation sites and thus reduce the amount of iron fed to each site. Thus, whisker formation would be suppressed by a high temperature heat treatment. Unfortunately, later experiments by the same author indicated that the calcium enhanced rather than inhibited the nucleation of metallic iron on the wüstite surface.[18]

Vom Ende[4,28] recognized that the nucleation of metallic iron on pure iron wüstite was very difficult, and proposed that calcium oxide would reduce the energy barrier of nucleation and enhance metallic iron nucleation. He interpreted the impurity effect in terms of a wüstite lattice distortion and of the iron activity in wüstite. The bulk property of wüstite would be strongly affected by the presence of the impurity. This explains how calcium oxide would enhance metallic iron nucleation, but it cannot explain why there is no whisker formation on a calciowustite solid solution and why there is whisker formation on a two phase calcium oxide-wüstite mixture after a brief heat treatment.[18] It is also difficult to explain why magnesium oxide can enhance metallic iron nucleation but not enhance whisker formation.[18]

Nicolle and Rist[29] followed the route of Lu and vom Ende, and treated the whisker formation in more detail. The whisker formation would be governed by three factors: the metallic iron nucleation site density on the wüstite surface, the critical degree of supersaturation of iron in wüstite, and the amount of supersaturated iron stored in wüstite before the metallic iron appears. They also showed how the amount of supersaturated iron was affected by the critical degree of supersaturation, the surface reaction rate on wüstite and the iron diffusivity in wüstite. It was claimed that a low nucleation site density, a high critical degree of supersaturation, a large amount of supersaturated iron, a slow wüstite surface reaction rate, and a high iron diffusivity in wüstite would favor whisker formation. The

impurities would alter the critical degree of supersaturation, the surface reaction rate, and the iron diffusivity in wüstite. This theory still cannot overcome the difficulty which vom Ende's mechanism faced: The enhancement of metallic iron nucleation by calcium oxide requires a lower critical degree of supersaturation, but calcium oxide should at the same time promote whisker formation that requires a higher critical degree of supersaturation. This theory also claimed that a slow oxide surface reaction rate would promote whisker formation which is exactly opposite to the observed result that a fast reaction rate favors whisker formation.

Another independent mechanism has been proposed recently by de Haas et al.[21] Except for the reaction occurring at the oxide surface, they suggested an additional reduction process occurring at the metal-oxide interface where carbon, dissolved in the metallic iron, would be reacting with the oxide. They further assumed that the reaction at the metal-oxide interface mainly caused radial growth of the metallic iron phase. Thus, if the interface reaction were inhibited, whiskers would have appeared. The role of sulphur was emphasized in their mechanism; even trace amounts of sulphur could prevent the carburization of iron and thus the interface reaction would be inhibited, and intensive whisker formation would result. This mechanism only deals with sulphur; the role of other impurities such as calcium, or magnesium, was unclear, and the assumption of radial growth by the proposed metal-oxide interface reaction is too artificial.

It can be concluded that mechanisms involving only metallic iron nucleation are inadequate to interpret abnormal swelling, and that the impurity effect on nucleation has no clear correlation with abnormal swelling. We will deal with the radial growth of whiskers, and explore the mechanism controlling the whisker diameter. Impurity effects on the whisker diameter will be discussed and applied to interpret the phenomenum of the abnormal swelling.

II. EXPERIMENTAL

Since whisker formation is the cause of abnormal swelling during reduction, the study of whiskers itself should reveal more about the basic mechanism. To observe whisker behavior on the oxide surface, we use dense, pure oxide, artificially introduce impurities in the surface, and reduce the oxide under controlled reaction conditions. Because whisker formation was also observed in reduction of readily available cobalt ferrites, cobalt ferrite was the primary material used in exploring the basic mechanism of the whisker formation. The phase diagram of the Co-Fe-O system is shown in Figure 3, cobalt ferrite behaves quite similarly to magnetite and can be considered representative of a broad class of iron bearing mixed transition metal oxides. In reduction of cobalt ferrite, also a highly nonstoichiometric layer of cobalt-iron wüstite formed before a metallic phase appears.[30,32] The basic oxides impurities employed in the experiments include magnesium, calcium, lithium, sodium, potassium and barium. Among these impurities, calcium and potassium were used the most often.

Most of the reduction experiments were conducted in a $CO-CO_2$ atmosphere, at various ratios and total pressures. In all the previous work on the whisker formation or abnormal swelling, the gas pressure was kept at 1 atm and the partial pressures of CO and CO_2 were adjusted by the introduction of inert gases such as N_2 or Ar. In our work, there is no addition of inert gas. The total gas pressure is directly controlled to be between 50 torr to 200 torr. The benefit of

this low pressure is to enhance the efficiency of gas phase mass transport and to minimize the gas composition difference between the main gas flow and the oxide surface.

1. Apparatus

A controlled atmosphere, vertical furnance is used in this study. The configuration is schematically shown in Figure 4. The specimen is hung by a chromel wire in a quartz tube; the wire is attached to a hook so that the specimen can be released by the action of a magnet causing it to drop out of the furnance hot zone onto a fan-cooled brass headpiece.

A digitized temperature controller is employed to regulate the furnance temperature, usually set at 900°C, to within 1°C. The specimen temperature is monitored by a separate K type thermocouple which is inserted into the furnance tube, just beneath the specimen.

The gas pressure is controlled by a back pressure control valve connected with a mechanical pump; in our operation conditions, it can be easily set in the range of 25 torr to 400 torr with a stability of about 1 torr. The absolute gas pressure is indicated on capacitance pressure gauges. The accuracy of the gauges was claimed to be within 7 percent by the manufacturer. The gas composition is adjusted by the relative flow rate of pure components and usually the CO/CO_2 ratio is set about 11.8. Pure gases were supplied by Matheson Co.: the carbon monoxide is a Matheson grade with a purity above 99.99 percent, the carbon dioxide is a Coleman grade with a purity above 99.5 percent.

The gas flow rate is measured by a Matheson type 602 rotameter, and adjusted by a downstream needle valve. Upstream, the gas goes through a two-stage regulator to keep the upstream pressure of the rotameter about 2 Psig; then, the gas flow rate is insensitive to the reaction tube pressure. For each of the gases, the actual flow rate was calibrated with a bubble meter as shown schematically in Figure 5. The bubble meter was exposed to air, and the time of a soapbubble film travelling through a known volume was measured to obtain the gas flow rate in terms of STP gas volume per unit time. The calibration curves of CO and CO_2 are shown separately in Figure 6 and in Figure 7. In our experiments, the gas flow rate was set to about 13.5 STP ml/sec with the inner diameter of reaction tube of only 0.75 inch. There was no flow rate effect on the reduction reaction rate detectable at such a flow rate.

2. Specimen Preparation:

The 99 percent dense, polycrystalline cobalt ferrite bars were manufactured by Countis Industires. A specimen was cut from the bar into 1 cm x 1 cm x 0.1 cm slabs. One side of the specimen was ground and polished to 0.03 μm. The specimen was ultrasonically cleaned in pure acetone and distilled water for 10 minutes. To remove the surface damage induced by the polishing process, the surfaces of specimens were further sputtered by argon ions under the following conditions: ion accelerating voltage: 7 kV, specimen current: 0.6 mA; incident angle: 55° from normal; time: 30 minutes.

Wüstite specimens were prepared by oxidizing, MARZ iron slabs with a purity of 99.99 percent. These iron slbas were ground on 600 grit silicon carbide paper to remove superficial oxides, and cleaned in pure acetone and distilled water. Then the iron was oxidized in a $CO-CO_2$ mixture with CO/CO_2 ratio of 1, at 900°C, and at total gas pressure of 400 torr, for 4 hours. After this oxidation prcess, the thickness of the wüstite layer on the metallic iron was about 10 μm. A magnetite specimen was also prepared by the oxidation of pure iron, in a N_2-air mixture, with an oxygen content of about 60 ppm, at 1200°C, for 3 days.

A solid solution of 2 atom percent calcium oxide in wüstite was prepared by standard ceramic powder methods. Measured amounts of chemical reagent grade calcium nitrate and ferric nitrate were dissolved in pure methyl alcohol to form a homogeneous solution, then the solution was dired, and decomposed on a heating plate into a fine powder mixture of CaO and Fe_2O_3. The powder was compressed in a 1/4" die to form thin slabs. These were reduced in a $CO-CO_2$ mixture with a CO/CO_2 ratio of 1, at total pressure of 400 torr, at 900°C, for 4 hours. The final product was checked by X-ray diffraction.

Impurities were introduced into the surface of a specimen by wetting it with a drop of a solution containing a specified impurity. The wet specimen was then dried on a heating plate to preserve all the impurities in the drop, or it was blown to dry by compressed air to remove most of the solution except for a small portion absorbed on the specimen surface; we name the former "heavily contaminated" specimens, and the latter "lightly contaminated" specimens. Table 1 is a list of the impurity solutions used.

When the specimen is ready in the reaction tube, the system is evacuated to 0.2 torr, and the specimen is heated to the desired temperature. The preadjusted gas flow then starts and reduction reaction takes place until the specimen is quenched. It takes about 30 minutes to stabilize the furnance temperature at 900°C, and about 30 seconds to reach the equilibrium pressure in the reaction tube.

To examine the whiskers in the scanning electron microscope, the quenched specimen does not need any further treatment. Sometimes, a 10 percent bromine solution in methyl alcohol was employed to etch away the metallic phase, leaving the oxide phase untouched. This exposed the metal-oxide interface structure under the whiskers.

The specimens were examined in ISI high resolution scanning electron microscope. Stereo micrographs were always taken to reveal the three dimensional structure of surface features.

III. RESULTS

1. Whisker growth in reduction of cobalt ferrite:

The general appearance of a specimen reduced at 900°C at CO/CO_2 ratio of 10 is shown in Figure 8 and 9. The original ferrite grain boundary has been preferentially attacked by the reducing gas. The separation between grains is in good agreement with what is expected from the volume change of the spinel-to-wüstite transformation and the additional reduction. Metal whiskers of diameters in the range of 0.1 to 1 μm are scattered on the oxide surface. Some whiskers have grown in the gap between grains, lifting not yet completely reduced oxide grains. The oxide surface becomes pitted and faceted during the reduction, as shown in Figure 10. The facets of this pits appear to be {111} planes, corresponding to the densest oxygen planar packing in these cubic oxides. Figure 10 also shows that the whiskers tend to facet. The metal-oxide interface under the whisker is revealed in Figure 11 where the same location is shown with and without whiskers after etching. The stereo pair micrograph, Figure 11c, shows that the metal-oxide interface is again faceted and indents the oxide. The tendency for faceting strongly suggests that selected orientation relationships occur between the metal whisker and the matrix. Such orientation relationships were studied earlier for reduction of cobalt ferrite by De Jonghe and Thomas.[31]

2. Impurity effects:

On polished and ion sputtered surfaces, metal appears preferentially near grain boundaries or near pores within a grain, as

shown in Figure 12. Examination of fracture surfaces with the scanning Auger microscope, as shown in Figure 13, shows that intrinsic impurities such as Na, and Ca are present on intergranular fracture surfaces and on pore surface, while no impurities are detected on transgranular fracture surfaces. Sulphur was also detected on pore surfaces, as shown in the Auger electron profile Figure 14. This indicates that Na, Ca, and S, segregated to the grain boundaries and pore surfaces. If a specimen is polished and not ion sputterd, metal whisker will appear uniformly as shown in Figure 23. Therefore, impurities on surfaces and on grain boundaries can stimulate metal nucleation.

To further verify the effect of surface impurities, contaminated specimens were used. Whisker growth on "lightly" contaminated specimen surfaces is shown for surface contamination of Ca ions, Figure 15, and for K ions, Figure 16. Compared with sputtered specimens, the number density of the metal phase does not increase much, but the lateral size of the metal phase on contaminated specimens is significantly smaller. Although the quantity of impurity deposited on the surface is very small, it is effective in causing whiskers to appear. Other impurities such as Ba, Na, Li, and even Mg also show some tendency towards enhancing whisker formation, as shown in Figure 17 to Figure 20. Surprisingly, no matter which impurity contaminated the surface, the whisker diameters appeared comparable.

For "heavily" contaminated surfaces, both Ca ion and K ion increase dramatically the number density of whiskers, while Ca ion is more

effective than K ion, as shown in Figure 21 and 22. Since the increase of the whisker number density by itself would not favor the swelling, a consideration of impurity effect on whisker diameter becomes necessary to interpret the swelling behavior.

It has been shown that the surface impurities can be very effective in enhancing metal nucleation and whisker formation. Therefore, the impurity concentration on surface should be an important factor in the whisker formation. In fact, it might be the key parameter affected by various factors such as the initial composition of the oxides, the heat treatment process, and the reduction reaction rate.

3. Effect of gas pressure on whisker diameter

It is observed that whiskers grown at 100 torr generally are thinner than those grown at 50 torr, as shown in Figure 23 and Figure 24, when all other reaction conditions are identical. Variations in whisker diameter are observed for a given specimen, and are probably due to variations in local impurity concentrations and in metal-oxide interfacial structure. The experiments in which the total pressures were changed during the course of reduction permitted the evaluation of the change in whisker diameter on the same whisker. Figure 25 shows the whisker diameter change for a specimen reduced at 100 torr for 3 min., followed by a 4 min reduction at 50 torr, at 900°C and at a CO/CO_2 ratio of 11.8. The whisker diameter increases significantly. For the opposite case, Figure 26 shows the change in whisker diameter

for a specimen reduced at 50 torr for 4 mins., followed by a reduction at 100 torr for 2 min., at a CO/CO_2 ratio of 11.8 and at 900°C. The whiskers tend to cluster, but the decrease in whisker diameter with increasing total gas pressure is quite evident. For larger gas pressure changes (from 50 torr to 200 torr or vice versa), the whisker diameter changes are more obvious as shown in Figure 27 and 28. The ratios of whisker diameter before and after total gas pressure changes are shown in Figure 29. These results indicate that the whisker diameter is inversely proportional to the total gas pressure.

The changes of the whisker diameter always happen in the whisker segment close to the oxide surface, as shown in Figure 25 to Figure 28. This clearly indicates that whiskers are grown from the bottom, and agrees with Wagner's model in which metal is fed to the whisker base by cation diffusion in wüstite during reduction. Further, it is evident that whisker formation is a continuous growth process rather than a nucleation controlled process.

4. Effect of gas composition on whisker diameter

In addition to the total gas pressure, one may expect an effect of gas composition on the whisker diameter. Polished "lightly" Ca contaminated specimens were employed for the assessment of this effect. Figure 30 shows the whisker diameter change for a specimen reduced at 900°C, at CO/CO_2 ratio of 11.8, for 4 min., followed by a reduction at CO/CO_2 ratio of 2.9, for 2.5 min., with the total pressure kept

constant at 100 torr. There is only a small increase in the whisker diameter. Figure 31 shows the whisker diameter change for a specimen reduced at 900°C, at 100 torr, at CO/CO_2 ratio of 11.8 for 4 min., followed by a 2.5 min. reduction at 123 torr, at CO/CO_2 ratio of 2.9 to keep the partial pressure of CO a constant. The whisker diameter changes very little. Compared with the effect of the total pressure, the whisker diameter appear relatively insensitive to the changes of CO/CO_2 ratio, under the present conditions.

5. Metal formation in reduction of wüstite

When pure wüstite is reduced in a CO/CO_2 mixture, with a CO/CO_2 ratio of 11.8, at a total pressure of 100 torr, at 900°C, no metallic iron is observable on wüstite, even after a 5 min. reduction time, as shown in Figure 32. However, if the surface of wüstite is contaminated by Ca ions or K ions, a complete layer of metallic iron will cover the oxide under the same conditions. For a 3 min reduction, metal patches about 1.25×10^{-2}cm in diameter were observed on Ca ion and K ion contaminated surface as shown in Figure 33a and 34a. These results reconfirm that impurities such as Ca and K stimulate metal nucleation in reduction of wüstite. At the center of some metal patches, metal spikes were found, which can be considered as whiskers with a diameter of about 10 μm, as shown in Figure 33b and 34b. The effect of impurity on whisker formation in reduction of bulk wüstite is clearly much weaker than that in reduction of cobalt ferrite.

The metal patch on wüstite seems to be a thin, dense layer growing laterally to cover the wüstite surface at a rather high spreading rate. By assuming the velocity was constant during reduction, it was estimated to be about 3.5×10^{-5} cm/sec at 900°C, at total pressure of 100 torr, and at CO/CO_2 ratio of 11.8. The metal layer is so thin that the contrast between metal and oxide in a secondary electron image is very low, as shown in Figure 33b and 34b. A cross section of the metal patch as shown in Figure 35, reveals the thickness of metal layer to be about 0.5 μm. The surface of the metal patch remains at about the same level as the neighboring unreduced wüstite. This implies that the metal layer extends at the expense of the oxide phase, and that the consumed oxygen at the metal-oxide interface has been removed by diffusion, at a rate of about 1.4×10^{-10} gmole O/cm sec under the present conditions.

6. Oxide-gas interface velocity:

The absolute oxide-gas interface velocity cannot be obtained from conventional thermogravimetric measurements because the gas-solid interface area is not constant for a polycrystalline specimen. In reduction of dense cobalt ferrite, it is observed that the incompletely reduced coablt-iron wüstite grains are separated from each other. The width of the gap between grains increases with reduction time, as shown in Figure 36, and thus can yield the approximate rate at which the oxide-gas interface recedes. In Figure 37, the average oxide-gas interface velocity at CO/CO_2 ratio of 11.8 at total pressure of 100

torr and at 900°C at time less than 10 minutes was found to be about $5x10^{-9}$ m/sec., corresponding to an oxygen flux about $5x10^{-8}$ gmole O/cm^2sec.

7. Diffusion of Ca and Mg in reduction of magnetite:

A pure iron magnetite surface was heavily contaminated by $2.5x10^{-2}$ M $Mg(NO_3)_2$ or a $Ca(NO_3)_2$. The specimens were reduced in CO/CO_2 mixture at total pressure 100 torr, at CO/CO_2 ratio 11.8 and at 900°C, for 3 minutes. The concentration profile of the Ca and the Mg was measured by Auger electron spectroscopy with argon ion sputtering. The Ca diffusion profile shows a typical concentration rise near the surface in Figure 38. But there was no detectable Auger electron signal of Mg as shown in Figure 39. The Mg diffusivity is obviously much greater than the Ca diffusivity in this reaction conditions, causing the Mg to dissolve almost completely in the oxide.

IV. DISCUSSION

1. Metal-oxide interface diffusion in reduction of wüstite:

Metal patches were observed to grow on the wüstite surface during the $CO-CO_2$ reduction at 900°C. Oxygen diffusion is thought to be necessary in this process and the rate of oxygen removal in the present case is estimated about 1.4×10^{-10} gmole atoms of O/cm sec.

There are three possible paths for oxygen diffusion out of the metal-oxide interface: 1) through the metal phase, 2) through the oxide phase, and 3) along the metal-oxide interface. The oxygen diffusivity in pure iron-wüstite is not available; however, it is expected to be very low and is estimated to be comparable to that in CoO, measured to be about $10^{-16}cm^2/sec$ at 900°C.[36]. The oxygen concentration in the oxide is about 10^{-1} gmole atoms of O/cm^3. The oxygen diffusivity in f.c.c. iron at 900°C,[37] is about 3×10^{-7} cm^2/sec and the oxygen solubility limit is about 3 ppm,[37] which corresponds to an oxygen concentration of 1.5×10^{-6} gmole atoms of O/cm^3. The oxygen flux can be expressed approximately in terms of diffusion parameters:

$$J = -\beta C \frac{D_O}{KT} \frac{\Delta\mu}{\lambda} \qquad (5)$$

where C is the oxygen concentration, D_O is the oxygen diffusivity, β is the effective width of diffusion path, $\Delta\mu$ is the oxygen chemical potential difference between the oxygen source and the sink, and λ is the diffusion distance. For lattice diffusion in the metal or the

oxide, occurring at the leading edge of metal path, β, λ and $\Delta\mu$ are equivalent. According to Eqn. (5), the diffusion through the metal phase is obviously faster than through the oxide phase. There are no data available for oxygen diffusion along metal-oxide interfaces to compare with the other mechanisms. The interface diffusion is, however, likely to be the dominant mechanism.

If the diffusion through the metal phase were the dominant mechanism, the thickness of the metal patch should follow a parabolic law:

$$Y^2 \propto (t-t_o) \tag{6}$$

where Y is the thickness of the metal scale, t is the time, and t_o is the time of metal phase nucleation. If we assume the metal patch to have an ideal circular shape and to start growing at time t = 0 with a constant velocity V_p, then at a distance r from the center of metal patch,

$$r = t_o V_p \tag{7}$$

For a metal patch quenched at time t_f, the thickness, Y, profile of a cross section through the center should be approximated by a parabola:

$$Y^2 \propto (t_f - \frac{r}{V_p}) = k_p(t_f - \frac{r}{V_p}) \tag{8}$$

where k_p is a proportional constant.

The cross-section, Figure 35a, shows instead that the metal patch has a rather uniform thickness profile.

For a more detailed analysis of the thickness profile, we have to consider the displacement of the cross-section from the center of the metal patch. Referring to Figure 40, the thickness of metal at the center of the cross section is:

$$Y_c^2 = k_p \left(t_f - \frac{t_1 V_p}{V_p}\right) = k_p t_f \left(1 - \frac{t_1}{t_f}\right) \tag{9}$$

The time of the metal phase appearance at x, t_x, follows from simple geometrical considerations:

$$t_x = \left[t_1^2 + \left(1 - \frac{x}{L}\right)^2 \left(t_f^2 - t_1^2\right)\right]^{1/2} \tag{10}$$

Then, the thickness of metal at x is:

$$Y_x^2 = k_p(t_f - t_x)$$

$$= k_p t_f \left\{1 - \left[\left(\frac{t_1}{t_f}\right)^2 + \left(1 - \frac{x}{L}\right)^2 \left(1 - \left(\frac{t_1}{t_f}\right)^2\right)\right]^{1/2}\right\} \tag{11}$$

and the thickness profile is:

$$\left(\frac{Y_x}{Y_c}\right)^2 = \frac{1 - \left[\left(\frac{t_1}{t_f}\right)^2 + \left(1 - \frac{x}{L}\right)^2 \left(1 - \left(\frac{t_1}{t_f}\right)^2\right)\right]^{1/2}}{1 - \left(\frac{t_1}{t_f}\right)} \tag{12}$$

when $t_1/t_f = 0$, this gives Eqn. (8).

When t_1/t_f approaches 1, an equation for a circle follows:

$$\left(\frac{Y_x}{Y_c}\right)^2 = 1 - \left(1 - \frac{x}{L}\right)^2 \qquad (13)$$

No matter which cross section is taken, a thickness profile between these two extremes, as shown in Figure 41, should be observed, and the thickness of metal should always gradually decrease from the center to the edge. No uniform thickness should be observed, if the dominant mechanism is the diffusion through metal phase.

On the other hand, if the diffusion along the metal-oxide interface is the dominant mechanism, the affected zone will be restricted to the leading edge of the metal patch and the remaining portion will be of a constant thickness. Thus, from the observed morphology, it follows that metal-oxide interface oxygen diffusion is the dominant transport mechanism.

Quantitative analysis of the oxygen flux at the edge of the metal patch may confirm the rejection of the diffusion through metal phase and provide some information about the metal-oxide interface diffusion.

The microstructure of the leading edge of the metal patch is schematically shown in Figure 35c. To simplify the analysis, the leading edge has been assumed to be perpendicular to the surface and to the bottom of the metal patch. Since the metal layer thickness is uniform, it can be assumed that the oxygen removal occurs only at the leading edge, either by the diffusion through metal or by diffusion along the metal-oxide interface.

If the diffusion through metal is the dominant mechanism, Poisson equation might describe the oxygen distribution within the metal:

$$\nabla^2 C_v = 0 \tag{14}$$

where C_v is the oxygen concentration in the metal. In rectangular coordination, Eqn. (14) is:

$$\frac{\partial^2 C_v}{\partial x^2} + \frac{\partial^2 C_v}{\partial y^2} = 0 \tag{15}$$

Under the steady state assumption, the oxygen removal rate at the leading edge is proportional to the growth velocity V_p:

$$-D_v \frac{\partial C_v}{\partial x} = V_p \rho \qquad \text{at } x = 0 \tag{16}$$

where D_v is the oxygen lattice diffusivity in the metal and ρ is oxygen concentration in the oxide. To keep the thickness constant, there should not be any oxygen flux across the bottom of the metal patch:

$$\frac{\partial C_v}{\partial y} = 0 \qquad \text{at } y = 0 \tag{17}$$

At the surface of the metal patch, the oxygen concentration may be assumed to be equilibriated with gas phase by Sievert's law:

$$C_v = K_v \, (P_{O_2}{}^g)^{1/2} \qquad \text{at } y = Y \tag{18}$$

where K_v is the proportional constant in Sievert's law, $P_{O_2}{}^g$ is the oxygen partial pressure in gas phase. Y is the thickness of the metal patch. In addition to the boundary conditions (16) to (18), there is one more requirement: the oxygen concentration is finite everywhere.

By the standard separation of variables method and by a Fourier series technique, the solution of Eqn. (15) is obtained:

$$C_v = K_v \, (P_{O_2}{}^g)^{1/2} + \frac{2YV_p\rho}{D_v} \sum_{n=0}^{\infty} \frac{(-1)^n}{k_n} \cos(k_n \tfrac{y}{Y}) \exp(-k_n \tfrac{x}{y}) \tag{19}$$

where

$$k_n = (\frac{2n+1}{2}) \quad , \quad n = 0,1,2,\ldots$$

The immobility of the metal-oxide interface at the bottom of the metal patch also implies that the oxygen concentration in the metal there is in equilibrium with that in the oxide.

$$C_v = K_v \, (P_{O_2}{}^e)^{1/2} \qquad \text{at } y = 0 \tag{20}$$

where $P_{O_2}{}^e$ is the metal-oxide equilibrium oxygen partial pressure. Putting this condition into Eqn (19), yields,

$$K_v \left[(P_{O_2}{}^{e})^{1/2} - (P_{O_2}{}^{g})^{1/2} \right] = 0.74 \frac{YV_p\rho}{D_v} \qquad (21)$$

If the diffusion through metal indeed is the dominant mechanism, the oxygen diffusivity could be estimated by Eqn. (21). The relevant parameters for the present experimental conditions are listed in Appendix 1, and the calculated oxygen diffusivity is 8.8×10^{-5} $cm^2/sec.$, which is three orders of magnitude less than the measured diffusivity.

In the case of the diffusion along the metal-oxide interface is dominant, Poisson's equation does not apply any more because every point along the metal-oxide interface acts as an oxygen source. Now, the supply rate of the oxygen source equals the divergence of the oxygen flux:

$$\nabla \cdot J = V_p \rho \qquad (22)$$

and the oxygen flux in terms of interface diffusion becomes:

$$J = - D_i \delta_i \frac{dC_i}{dy} \qquad (23)$$

where D_i is the oxygen diffusivity at the metal-oxide interface, δ_i is effective width of the interface diffusion path, C_i is the oxygen concentration at the metal-oxide interface. Combining Eqn. (22) and (23), yields the governing equation of the interface diffusion:

$$\frac{d^2C_i}{dy^2} = -\frac{V_p\rho}{D_i\delta_i} \tag{24}$$

The boundary conditions are similar to those in the previous case:

$$C_i = K_i\,(P_{O_2}{}^{g})^{1/2} \qquad \text{at } y = Y \tag{25}$$

and

$$\frac{dC_i}{dy} = 0 \qquad \text{at } y = 0 \tag{26}$$

where K_i is the proportional constant in Sievert's law applied to the metal-oxide interface.

The solution of Eqn. (24) is:

$$C_i = K_i(P_{O_2}{}^{g})^{1/2} + \frac{1}{2}\frac{V_p\rho}{D_i\delta_i}\,(Y^2 - y^2) \tag{27}$$

At the bottom of the metal patch, we also have

$$C_i = K_i\,(P_{O_2}{}^{e})^{1/2} \qquad \text{at } y = 0 \tag{28}$$

yielding

$$K_i\,[(P_{O_2}{}^{e})^{1/2} - (P_{O_2}{}^{g})^{1/2}] = \frac{1}{2}\frac{Y^2V_p\rho}{D_i\delta_i} \tag{29}$$

The oxygen diffusion along the metal-oxide interface is the most likely mechanism in the metal patch formation on wüstite. Some quantities concerned with the interface diffusion would follow from the present experiments. The parameter group $D_i\delta_i K_i$ was evaluated by Eqn. (29) to be 1.2×10^{-6} gmole atoms of $O/atm^{1/2}$ sec. If C_i in the iron-wüstite equilibrium is estimated to be the oxygen concentration in the oxide bulk, K_i would be about 2.2×10^{7} gmole atoms of O/cm^3 $atm^{1/2}$, and $D_i\delta_i$ would be 5×10^{-14} cm^3/sec. With the usual assumption that $\delta_i \cong 10^{-7}$ cm, it would follow that $D_i \cong 5\times10^{-7}$ cm^2/sec at 900°C.

2. Steady state whisker diameter:

When oxide is reduced to metal, and the metal remains in contact with the oxide, as is the case for the whiskers, the metal-oxide interface will have to advance. In Figure 11 it was shown that the metal-oxide interface under th whisker has advanced slightly below the neighboring surface. Thus, oxygen must be removed from the whisker-oxide interface at a rate that is compatible with the rate at which the surrounding oxide-gas interface recedes. This rate was measured about 5×10^{-9} cm/sec, corresponding to a flux of 5×10^{-8} gmole atoms of O/cm^2 sec. The axial growth of the whisker is determined by the oxide-gas interface velocity, the whisker diameter, and the whisker density. The diameter of the whisker is determined by a balance between reactions and transport processes at the whisker base, as discussed now.

Similar to the argument in the previous section, there are three possible mechanisms of oxygen removal from the metal-oxide interface: 1) diffusion through the metal whisker, 2) diffusion through the oxide bulk, and 3) diffusion along the metal-oxide interface. In the present experiments, the metal and the oxide contain cobalt as well as iron. The oxygen diffusion in cobalt-iron alloy is not available, but it should be of the same order of magnitude as that in pure cobalt or iron. The oxygen diffusivity in cobalt at 900°C might be extrapolated from diffusion data obtained by Grundy and Nolan,[39] giving about 3×10^{-9} cm^2/sec. The oxygen solubility limit in cobalt was determined to be about 6×10^{-5} gmole atoms of O/cm^3 at 900°C.[38] Thus, the diffusion rate of oxygen in cobalt is comparable with that in iron. The oxygen diffusion through the oxide, as discussed before, is much slower than that through the metallic iron and presumably also through the metallic cobalt-iron alloy. Diffusion data of oxygen along a metal-oxide interface are only available for the pure iron-wustite system, from the work presented in the previous section. It is expected that the oxygen diffusion along the whisker-oxide interface would have similar properties and would dominate over diffusion through the whisker.

A more rigorous, mathematical treatment of the diffusion geometries of the whisker will demonstrate that the oxygen diffusion along the metal-oxide interface is indeed the dominant mechanism in determining the whisker diameter. The whisker geometry is assumed to be a cylinder having a flat metal-oxide interface, as shown schematically in Figure 42.

In the case of oxygen diffusion through the whisker, the governing relationship is Poisson's equation in cylindrical coordinates:

$$\frac{\partial C_v}{\partial z} + \frac{1}{r}\frac{\partial}{\partial r}\left(r \frac{\partial c_v}{\partial r}\right) = 0 \qquad (30)$$

The boundary conditions are, set similar to those in the discussion of the metal patch formation:

$$C_v = K_v(P_{O_2}{}^g)^{1/2} \qquad \text{at } r = \frac{D}{2} \qquad (31)$$

and

$$\frac{\partial C_v}{\partial r} = 0 \qquad \text{at } r = 0 \qquad (32)$$

where D is the whisker diameter.

A uniform oxygen removal occurs at the metal-oxide interface in the steady state:

$$-D_v \frac{\partial C_v}{\partial z} = Vp \qquad \text{at } z = 0 \qquad (33)$$

The oxygen concentration at the tip of whisker is assumed in equilibrium with gas phase:

$$C_v = K_v (P_{O_2}{}^g)^{1/2} \qquad \text{at } z = \infty \qquad (34)$$

By a separation of variables method and use of Bessel functions, the solution of Eqn. (30), under boundary conditions (31) to (34) is found to be:

$$C_v = K_v(P_{O_2}\, g)^{1/2} + \frac{V\rho D}{D_v} \sum_{n=1}^{\infty} \frac{1}{k_n^2\, J_1(k_n)}\, J_o(k_n r)\exp(-k_n z) \qquad (35)$$

where k_n is the nth zero of Bessel function Jo.

The maximum oxygen concentration difference occurs between the periphery of the whisker base at $r = D/2$, $z = 0$, and the center of the whisker base at $r = 0$, $z = 0$ so that:

$$\Delta C_{v_{max}} = \frac{V\rho D}{D_v} \sum_{n=1}^{\infty} \frac{1}{k_n^2\, J_1(k_n)} \qquad (36)$$

The oxygen concentration difference in Eqn. (36) can be expressed in terms of oxygen partial pressure and the Σ term is calculated to be about 0.26 from numerical tables of Bessel functions; thus:

$$K_v \Delta(P_{O_2}{}^{1/2})_{max} = 0.26\, \frac{V\rho D}{D_v} \qquad (37)$$

In the case of oxygen diffusion along the whisker-oxide interface, the governing equation is:

$$J = -\frac{1}{r}\frac{d}{dr}\left(r\, D_i \delta_i \frac{dC_i}{dr}\right) = V\rho \qquad (38)$$

and the boundary conditions are:

$$C_i = K_i\, (P_{O_2}\, g)^{1/2} \qquad \text{at } r = \frac{D}{2} \qquad (39)$$

$$\frac{dC_i}{dr} = 0 \qquad \text{at } r = 0 \qquad (40)$$

Solution of Eqn (38) yields straightforwardly:

$$C_i = K_i \, (P_{O_2}{}^{g})^{1/2} + \frac{v\rho}{4D_i\delta_i} \left(\frac{D^2}{4} - r^2\right) \tag{41}$$

The maximum oxygen concentration difference is then obtained:

$$\Delta C_{i_{max}} = K_i \Delta(P_{O_2}{}^{1/2})_{max} = \frac{V\rho D^2}{16 D_i \delta_i} \tag{42}$$

Eqn (37) and Eqn (42) describe the required driving forces, $\Delta(P_{O_2}{}^{1/2})$ for these two diffusion mechanism at the whisker base. In the case of pure iron oxide reduction, as shown in Figure 43, $\Delta(P_{O_2}{}^{1/2})$ for the metal-oxide interface diffusion is less than that for the metal lattice diffusion when the whisker diameter is smaller that 5×10^{-2} cm, no matter what the oxide-gas interface velocity is. The oxygen diffusion along the metal-oxide interface is thus overwhelmingly dominating for whisker diameters smaller than 1 μm, usually observed in the reduction of iron ores and cobalt ferrite.

No matter which mechanism is dominant in removing oxygen from the metal-oxide interface, the oxygen has to be removed steadily from the whisker surface or from the metal-oxide-gas triple junction by some chemical reaction. This reaction characteristically occurs on the metal surface. The chemical reaction and the oxygen diffusion can be considered as reactions in series. The total chemical reaction driving force---the oxygen partial pressure difference between the gas stream and the center of the whisker base--is distributed between the whisker surface reaction and the oxygen diffusion. In the previous analysis, we assumed that the oxygen concentration at the whisker surface is in

equilibrium with the gas phase; this is not valid any more. A pseudo-equilibrium oxygen partial pressure, $P_{O_2}{}^t$, should prevail at the whisker surface. The boundary condition (31) and (39) should then be written as:

$$C_i \text{ or } v = K_i \text{ or } v \ (P_{O_2}{}^t)^{1/2} \qquad \text{at } r = \frac{D}{2} \tag{43}$$

In the case of oxygen diffusion through the whisker, $P_{O_2}{}^t$ is a function of the axial coordinate, z, and would be unobtainable unless a surface reaction rate equation has been assumed. Regardless of the detailed mechanism of the metal surface reaction, the surface reaction always offers a resistance in the sequential reaction, and $P_{O_2}{}^t$ is always greater than $P_{O_2}{}^g$.

The boundary condition (34) then is a limiting case and the required driving force for diffusion in Eqn. (37) is a lower limit for oxygen diffusion through the whisker bulk. Therefore, in this more realistic situation, the oxygen diffusion along the metal-oxide interface is more important.

When oxygen is transported out along the metal-oxide interface, the chemical reaction is concentrated at the metal-oxide-gas junction. This triple junction reaction has a rate R_t per unit length of the triple junction. In the steady state, the triple junction reaction has to consume all the oxygen generated by the advancing of the metal-oxide interface:

$$\pi D \ R_t = \frac{\pi D^2}{4} V_p \tag{44}$$

Combining Eqn. (42) and Eqn. (44), the steady state whisker diameter can be expressed in terms of either the oxygen interface diffusivity or the triple junction reaction rate:

$$D = \left\{ \frac{16\, D_i \delta_i}{V_\rho\, K_i\, [(P_{O_2}{}^c)^{1/2} - (P_{O_2}{}^t)^{1/2}]} \right\}^{1/2} = \frac{4\, R_t(P_{O_2}{}^t)}{V_\rho} \qquad (45)$$

where $R_t(P_{O_2}{}^t)$, representing the triple junction reaction rate, might be a function of the triple junction oxygen partial pressure, $P_{O_2}{}^t$, at a constant total pressure. $P_{O_2}{}^c$ is the oxygen partial pressure at the center of the whisker base for which it is reasonable to assume that:

$$P_{O_2}{}^c \sim P_{O_2}{}^e \qquad (46)$$

Since the metal-oxide interface diffusion and the triple junction reaction are coupled in series, either one of them may be a rate determining step. If the interface diffusion is the rate determining step, most of the chemical driving force for oxygen removal would be exerted on the diffusion step, the oxygen partial pressure at the triple junction would be close to that in the gas phase:

$$P_{O_2}{}^t \sim P_{O_2}{}^g \qquad (47)$$

and the steady state whisker diameter is:

$$D = \left[\frac{16\, D_i \delta_i}{V_\rho\, K_i\, [(P_{O_2}{}^e)^{1/2} - (P_{O_2}{}^g)^{1/2}}\right]^{1/2} \tag{48}$$

On the other hand, if the triple junction reaction is the rate determining step, the oxygen chemical potential difference along the metal-oxide interface would be rather small and the triple junction reaction would be occurring under $P_{O_2}{}^e$:

$$R_t\,(P_{O_2}{}^t) \sim R_t(P_{O_2}{}^e) \tag{49}$$

and the steady state whisker diameter is:

$$D = \frac{4\, R_t(P_{O_2}{}^e)}{V_\rho} \tag{50}$$

Eqn. (48) and Eqn. (50) give an experimental means of distinguishing these two regimes. The dependence of the whisker diameter should be inversely proportional to 1/2 power of the oxide-gas interface velocity if the whisker is grown in the interface diffusion controlled regime.

The oxide-gas interface reaction rate for a CO-CO_2 mixture with a simple oxide, such as FeO, Fe_3O_4, CoO or ZnO can be simply expressed as a reversible reaction:[40-42]

$$V_\rho = K_s(P_{CO} - P_{CO_2}\ (\frac{P_{CO}}{P_{CO_2}})_e) \tag{51}$$

where P_{CO} and P_{CO_2} are the partial pressures of CO and CO_2, $(\frac{P_{CO}}{P_{CO_2}})_e$ is the gas ratio for metal-oxide equilibrium, k_s is the rate constant, which is a function of nonstoichiometry of oxide. The reaction rate equation also can be rewritten as:

$$V_\rho = \frac{k_s P_T}{1+R_a} (1 - \frac{R_a}{R_{a_e}}) \tag{52}$$

where P_T is the total pressure of CO and CO_2; R_a is the P_{CO_2}/P_{CO} ratio, which is directly related to oxygen partial pressure by the equation:

$$R_a = \frac{P_{CO_2}}{P_{CO}} = K(P_{O_2})^{1/2} \tag{53}$$

where K is the equilibrium constant.

In the cobalt-iron-oxygen system, we expect a similar behavior as in the pure iron-oxygen system, and the oxide-gas interface reaction rate should follow a rate equation similar to Eqn. (52).

In the interface diffusion control regime, when the gas ratio is kept constant, the whisker diameter would then be simply related to the total pressure by:

$$D \propto P_T^{-1/2} \tag{54}$$

But experimental results in Figure 29 show the whisker diameter to be inversely proportional to the total pressure rather than to the 1/2 power of the total pressure. The assumption of the interface diffusion control is thus inappropriate. It thus can be concluded that the whiskers grow in the triple junction reaction control regime.

If the pure wüstite-gas reaction rate is estimated to be in the range of 10^{-7} to 10^{-9} gmole O/cm^{2}sec, the required $\Delta(P_{O_2}^{1/2})$ for the oxygen interface diffusion is below the overall $\Delta(P_{O_2}^{1/2})$ in the system by at least two orders of magnitude as shown in Figure 43. For cobalt ferrite, the $P_{O_2}^{e}$ is higher than that for pure iron wüstite, and the $\Delta(P_{O_2}^{1/2})$ for the interface diffusion becomes more negligible in the overall $\Delta(P_{O_2}^{1/2})$. The triple junction reaction thus takes the predominant share of the overall driving force and controls the whisker diameter. Eqn. (50) should correctly describe the steady state whisker diameter.

When the gas ratio is kept constant, Eqn. (50) should fit the experimental results:

$$D \propto P_T^{-1} \tag{55}$$

It is found that as long as R_t is independent of the total pressure, Eqn. (55) holds. The implication of this on the mechanism of the triple junction reaction will be discussed later.

When the total gas pressure is kept constant, the dependence of the whisker diameter on the gas ratio can be obtained by combining Eqn. (50) and (52):

$$D \propto \frac{1 - \frac{R_a}{R_{a_e}}}{1 + R_a} \tag{56}$$

For iron oxide, R_{a_e} is about 0.4; for cobalt iron oxide alloy, R_{a_e} is about one order of magnitude higher. If R_a is much smaller than 1, the whisker diameter would be very insensitive to the change of the gas ratio. Under the present experimental conditions, R_a changes from 1/11.8 to 1/2.9, the corresponding increase of the whisker diameter should be about 20 to 30 percent only. The experimental result, Figure 30, fits this prediction quite well.

When the partial pressure of CO is kept constant, the dependence of the whisker diameter on the gas ratio should be even less. When the triple junction reaction rate is assumed to be independent of P_{CO}, the whisker diameter would follow:

$$D \propto \left(1 - \frac{R_a}{R_{a_e}}\right) \tag{57}$$

The change of the whisker diameter predicted by Eqn. (57) under the present conditions is less than 10 percent--a plausible prediction for Figure 31.

3. The metal-oxide-gas triple junction reaction

The analysis in the previous section showed that the steady state whisker diameter followed the equation:

$$D = \frac{4 R_t}{V\rho} \qquad (58)$$

The whisker diameter depends on two parameters which are affected by the reaction conditions: the triple junction reaction rate and the oxide-gas interface velocity. The overall impurity effect on the whisker diameter can thus be understood by considering the effect on these two factors.

The impurity effect on the oxide-gas interface velocity is reflected in the effect on the overall reduction rate, and can be measured thermogravimetrically. In the reaction of hematite, Schneider and Koch[20] showed that additions of SiO_2 and MgO had no effect on the reaction rate, and additions of K_2O, Na_2O and CaO only slightly slowed down the initial reaction rate.

In the whisker formation process, the presence of basic oxide impurities has been shown to have a drastic influence on the whisker diameter. Since impurities have only a minor effect on the oxide-gas interface velocity, the triple junction reaction rate should be significantly affected by impurities. For different impurity species, as shown before, the induced whisker diameters are quite similar so that their effects on the triple junction reaction should be similar also.

The overall reaction at the triple junction can be written as:

$$CO_{(g)} + O_{(ad)} \longrightarrow CO_{2(g)} \qquad (59)$$

This reaction has been studied on various metals as well as oxides surfaces.[40,52,53] No matter where it is occurring, the rate equation in the present conditions can be expressed as Eqn. (51) where the reaction rate is always proportional to the total pressure. Since the rate of the triple junction reaction has been suggested to be independent of the total pressure in the previous section, the reaction mechanism on such a heterogeneous junction could not be the same as that on a homogeneous surface.

Usually, there are two types of surface reaction mechanisms discussed in this reaction: Eley-Rideal (ER) and Langmuir-Hinshelwood (LH). In the ER mechanism, molecular CO gas is involved directly in removing oxygen; the reaction mechanism is exactly the same as Eqn. (59).

In the LH mechanism, CO gas is adsorbed on the surface, and then reacts with oxygen:

$$\begin{aligned} &(1) \quad CO_{(g)} \longrightarrow CO_{(ad)} \\ &(2) \quad CO_{(ad)} + O_{(ad)} \longrightarrow CO_{2(g)} \end{aligned} \tag{60}$$

The proportionality of the total pressure occurs in the ER mechanism or in the LH mechanism with the adsorbed CO far from saturation. The reaction rate would be constant when the surface is saturated by the adsorbed CO. This mechanism is unlikely because constant reaction rate has never been reported on either metal or oxide surface under the present reaction conditions, and there is no reason why CO molecules should adsorb preferentially at the triple junction to reach saturation.

Since either gaseous CO or molecularly adsorbed CO is unlikely to directly participate in the triple junction reaction, there should be other species involved in this mechanism. It has been found that CO molecules would dissociate readily on metal surface at temperature of 150°C and above.[43-49] The dissociation of CO will generate adsorbed carbon on the metal surface which might be a good oxygen removing agent, as in a $CO-CO_2$ decarburization reaction[51,52] where the adsorbed oxygen reacted with the dissolved carbon.

Inhibition of the dissociation of CO has been reported to be induced by sulphur and by oxygen adlayers on iron (100),[43] while no dissociation of CO has been observed on the oxide surface. Unreducible oxides on the metal surface would be expected to reduce drastically the dissociation of CO, and, thus to slow down the triple junction reaction, if the dissociated CO indeed is involved in the reaction mechanism. The similarity between the impurity effect on the dissociation of CO on the metal surface and that on the triple junction reaction suggests that the dissociated CO could be involved in the reaction mechanism.

We might presume the oxygen removal step in the triple junction reaction to be:

$$C_{(ad)} + O_{(ad)} \longrightarrow CO_{(ad)} \qquad (61)$$

The adsorbed oxygen or the adsorbed carbon has to move around the triple junction to accomplish this step. It was found that both of them were of low mobility; the mobility of carbon was thought to be

higher.[43] Thus, more precisely, reaction (61) is probably accomplished by the diffusion of the adsorbed carbon from the nearby metal surface to the triple junction.

The overall reaction mechanism is then made up as follows:

On the metal surface, the adsorbed carbon is generated:

$$
\begin{aligned}
&(1) \quad CO_{(g)} \rightleftharpoons CO_{(ad)} \\
&(2) \quad CO_{(ad)} \rightleftharpoons C_{(ad)} + O_{(ad)} \\
&(3) \quad CO_{(ad)} + O_{(ad)} \rightleftharpoons CO_{2(g)} \\
&(4) \quad C_{(ad)} \text{ diffusion to the triple junction}
\end{aligned}
\tag{62}
$$

and at the triple junction, the oxygen coming from the metal-oxide interface is removed by the adsorbed carbon:

$$(5) \quad C_{(ad)} + O_{(ad)} \longrightarrow CO_{(g)}$$

The rate determining step is either step (4) or step (5).

No matter which step is the actual rate determining step, the reaction rate should depend on the concentration of the adsorbed carbon and follow a kinetics similar to the Langmuir-Hinshelwood kinetics. A constant reaction rate would occur when the surface has been saturated with adsorbed carbon, i.e. when a surface carbide has been formed. Since the thermal desorption peak of dissociatively adsorbed CO is as high as 900°K,[43] indicating that its heat of adsorption might reach 50 kcal/gmole, surface carbide formation at 900°C and at 100 torr should be possible.

4. Impurity dissipation and the swelling of iron ore

It was observed that basic oxides, including MgO, would slow down the triple junction reaction rate and enhance the whisker formation; yet MgO does not cause abnormal swelling. Whiskers are easily formed in reduction of bulk wüstite. Whiskers were grown during reduction of mixed calcium oxide and wüstite powders, but not grown in reduction of calcio-wüstite solid solution. What is the interpretation for these facts?

In the previous section, the triple junction was shown to be severely retarded by impurities; if there are no impurities on the surface, the triple junction reaction rate could increase several orders and the whisker would not be formed. Thus, the presence of an impurity on the surface is necessary for the whisker formation, and the persistence of the surface impurity should be a decisive factor in sustaining whisker formation during the reduction process.

In the reduction of calcium contaminated wüstite, a metal spike was observed at the center of metal patch as shown in Figure 34. Since calcium oxide has a wide solubility range in wüstite at 900°C, it is easy for calcium to dissolve into wüstite in the heating process and in the reduction process. The spike formation can be treated as a whisker growth with decreasing impurity concentration at the triple junction.

When the surface impurity concentration is high enough, as in the previous discussion, the whisker diameter looks quite uniform and is controlled by the triple junction reaction. The decrease of the

impurity concentration will speed up the triple junction reaction and increase the importance of the oxygen diffusion along the metal-oxide interface. While the impurity concentration decreases, the whisker diameter will grow large and shift gradually from the reaction control regime to the diffusion control regime where the oxygen removal rate is limited by the interface diffusion and the gas P_{O_2}.

A maximum steady state whisker diameter results when the oxygen removal rate from the metal-oxide interface equals the maximum interface diffusion capability, that is:

$$P_{O_2}{}^{t} = P_{O_2}{}^{g} \tag{63}$$

in Eqn. (45). And the maximum whisker diameter is expressed as:

$$D_{max}^2 = \frac{16\, D_i \delta_i}{V_\rho\, K_i [(P_{O_2}{}^{e})^{1/2} - (P_{O_2}{}^{g})^{1/2}]} \tag{64}$$

If the oxide-gas interface velocity for wüstite is assumed to equal to that for cobalt ferrite of 5×10^{-8} gmole $O/cm^2 sec$, the maximum whisker diameter would be about 10 μm which is in agreement with the observed spike diameter, as shown in Figure 43.

The shift from the triple junction reaction control regime to the interface diffusion control regime is based on the assumption that oxygen is uniformly removed from the metal-oxide interface so that the triple junction reaction rate presumably could not be faster than the oxygen interface diffusion rate at the maximum whisker diameter. When the impurity concentration decreases, this maximum triple junction reaction rate would be exceeded and this assumption would be broken.

The metal-oxide interface close to the triple junction could consume oxygen more easily and would advance faster than that at the center. Thus, the metal-oxide interface would extend horizontally and its area would be so broad that axial growth of the metal would become negligible, i.e. the metal patch would be formed. The whole process is schematically shown in Figure 44.

The metal patch then could be considered as a two dimensional whisker lying on the oxide surface, and having a triple junction reaction with little impurity effect. The metal patch grows so fast that the oxide-gas interface velocity becomes relatively too slow to play any effective role in the metal patch formation.

The impurity concentration required for the nucleation of metal during reduction might not be as high as that required for the whisker formation and the impurity, such as calcium, would readily dissolve in wüstite. Therefore, whiskers are not easily formed in reduction of wüstite unless there is a large impurity source to maintain a high surface concentration as in calcium oxide and wüstite two phase powder mixtures.

In cobalt ferrite and Mn-Zn ferrite, it has been found that calcium or sodium is segregated to grain boundaries.[55,56] Thus, calcium might also be segregated to the grain boundary of magnetite and could not readily diffuse into the magnetite grains. Impurities have a higher probability to remain on the surface in the reduction of magnetite than of wüstite.

The dissipation rate of MgO from the surface has been demonstrated to be much faster than that of CaO in reduction of contaminated magnetite. Since MgO cannot stay on the surface for a long time, the whisker development should be expected to result in a lower abnormal swelling. Examination of ionic radii of various impurities as shown in Table 2, indicates that all those impurities which have been reported to cause the abnormal swelling have larger ionic radii than ferrous or ferric ion, and those impurities which have no reported effect have smaller ionic radii, except for Mn^{+2} which is more easily reduced than Fe^{+2} or Fe^{+3} and would thus be removed as metal by the metal phase. It seems that any metal oxide whose cation radius is greater than ferrous and ferric ion radius would enhance the abnormal swelling. From the point of view of diffusion, it is reasonable to expect that large ions are slower to diffuse and dissolve into an oxide host lattice of smaller ions, so that large ions would stay longer to enhance the whisker formation.

From the point of view of whisker nucleation, the higher the surface impurity concentration, the easier of the whisker nucleation. This would reduce the swelling. Thus, the correlation between the abnormal swelling and the impurities with larger ionic radii suggests that whisker growth is more important than whisker nucleation in control of the abnormal swelling.

5. Atomic mechanism of whisker diameter change

A last point which is worth discussing is the atomic mechanism by which the whiskers change diameter when the reaction conditions

change. The changes in whisker diameter cannot be explained on the basis of restricted radial growth after nucleation. However, the changes in whisker diameter can be understood if we consider their increasing and decreasing diameter together with the interface oxygen removal. A schematic series of drawings in Figure 45, illustrates how the diameter changes may be accomplished simply when the quasi-steady state has not yet been reached.

In the steady state, in Figure 45c, the velocity of the advancing oxide-gas interface equals that of the metal-oxide interface, and the whisker diameter is unchanged. When the oxide-gas interface velocity is faster than the metal-oxide interface velocity, due to the total pressure increase, as in Figure 45b, the triple junction will gradually move inward to shrink the whisker diameter. On the other hand, when the total pressure or the triple junction impurity concentration decreases, the metal-oxide interface will advance faster and the triple junction will move outward to extend the whisker diameter as in Figure 45d.

V. CONCLUSION

During $CO-CO_2$ reduction of cobalt ferrite and other iron bearing ores, metal whiskers may grow if impurities, such as basic oxides and sulphur, contaminate the surface. The whisker diameter is determined by the balance of oxygen removal from the oxide-gas interface and from the metal-oxide interface.

Oxygen transport along the metal-oxide interface might be limited by an impurity inhibited, ineffective catalytic process at the metal-oxide-gas triple junction, resulting in thin whiskers. Rapid oxygen diffusion along the metal-oxide interface has been observed in reduction of pure wüstite.

At constant temperature, the oxide-gas interface velocity is a function of the reaction conditions: the total pressure and the gas composition. The changes of reaction conditions will increase or decrease the whisker diameter. Specifically, it has been found that the whisker diameter is inversely proportional to the total pressure, but relatively insensitive to the gas ratio when the CO/CO_2 ratio of the gas is much higher than that of the metal-oxide equilibrium.

Adsorbed carbon from the dissociation of CO on metal surface is very likely play a major role in the catalytic process at the triple junction. Basic oxides and sulphur can inhibit this dissociation and drastically slow the triple junction reaction leading to thin whisker and enhancement of swelling.

Spike formation in reduction of wüstite is another form of whisker growth with decreasing surface impurity concentration. When the

surface impurity concentration is below a certain level, reduced metal will grow laterally to form a metal patch rather than grow upward to form a whisker.

Faster diffusion and higher solubility of impurities in wüstite than in iron bearing oxides with other crystal structures is the reason why whiskers are not readily formed in reduction of wüstite.

Impurity segregation in grain boundaries of ferrites or magnetite contributes to the whisker formation. The previous explanations of swelling of iron bearing ores in $CO-CO_2$ reduction by whisker nucleation effects do not appear satisfactory. A new interpretation which considers the growth of whisker and the effects of whisker diameter changes has been advanced.

The swelling of iron oxides during reduction depends on the persistence of impurities on the gas-solid surface. Impurities with a large ionic radius are expected to have a low diffusivity in wüstite and to induce the swelling.

APPENDIX 1

Values of the parameters used in Eqn. (21) and Eqn. (29).

1. Iron–wüstite equilibrium at 900°C

$$P_{O_2}^{\,e} = 1.44 \times 10^{-17} \text{ atm}$$

2. In CO–CO_2 mixture, at CO/CO_2 ratio of 11.8 and at 900°C.

$$P_{O_2}^{\,g} = 7.59 \times 10^{-19} \text{ atm}$$

3. In iron–wüstite equilibrium at 900°C, the oxygen concentration in iron, $C = 1.5 \times 10^{-6}$ gmole atoms of O/cm^3, and the Sievert's law constant is:

$$K_v = \frac{C}{(P_{O_2}^{\,e})^{1/2}} = 400 \text{ gmole atoms of } O/atm^{1/2}\ cm^3$$

Table 1

Impurity solutions and their concentrations

Impurity	Solution type	Concentration
Ca	$CaO-H_2O$	Saturated at R.T.
	$Ca(NO_3)_2$-MeOH*	2.5×10^{-2}M
K	$K(OH)-H_2O$	2.5×10^{-2}M
Li	$Li(NO_3)$-MeOH	2.5×10^{-2}M
Na	$Na(NO_3)$-MeOH	2.5×10^{-2}M
Mg	$Mg(NO_3)$-MeOH	2.5×10^{-2}M
Ba	$Ba(OH)_26H_2O-H_2O$	Saturated at R.T.

* only used in diffusion experiment.

Table 2

Comparison of ionic radii of various impurities:

	species	ionic radius (Å)
abnormal swelling:	Na^{+}	0.95
	K^{+}	1.33
	Ca^{+2}	0.99
	Ba^{+2}	1.35
	Zn^{+2}	0.74
	Fe^{+2}	0.76
	Fe^{+3}	0.64
no abnormal swelling:	Mn^{+2}	0.80*
	Li^{+}	0.60
	Mg^{+2}	0.65
	Al^{+3}	0.50
	Si^{+4}	0.40

* Mn^{2+} has higher reduction potential than Fe^{2+}, thus no Mn^{2+} can exist on metallic iron surface.

ACKNOWLEDGEMENTS

I wish to express my sincere appreciation to Professor Lutgard C. DeJonghe for his continuous, patient guidance and support through this work. Further thanks are extended to Professor Alan Searcy and Professor Donald Olander for reviewing this manuscript and providing necessary help to develop this research.

I would like to thank the support staff, especially Ken Gaugler and Erlene Fong for their good service on Auger analysis and SEM.

I would like to thank my colleagues and friends, especially Dr. S. S. Chiang and Dr. C. H. Hsueh for their many enlightening discussions.

I would also like to thank Ms. Diana Morris in T.I.D., without her help this thesis could not be finished in time.

Finally, I would like to thank my wife, Mei-Ying, for her constant encouragement and support.

This work was supported by the Division of Materials Sciences, Office of Basic Energy Sciences of the U.S. Department of Energy under Contract No. DE-AC03-76SF00098.

REFERENCES

1. J. Szekely, J. W. Evans and H. Y. Sohn; "Gas Solid Reaction," Academic Press (1976) pp. 57
2. E. Mazanek, S. Jasienska and C. Bryk; Arch. Eisen., 50, 57-62 (1979)
3. V. H. vom Ende, K. Grebe, S. Thomalla and E. E. Hofmann; Stahl u. Eisen. 90, 667-76 (1970)
4. V. H. vom Ende, K. Grebe and S. Thomalla; Stahl u. Eisen, 91, 815-24 (1971)
5. T. Fuwa and S. Ban-Ya; Trans. Iron Steel Inst. Japan, 9, 137-47 (1969)
6. R. L. Bleifuss; Trans. Soc. Mining Eng. AIME, 247, 225-31 (1970)
7. W.-K. Lu; Scand. J. Metallurgy, 2, 65-67 (1973)
8. W.-K. Lu; Scand. J. Metallurgy, 2, 169-72 (1973)
9. P. K Strangway and H. U. Ross; Trans. Met. Soc. AIME, 242, 1968-81 (1968)
10. E. T. Turkdogan and J. V. Vinters; Met. Trans., 2, 3175-88 (1971)
11. L. S. Darken and R. W. Gurry; J. Am. Chem. Soc., 68, 798 (1946)
12. J. S. Sheasby and J. F. Gransden; Can. Met. Quar., 13, 479-83 (1974)
13. A. Ishimitsu; Tetsu-to-Hagane Overseas, 5, 214-16 (1965)
14. S. Watanabe and M. Yoshinaga; Tetsu-to-Hagane, 51, 583-86 (1965)
15. N. Ponghis, R. Vidal, A. Bragard and A. Poos; Ironmaking proceedings, Met. Soc. AIME, Vol. 26., (1967) pp. 146-156

16. K. Grebe, H. de Haas, and H. Keddeinis; Stahl u. Eisen. 93, 472-80 (1973)

17. W. Wenzel and H. W. Gudenau; Stahl u. Eisen, 90, 689-97 (1970)

18. T. El Kasabgy and W.-K. Lu; Met. Trans., 11B, 409-14 (1980)

19. W.-K. Lu; Scand. J. Metallurgy, 3, 49-55 (1974)

20. A. Scheneider and K. Koch; Arch. Eisen., 50, 283-88 (1979)

21. H. de Haas and K. Grebe and F. Oeters; Arch. Eisen., 51, 167-72 (1980)

22. W.-K. Lu; Scand. J. Metallurgy, 2, 273-76 (1973)

23. M. C. Chang, J. Vlnaty and D. W. Kestner; Ironmaking proceedings, Met. Soc. AIME, Vol. 26., (1967) pp. 140-45

24. C. Wagner; J. Metals, 4, 214-16 (1952)

25. C. Wagner; Steelmaking: The Chipman Conference, (1962) pp. 19-26

26. R. A. Swalin; "Thermodynamics of Solids" John Wiley a Sons, 2nd ed. (1972) pp. 322

27. W.-K. Lu; Ironmaking proceedings, Iron and Steel Soc. AIME, Vol. 33, (1974) 61-72

28. V. H. vom Ende, K. Grebe; Stahl u. Eisen, 91, 815-24 (1971)

29. R. Nicolle and A. Rist; Met. Trans., 10B, 429-38 (1979)

30. J. R. Porter and L. C. DeJonghe; Met. Trans., 12B, 299-309 (1981)

31. L. C. De Jonghe and G. Thomas; Mater. Sci. Eng., 8, 259-74 (1971)

32. M. C. Ray and L. C. De Jonghe; J. Mat. Sci. 15, 2241-52 (1980)

33. L. S. Darken and R. W. Gurry; J. Am. Chem. Soc., 67, 1398 (1945)

34. L. Himmel, R. F. Mehl and C. E. Birchenall; J. Metals, 5, 827 (1953)

35. A. Muan; Am. Ceram. Soc. Bull., 37, 81 (1958)

36. W. K. Chen and R. A. Jackson; J. Phys. Chem. Solids, 30, 1309-1314 (1969)

37. J. H. Swisher and E. T. Turkdogan; Trans. Met. Soc. AIME, 239, 426-31 (1969)

38. A. U. Seybolt and C. H. Mathewson; Trans. AIME, 117, 156-72 (1935)

39. P. J. Grundy and P. J. Nolan; J. Mat. Sci., 7, 1086-87 (1972)

40. V. H. Grabke; Ber. Bunsenges. Phys. Chem., 69, 48-57 (1965)

41. K. H. Ulrich, K. Bohnenkamp and H. J. Engell; Arch. Eisen., 9, 611-18 (1965)

42. E. Riecke and K. Bohnenkamp; Arch. Eisen., 40, 717-25 (1969)

43. J. Benziger and R. J. Madix; Surface Sci., 94, 119-53 (1980)

44. G. Broden, G. Gafner and H. P. Bonzel; Appl. Phys., 13, 333 (1971)

45. T. N. Rhodin and C. F. Brucker; Solid State Commun., 23, 341 (1970)

46. C. R. Brundle; IBM J. Res. Develop., 22, 235 (1978)

47. M. Textor, I. D. Gay and R. Mason; Proc. Roy. Soc. (London), A356, 37 (1977)

48. M. P. Hooker and J. T. Grant; Surface Sci., 62, 21-35 (1977)

49. R. W. Joyner; Surface Sci., 63, 291-314 (1977)

50. P. Hayes; Met. Trans. 10B, 489-96 (1979)

51. S. R. Shatynski and h. J. Grabke; Arch. Eisen., 49, 129-33 (1978)

52. H. J. Grabke; Arch. Eisen., 46, 75-81 (1975)

53. H. J. Grabke; "Proceedings of 3rd International Congress of Catalysis" ed. by W.M.H. Sachlter, G.C.A. Schuit and P. Zwietering, North-Holland Publ. Co., Amsterdam, (1965) pp. 928-38

54. H. J. Grabke; Ber. Bunsenges. Phys. Chem., 71, 1067-73 (1967)

55. P.E.C. Franken, W. T. Stacy; J. Am. Ceram. Soc., 63, 315-319 (1980)

56. R. Mishra; J. Appl. Phys., 49, 1876-8 (1978)

FIGURE CAPTIONS:

Figure 1. Phase diagrams of Fe-O systems. Oxygen scale is in unit of weight percent in figure a, in unit of CO_2/CO ratio in figure b.

Figure 2. Possible material transport mechanisms and accompanying chemical reaction at oxide-gas interface, at metal-oxide-gas triple junction and at metal-gas interface.

Figure 3. Phase diagrams of Fe-Co-O system at 1000°C. A continuous area of wüstite phase is shown between spinel and metal.

Figure 4. Schematical diagram of apparatus.

Figure 5. Schematical diagram of bubble meter.

Figure 6. Calibration chart of flowmeter for CO, the upstream pressure is kept at 2 Psig.

Figure 7. Calibration chart of flowmeter for CO_2, the upstream pressure kept at 2 Psig.

Figure 8. Stereo micrograph of cobalt ferrite reduced at $CO/CO_2=10$. Some partly reduced grains have been lifted off the surface. Metal whiskers tangle where their density is high. The separation between the grains in the substrate is due to the spinel to wüstite transformation as well as to further wüstite reduction.

Figure 9. Cobalt ferrite reduced at $CO/CO_2=10$. Partly reduced grain has not been completely seperated from the substrate.

Figure 10. Metal whisker and pitting of the oxide surface. The pit facets are {111} planes. The metal whisker also tends to facet.

Figure 11. The whiskers (900°C, CO/CO_2 = 11.8, 50 torr, 5 min) in figure a, have been removed by etching with 10 percent Br_2 solution of methanol for 1 min in figure b. The area boxed in figure b is shown enlarged in the stereo micrograph figure c. The metal-oxide interface under the whiskers is slightly below the neighboring surface, and tends to facet.

Figure 12. For polished and ion sputtered surface, whisker nucleation is confined to the grain boundary area of near the pore.

Figure 13. Fracture surface of the cobalt ferrite. Figure a is a SEM image of the same area shown by Ca mapping in figure b and by Na mapping in figure c with the scanning Auger microscope.

Figure 14. Auger electron spectrum from a pore of fracture surface of the cobalt ferrite shows the presence of Na, Ca and S.

Figure 15. Whisker formation on "lightly" Ca contaminated surface reduced at 900°C, CO/CO_2 = 11.8, 100 torr, 5 min.

Figure 16. Whisker formation on "lightly" K contaminated surface reduced at 900°C, CO/CO_2 = 11.8, 100 torr, 5 min.

Figure 17. Whisker formation on Ba contaminated surface reduced at 900°C, CO/CO_2 = 11.8, 100 torr, 5 min.

Figure 18. Whisker formation on Na contaminated surface reduced at 900°C, CO/CO_2 = 11.8, 100 torr, 5 min.

Figure 19. Whisker formation on Li contaminated surface reduced at 900°C, CO/CO_2 = 11.8, 100 torr, 5 min.

Figure 20. Whisker formation on Mg contaminated surface reduced at 900°C, CO/CO_2 = 11.8, 100 torr, 5 min. The equilateral triangle etching pits in figure a demonstrate {111} facets.

Figure 21. Whisker formation on "heavily" Ca contaminated surface reduced at 900°C, CO/CO_2 = 11.8, 100 torr, 5 min.

Figure 22. Whisker formation on "heavily" K contaminated surface reduced at 900°C, CO/CO_2 = 11.8, 100 torr, 5 min.

Figure 23. Stereo micrograph of whiskers on polished cobalt ferrite reduced at 900°C, CO/CO_2 = 10, 100 torr, 5 min.

Figure 24. Stereo micrograph of whisker on polished cobalt ferrite reduced at 900°C, CO/CO_2 = 10, 50 torr, 10 min.

Figure 25. Stereo pairs of whisker diameter change for a "lightly" Ca contaminated specimen reduced at 900°C for 3 min at 100 torr followed by a 4 min reduction at 50 torr, at CO/CO_2 = 11.8. The whisker diameter changes by about a factor of 2.

Figure 26. Stereo pair of whisker diameter change for a "lightly" Ca contaminated specimen reduced at 900°C for 4 min at 50 torr, followed by a 2 min reduction at 100 torr, at CO/CO_2 = 11.8. The whisker diameter shrinks.

Figure 27. Stereo pair of whisker diameter change for a "lightly" Ca contaminated specimen reduced at 900°C for 6 min at 50 torr, followed by a 0.5 min reduction at 200 torr at CO/CO_2 = 11.8.

The whisker diameter splits up into several smaller diameter whiskers.

Figure 28. Stereo pair of whisker diameter change for a "lightly" Ca contaminated specimen reduced at 900°C for 2.5 min at 200 torr followed by a 5 min reduction at 50 torr, at CO/CO_2 = 11.8.

Figure 29. Whisker diameter ratio as a function of total gas pressure ratio for experiments of the type shown in Figure 25 to 28. The theoretical line for the metal-oxide interface oxygen diffusion control regime cannot fit the data.

Figure 30. Stereo pair of whisker diameter change for a "lightly" Ca contaminated specimen reduced at 900°C for 4 min at CO/CO_2 = 11.8, followed by a 2.5 min reduction at CO/CO_2 = 2.9, at 100 torr. The whisker diameter increases very slightly.

Figure 31. Stereo pair of whisker diameter change for a "lightly" Ca contaminated specimen reduced at 900°C for 4 min at CO/CO_2 = 11.8, at 100 torr, followed by a 2.5 min reduction at CO/CO_2 = 2.9, at 123 torr. The whisker diameter almost has no change.

Figure 32. Surface features on pure FeO reduced at 900°C, CO/CO_2 = 11.8, 100 torr, for 5 min. Optical micrograph of figure a and SEM images of figure b, c show only faceting of the FeO, no sign of metal.

Figure 33. Metal patch formation and spike formation on Ca contaminated FeO surface reduced at 900°C, CO/CO_2 = 11.8, 100 torr, for 3 min. Figure a is an optical micrograph showing clear contrast between metal and oxide which is not clearly shown on SEM image in figure b.

Figure 34. Metal patch formation and spike formation on K contaminated FeO surface reduced at 900°C, CO/CO_2 = 11.8, 100 torr, for 3 min.

Figure 35. Cross section of a metal patch. Arrows in figure a, b, indicate the leading edge of the metal patch which is schematically shown in figure c.

Figure 36. The separation of oxide grains for specimens reduced at 900°C, CO/CO_2 = 11.8, 100 torr, for 3, 5 and 7 min in figure a, b and c, respectively.

Figure 37. The separation of oxide grains as a function of reduction time.

Figure 38. Element depth profiles for Ca contaminated magnetite reduced at 900°C, CO/CO_2 = 11.8, 100 torr, for 3 min.

Figure 39. Auger electron spectrum for Mg contaminated magnetite reduced at 900°C, CO/CO_2 = 11.8, 100 torr, for 3 min. Mg signal should appear about 1186 eV.

Figure 40. Geometry of dense Fe on FeO expected when oxygen diffusion through the dense Fe product would be rate controlling.

Figure 41. Thickness profile of dense Fe on FeO expected when oxygen diffusion through the dense Fe product would be rate controlling. Any profile should fall between the two limit cases, $t_1/t_f = 1$ and 0.

Figure 42. Whisker geometry. The oxide-gas interface is advancing with a velocity V.

Figure 43. For oxygen diffusion through the whisker and along the metal-oxide interface, the required driving forces as a function of the whisker diameter. The whisker diameter where these two mechanisms are comparable is independent of the oxide-gas interface velocity. At the size of whisker diameter observed on cobalt ferrite, the metal-oxide interface diffusion is dominated over the whisker lattice diffusion.

Figure 44. Schematic illustration of the transition from the spike formation to the metal patch formation.

Figure 45. Schematic illustration of the mechanism by which the changes in whisker diameter can occur. The shaded area is the new metal formed. The axial growth at rate, $\dot{a}$, is accomplished by a supply of metal ions from the neighboring oxide-gas interface and from the metal-oxide interface.

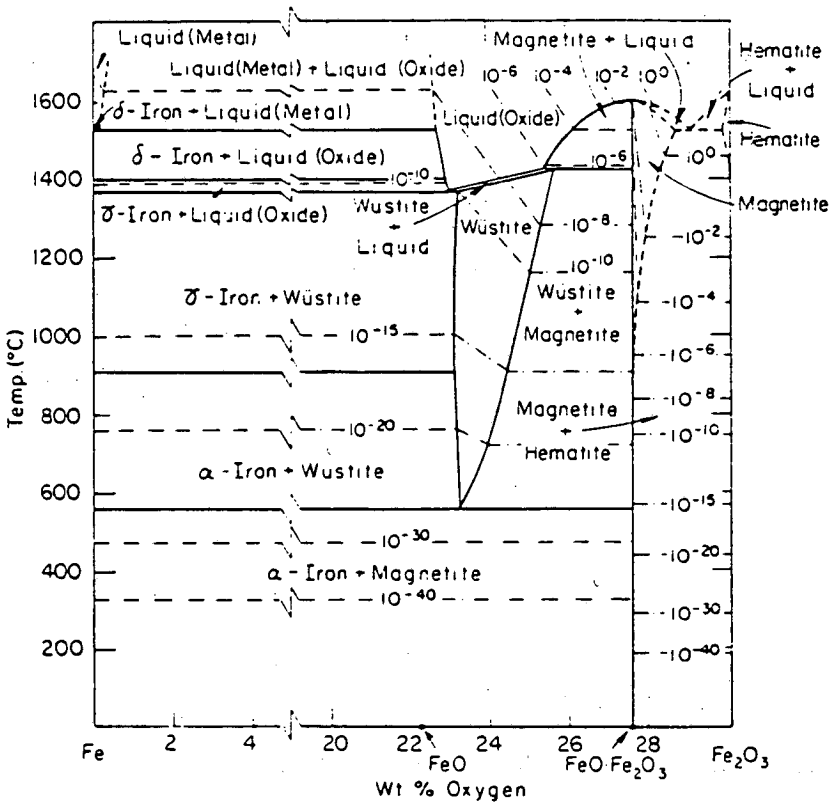

A

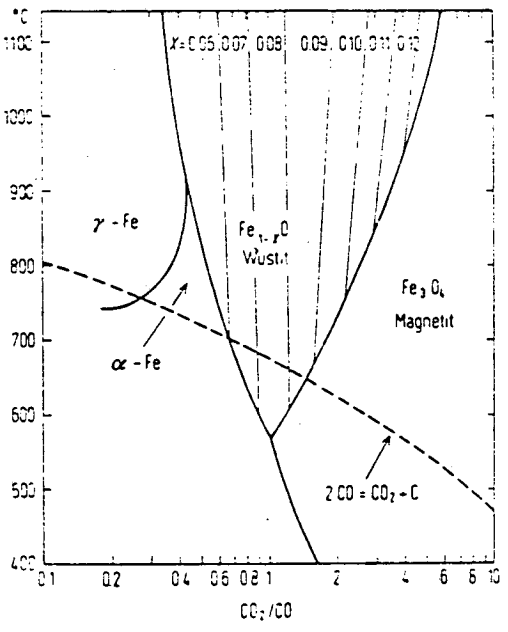

B

Figure 1. XBL 834-9032

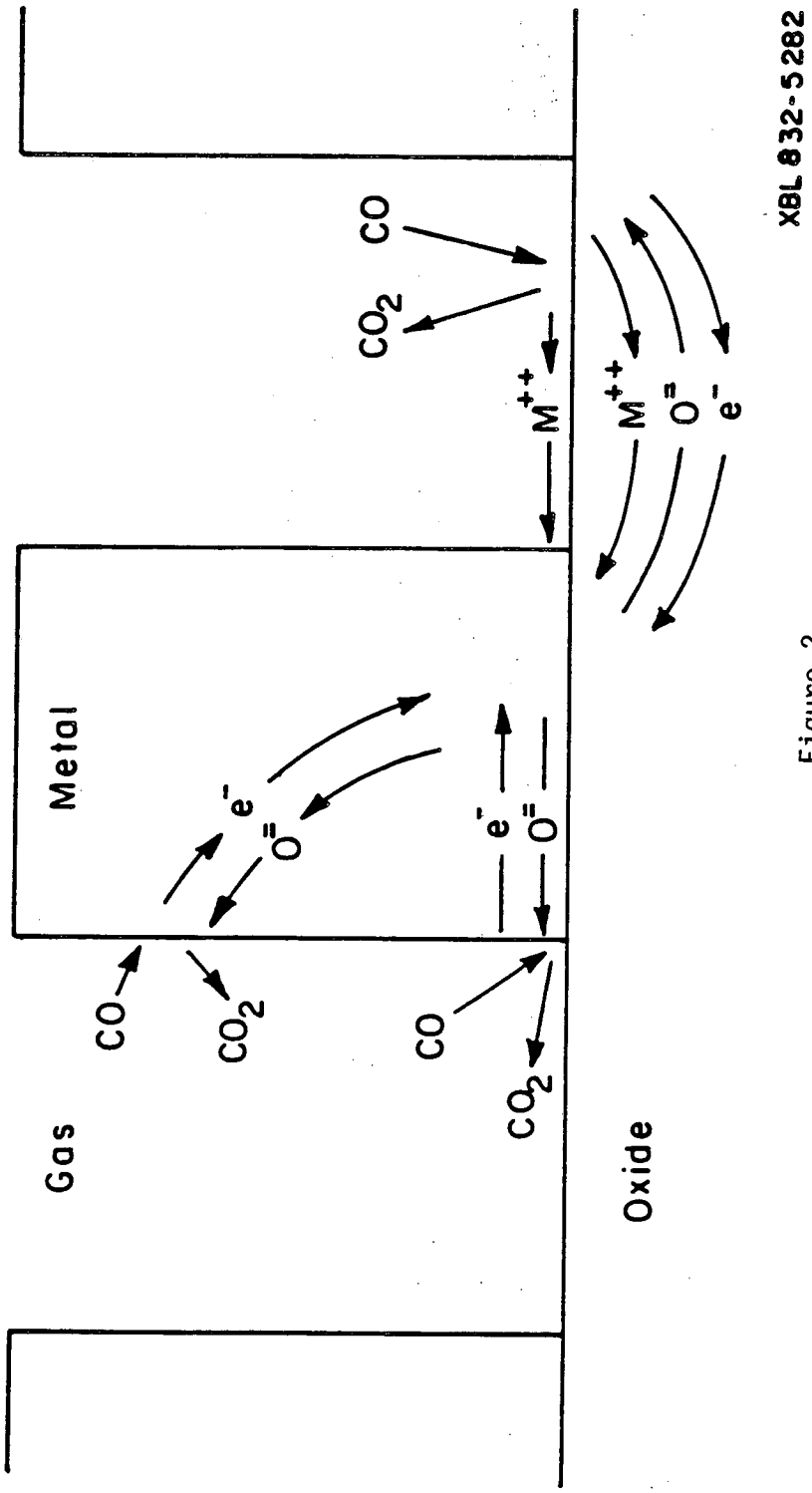

Figure 2.

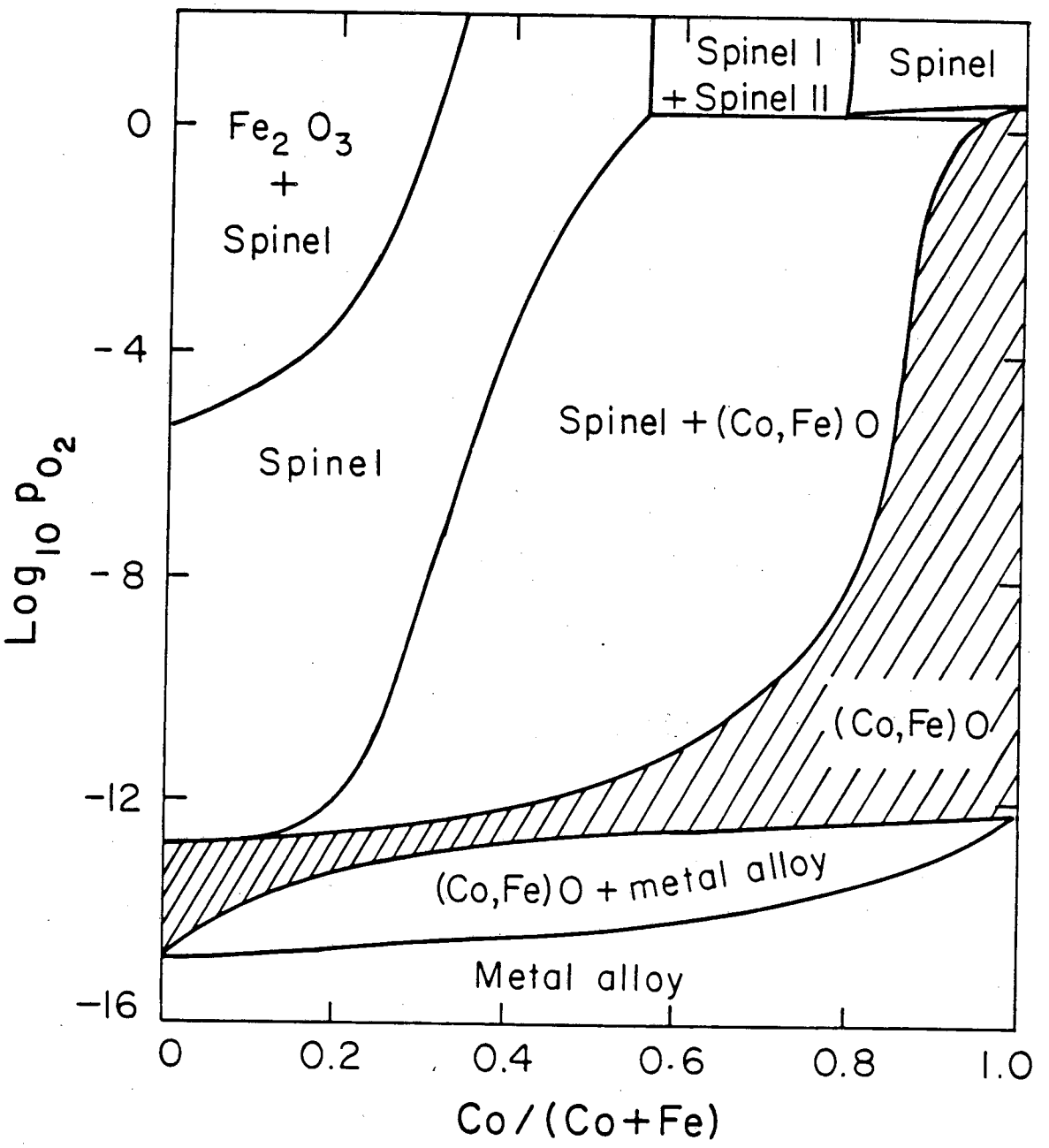

Figure 3.

XBL 807-1523

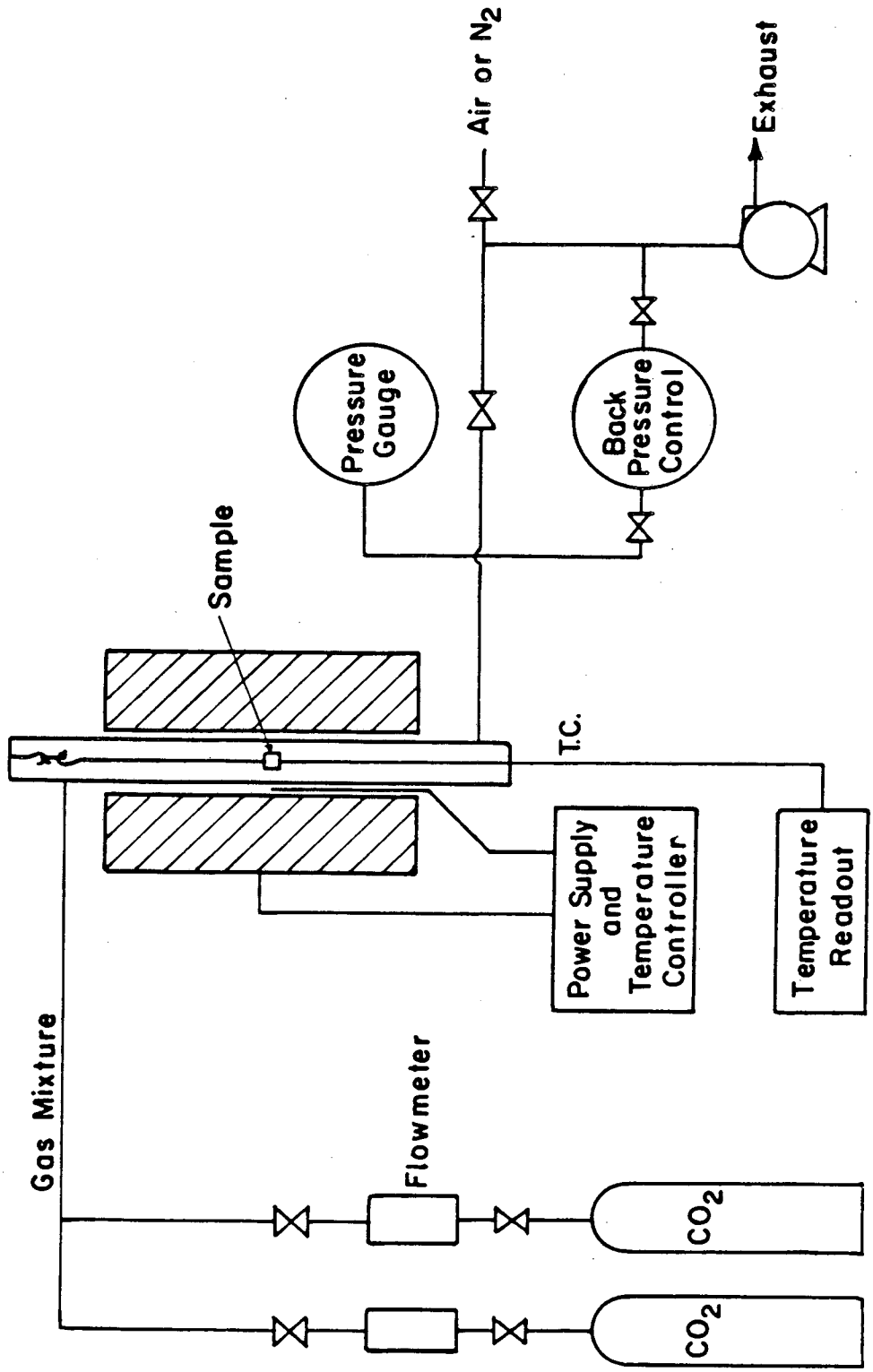
Air or N_2
Exhaust
Pressure Gauge
Back Pressure Control
Sample
T.C.
Power Supply and Temperature Controller
Temperature Readout
Gas Mixture
Flowmeter
CO_2
CO_2
XBL 832-5281

Figure 4.

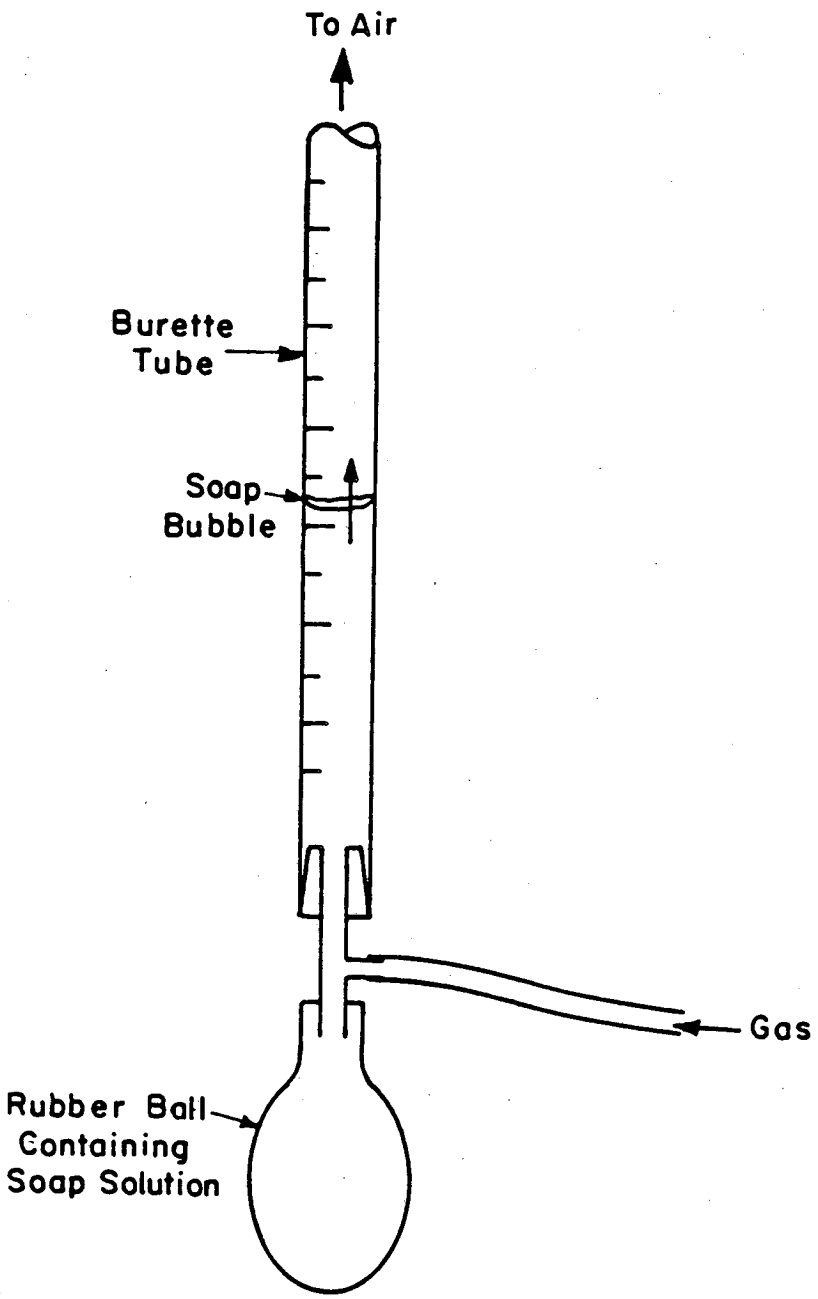
To Air
Burette Tube
Soap Bubble
Gas
Rubber Ball Containing Soap Solution
XBL832-5280

Figure 5.

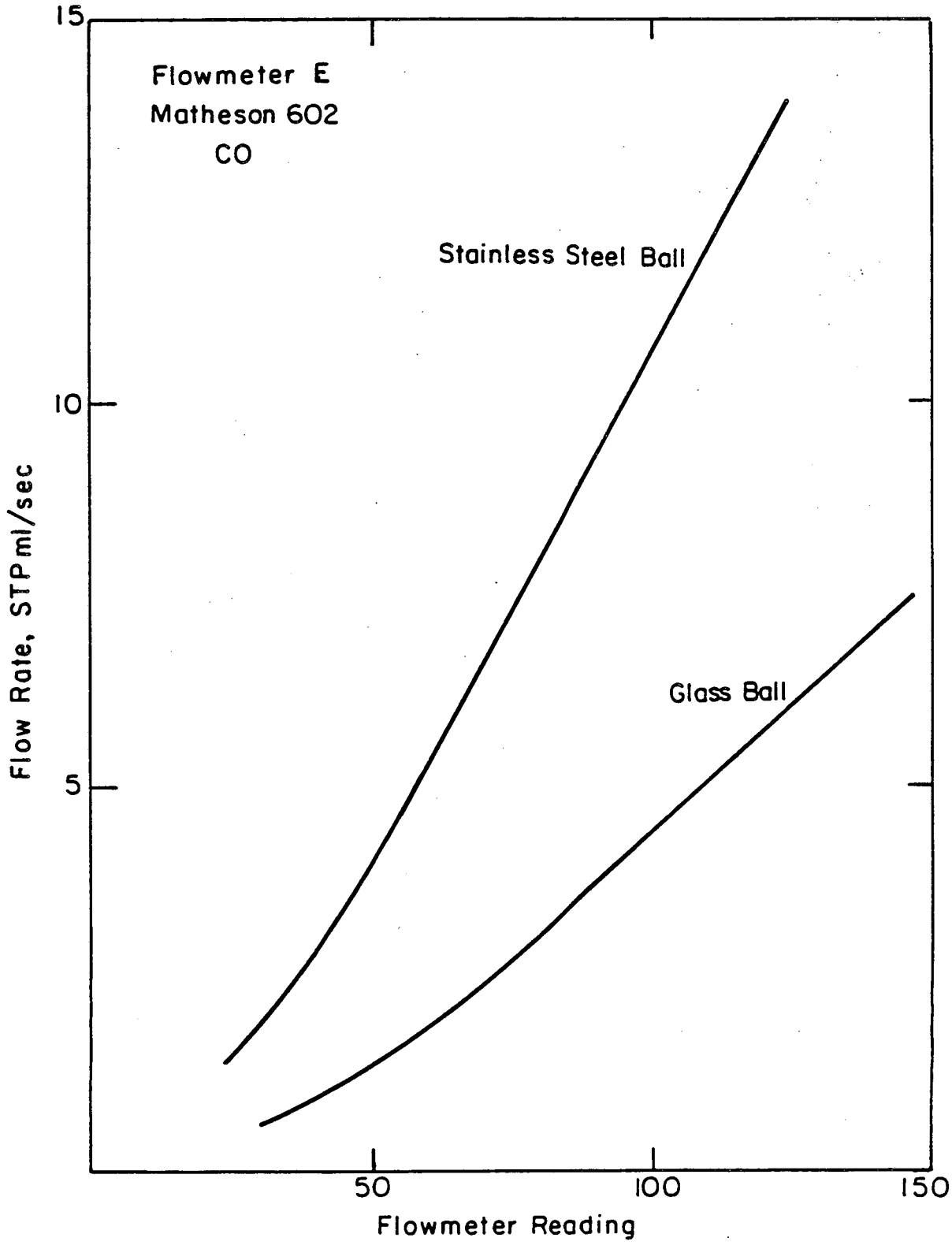

Figure 6.

XBL 832-5274

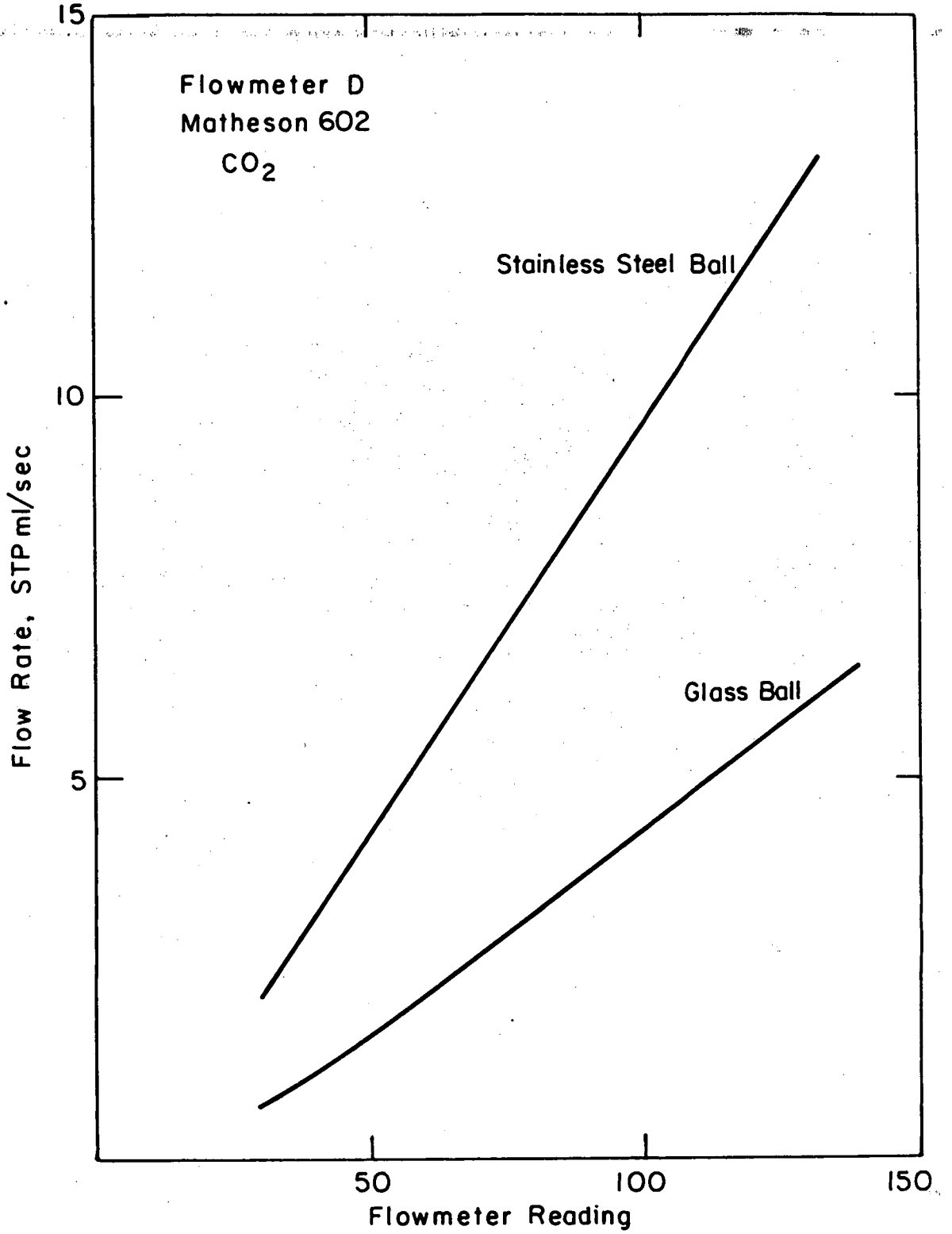
Flowmeter D
Matheson 602
CO_2
Stainless Steel Ball
Glass Ball
Flow Rate, STP ml/sec
15
10
5
50
100
150
Flowmeter Reading
XBL 832-5273

Figure 7.

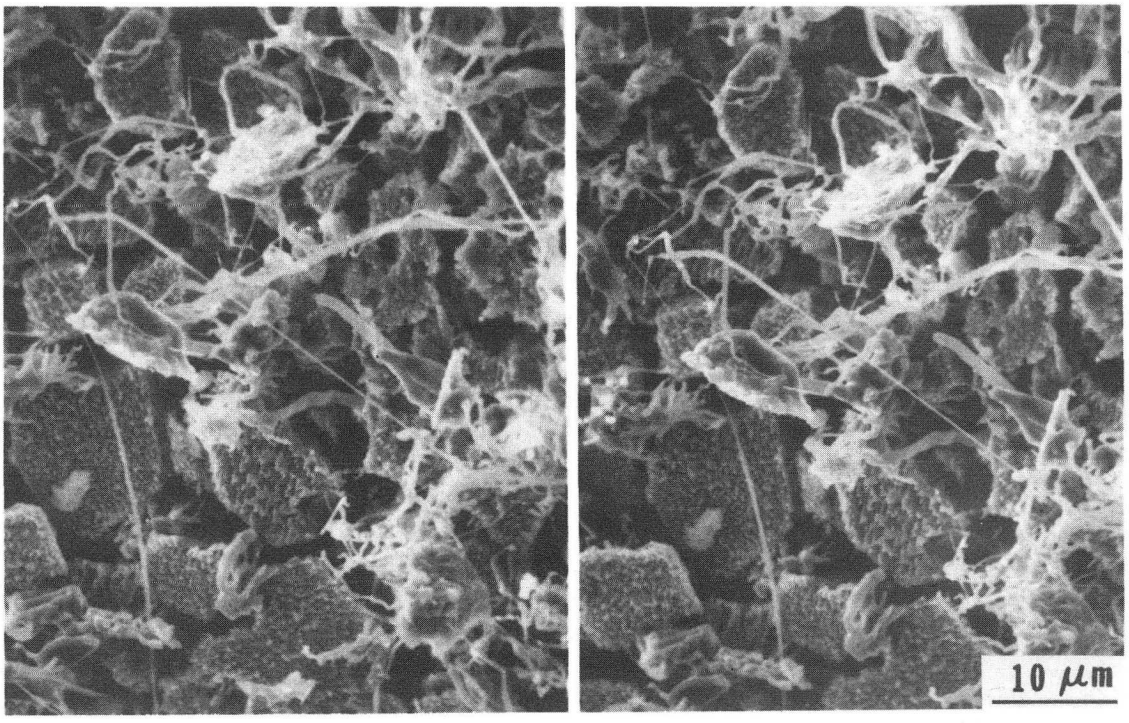

XBB 832-1118

Figure 8.

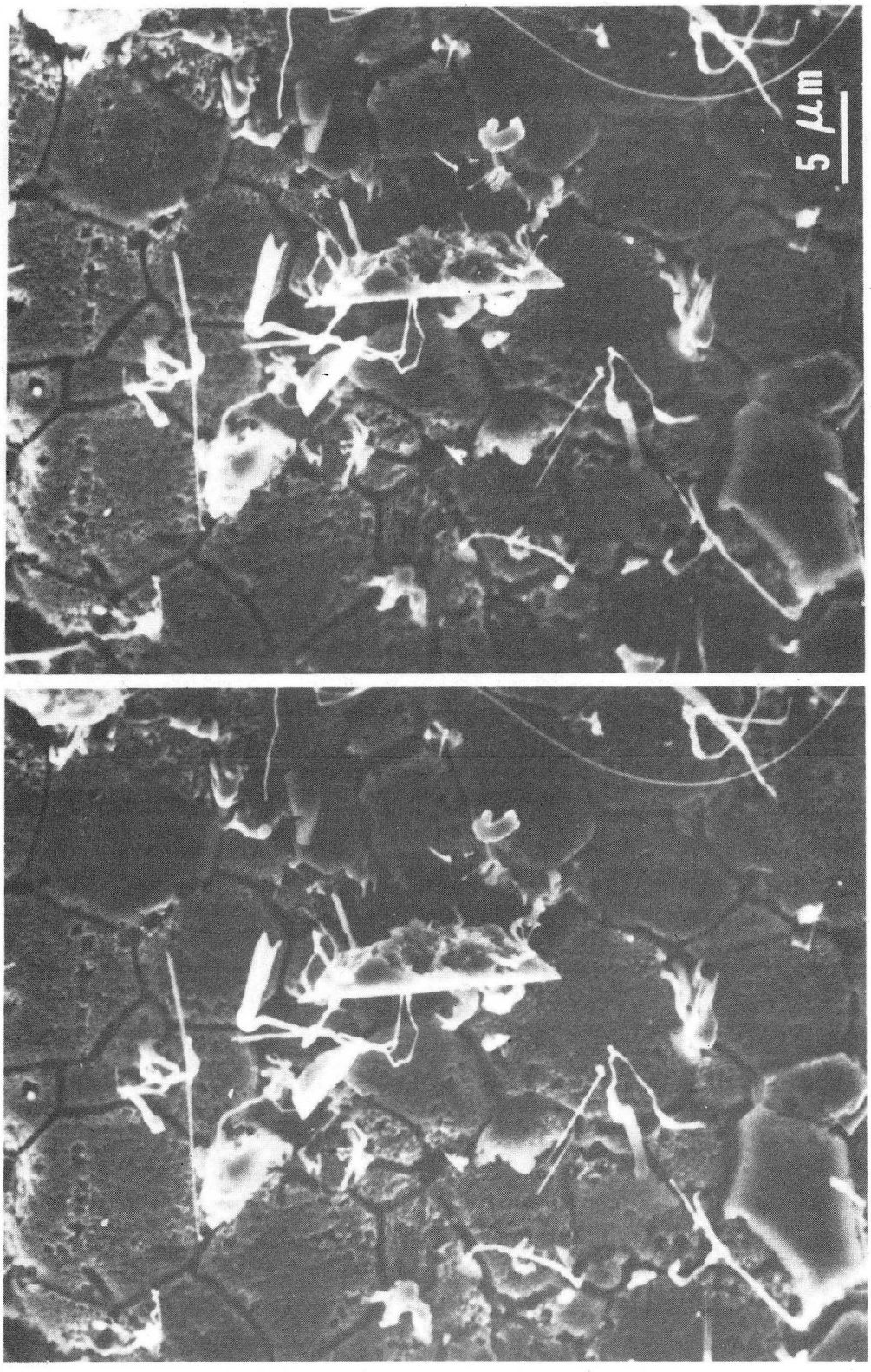

XBB 833-2623

Figure 9.

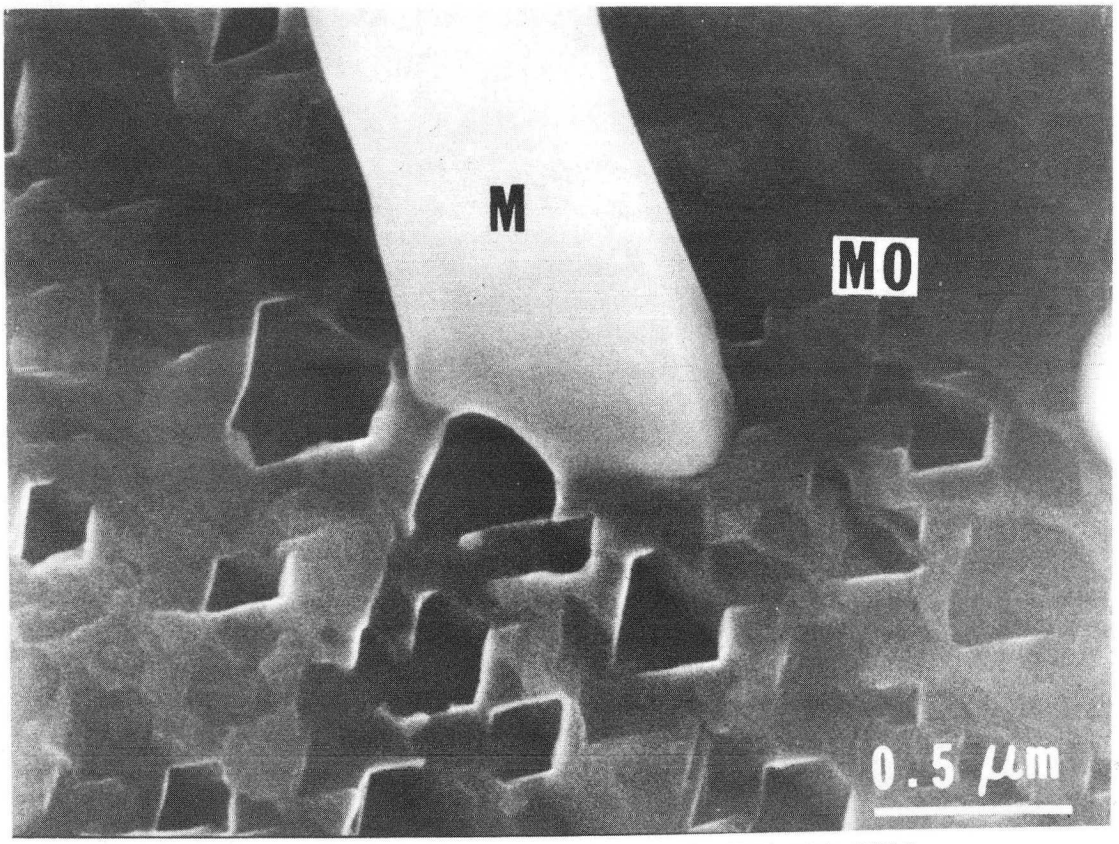

XBB 819-8722

Figure 10.

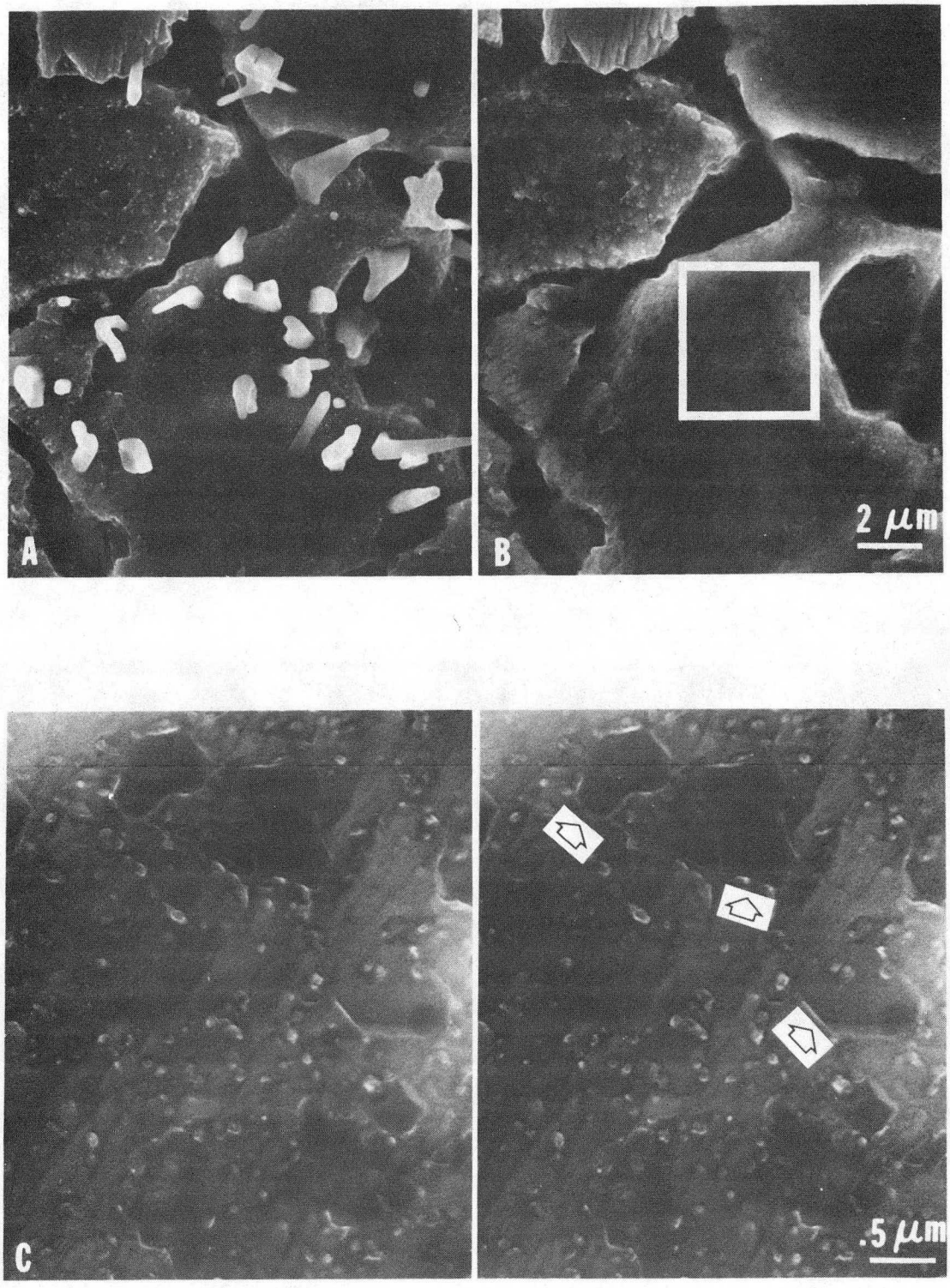

XBB 832-1114A

Figure 11.

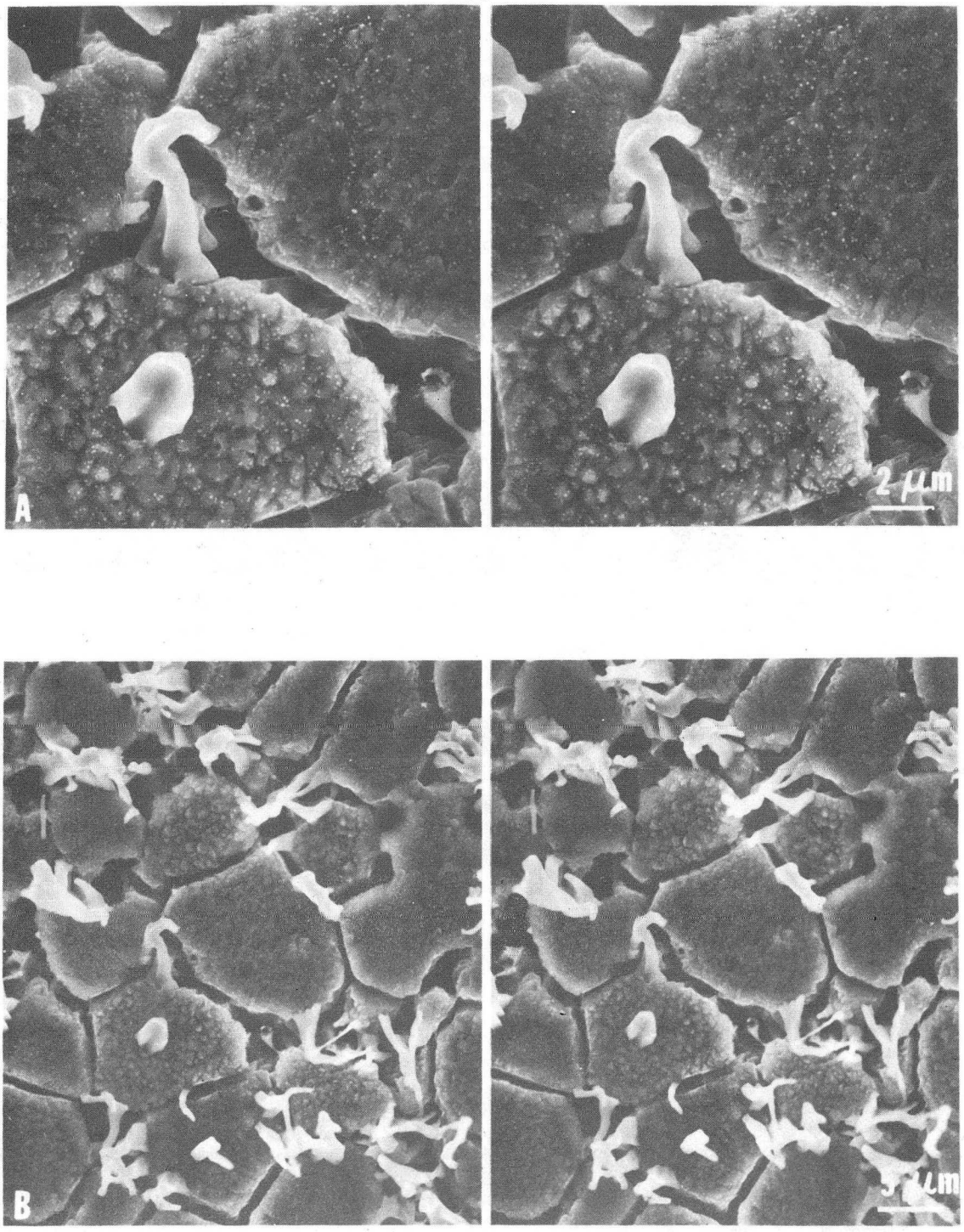

XBB 832-1106A

Figure 12.

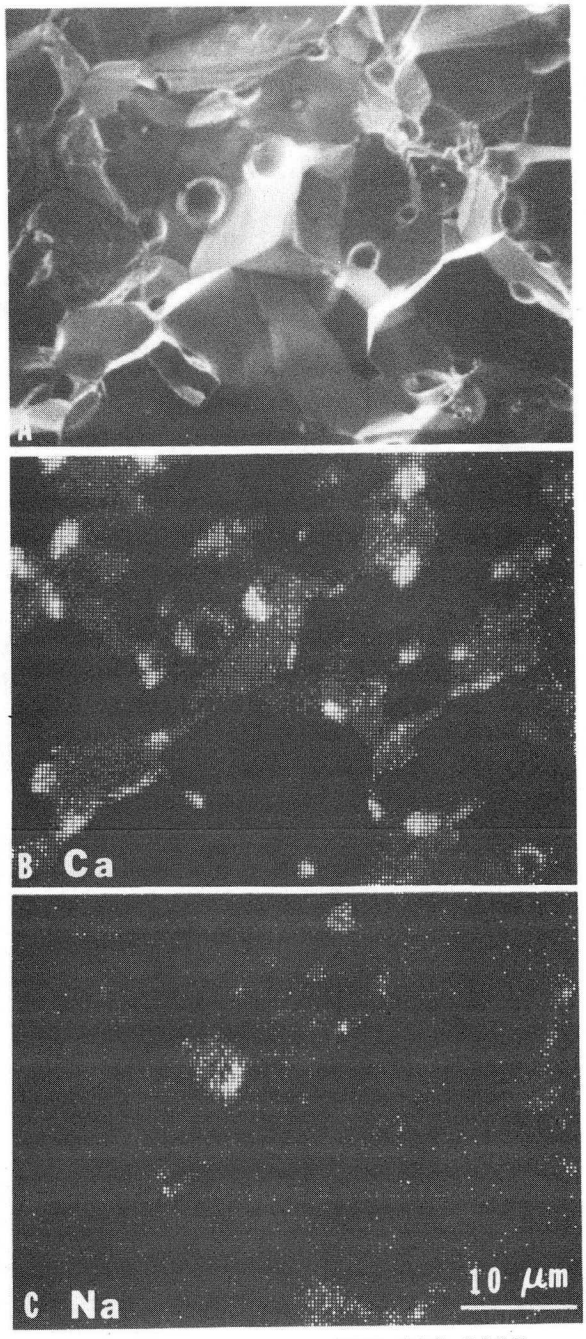

XBB 832-1117

Figure 13.

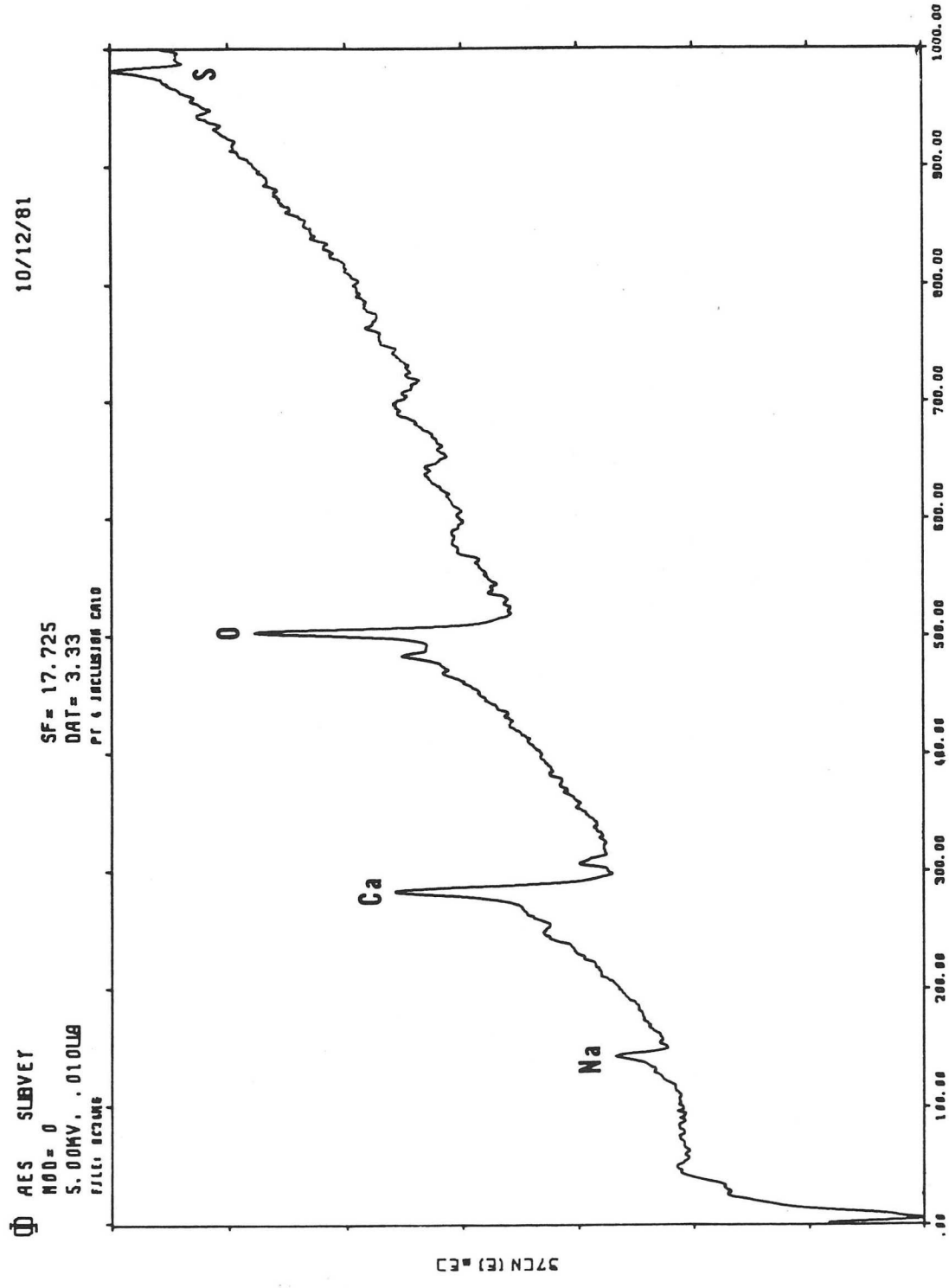

XBL 834-9031

Figure 14.

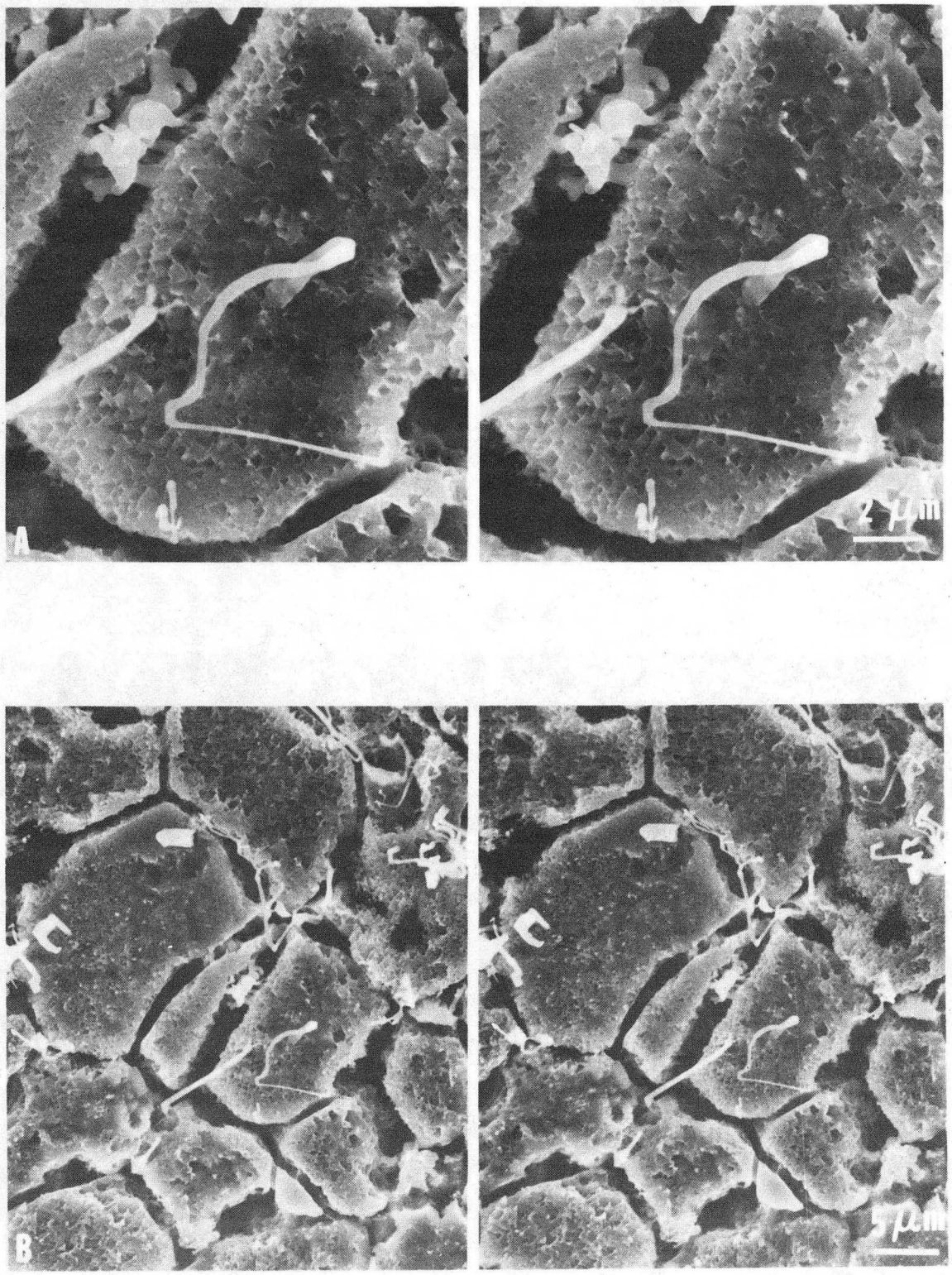

XBB 832-1104A

Figure 15.

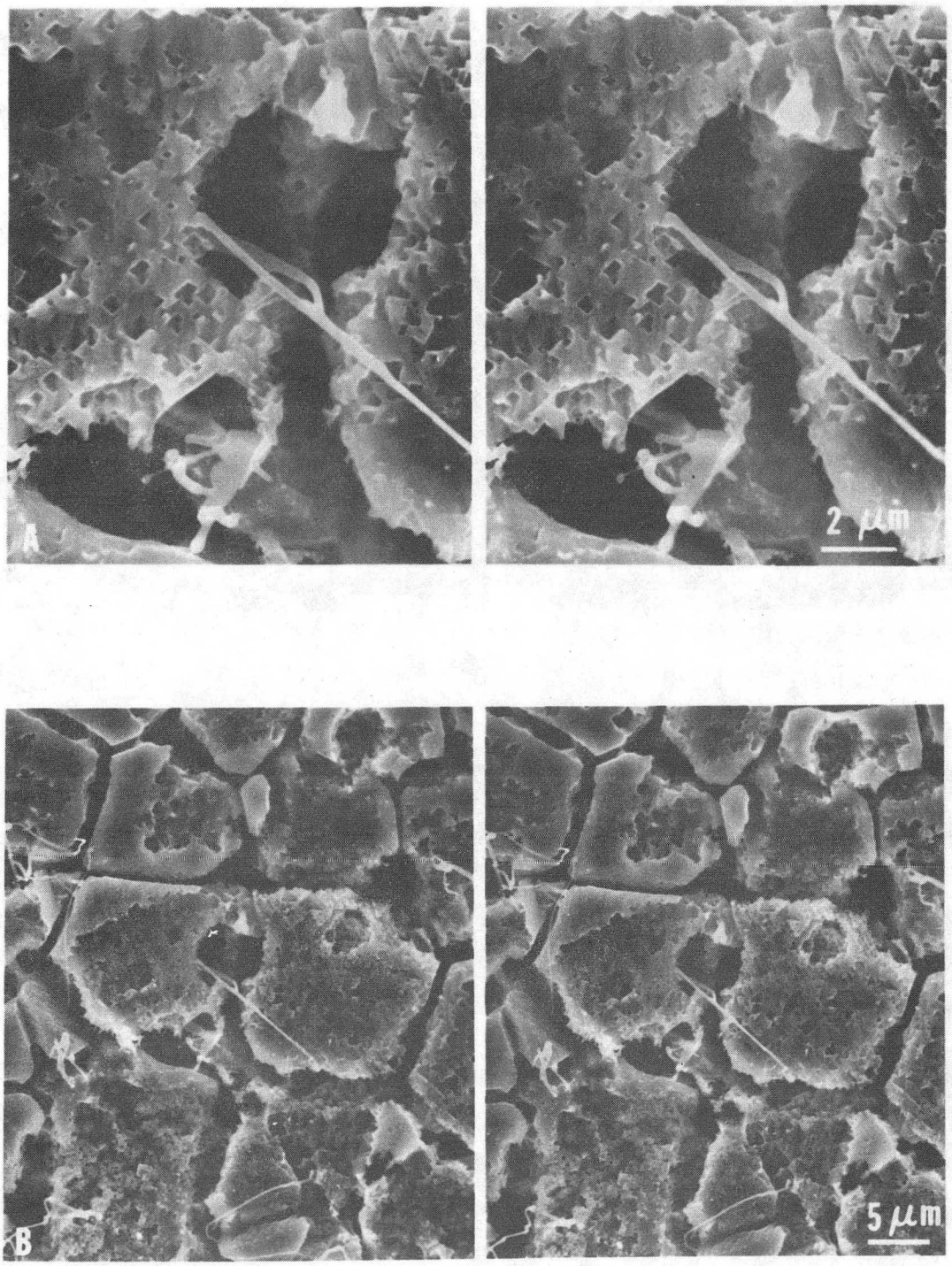

XBB 832-1112A

Figure 16.

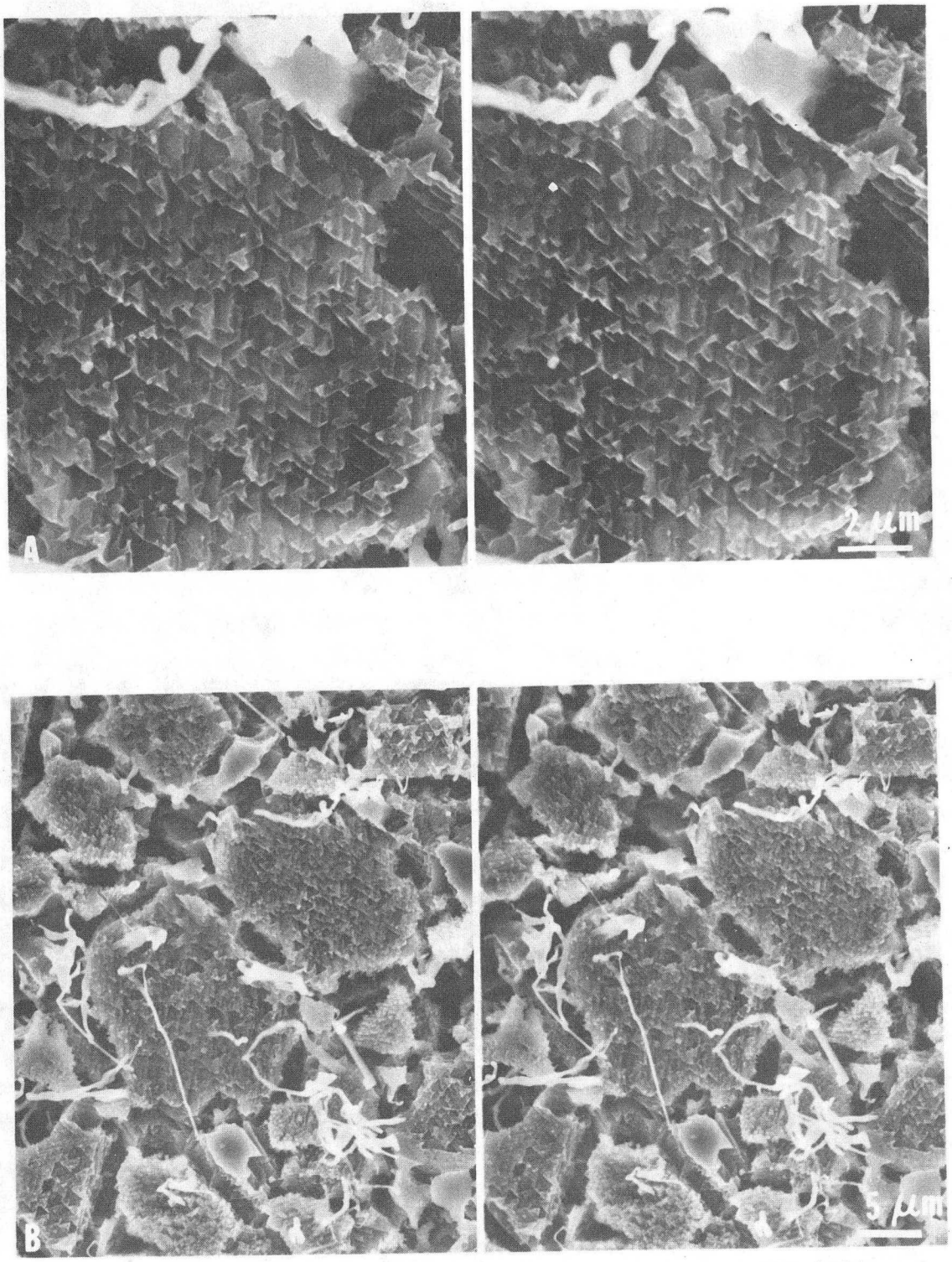

XBB 833-2624

Figure 17.

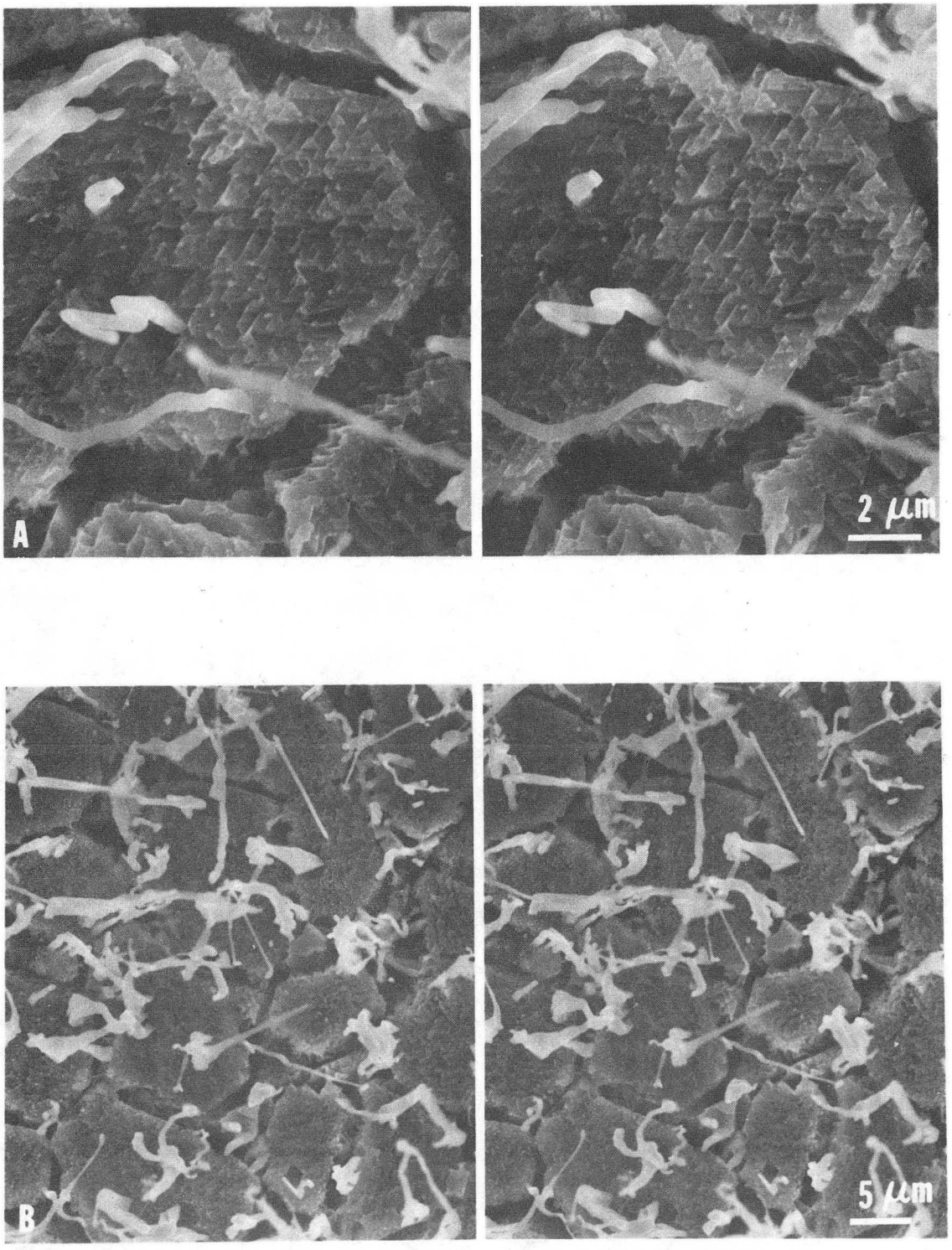

XBB 833-2625

Figure 18.

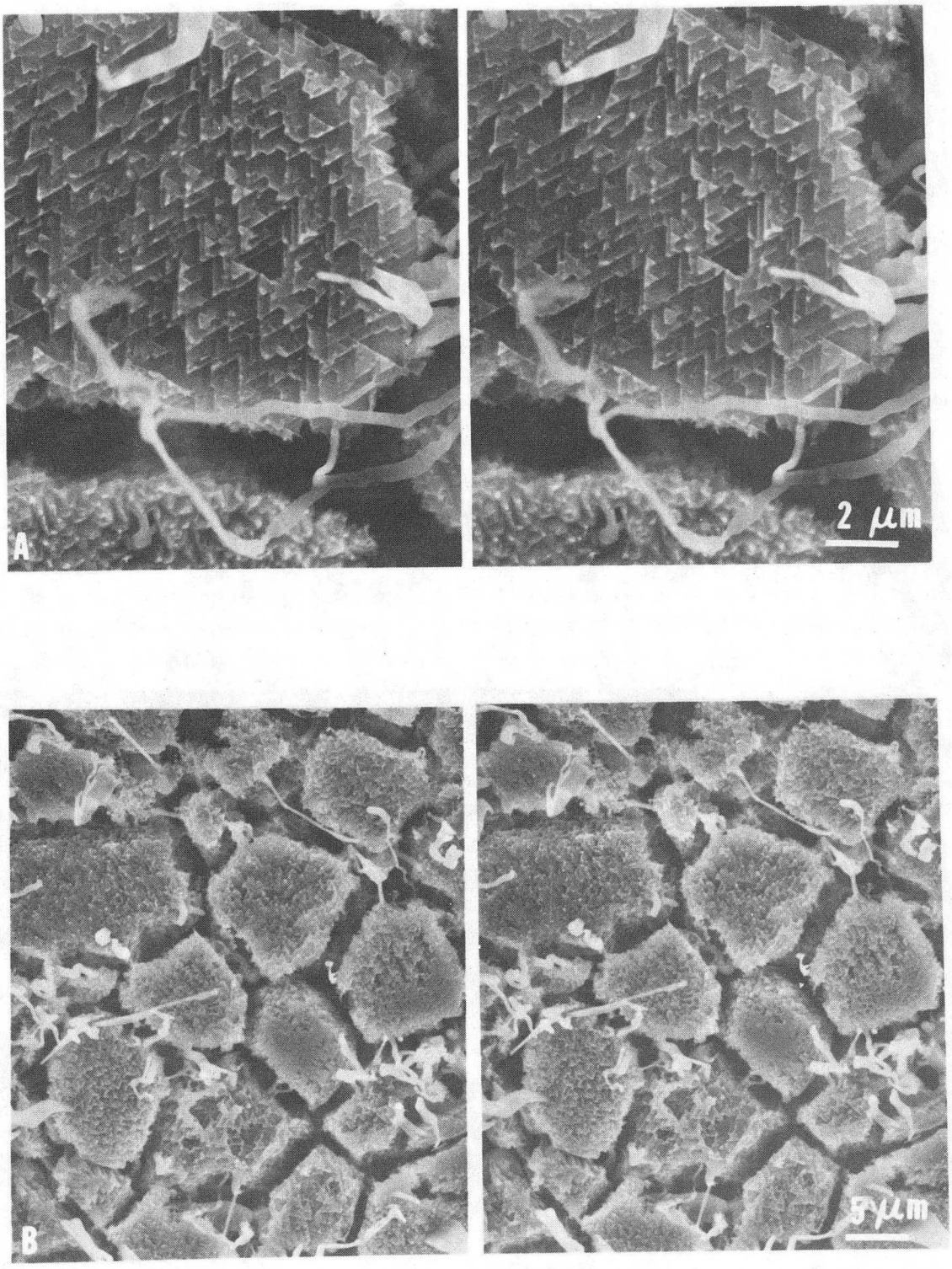

XBB 833-2626

Figure 19.

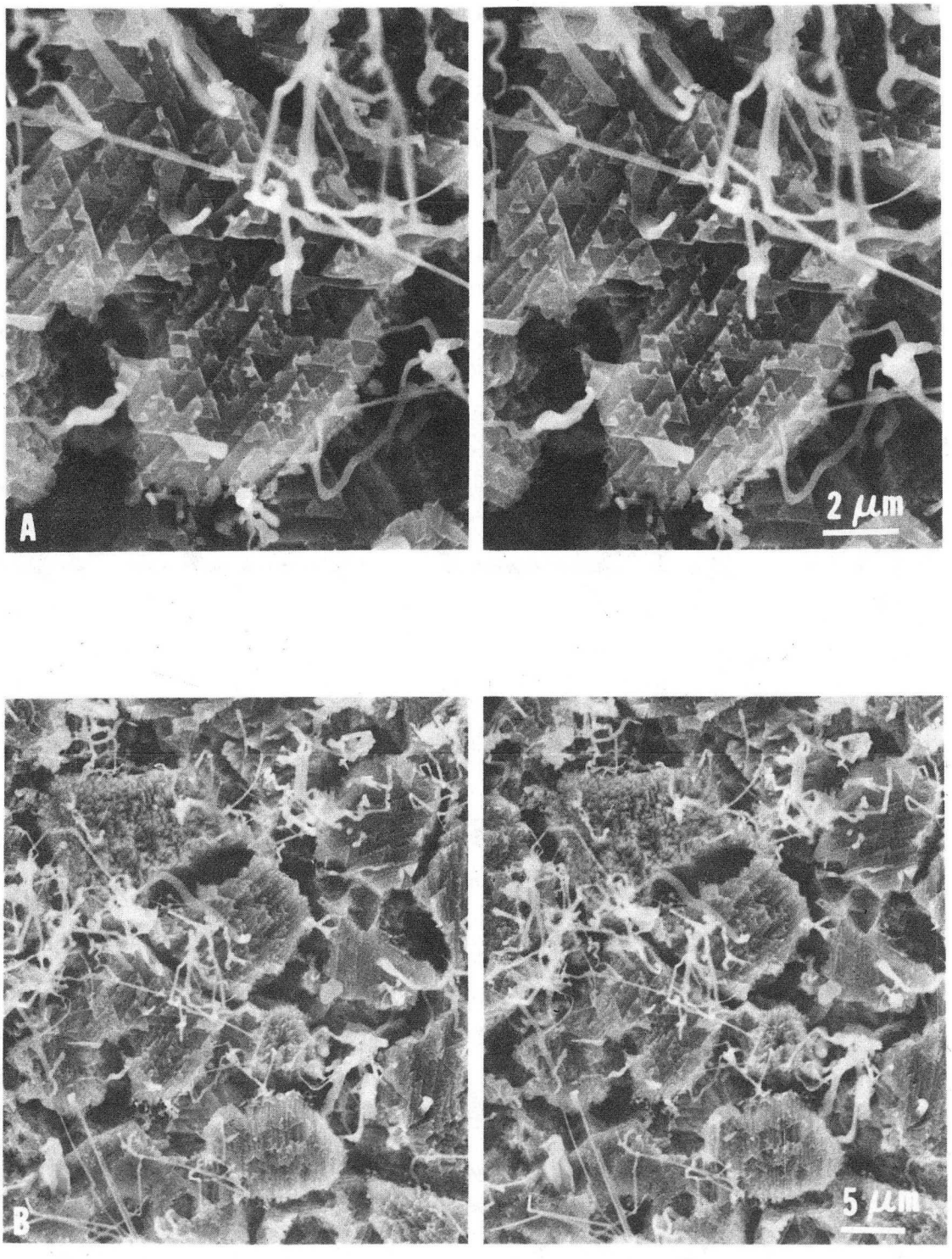

XBB 833-2627

Figure 20.

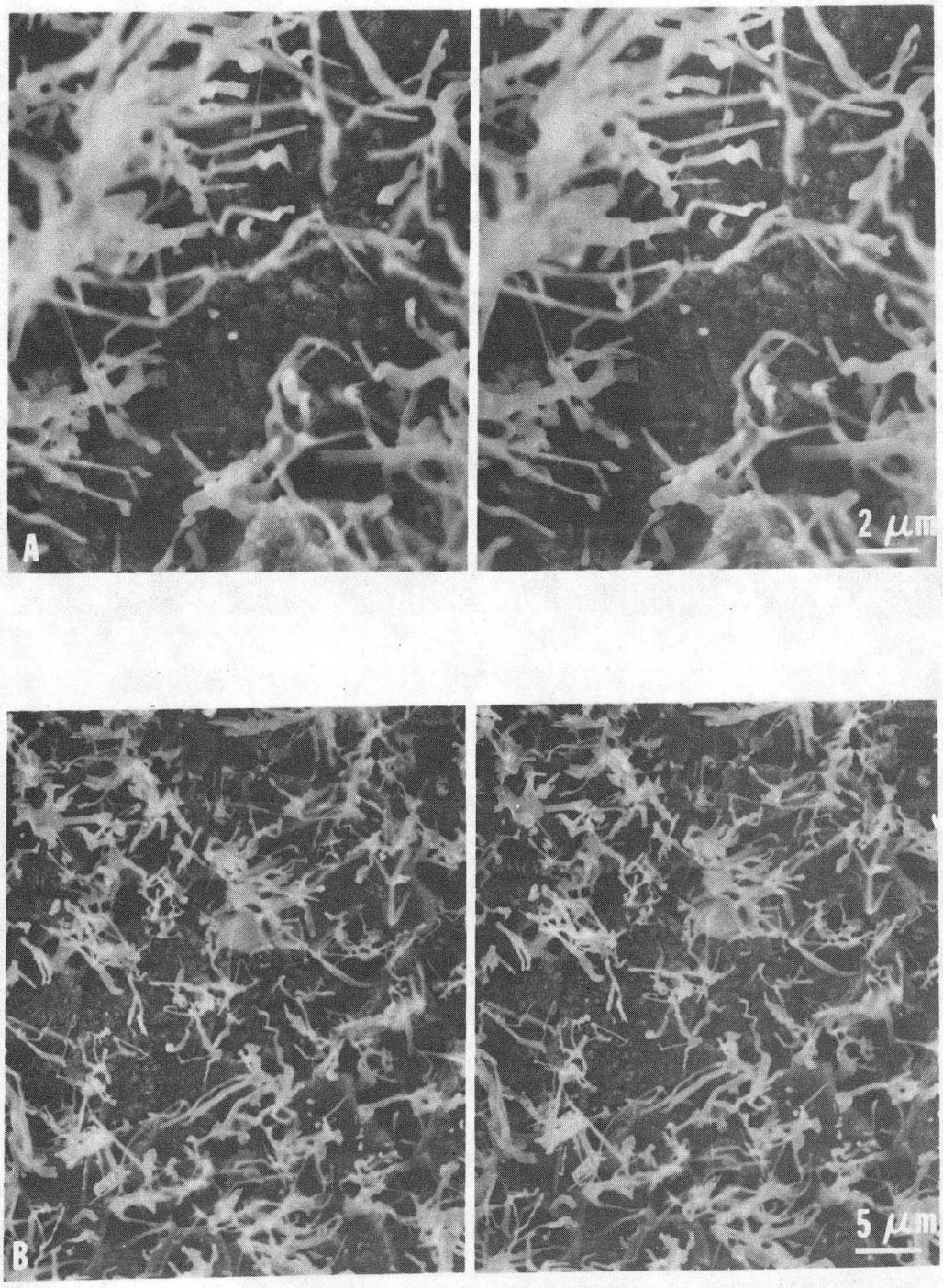

XBB 832-1102A

Figure 21.

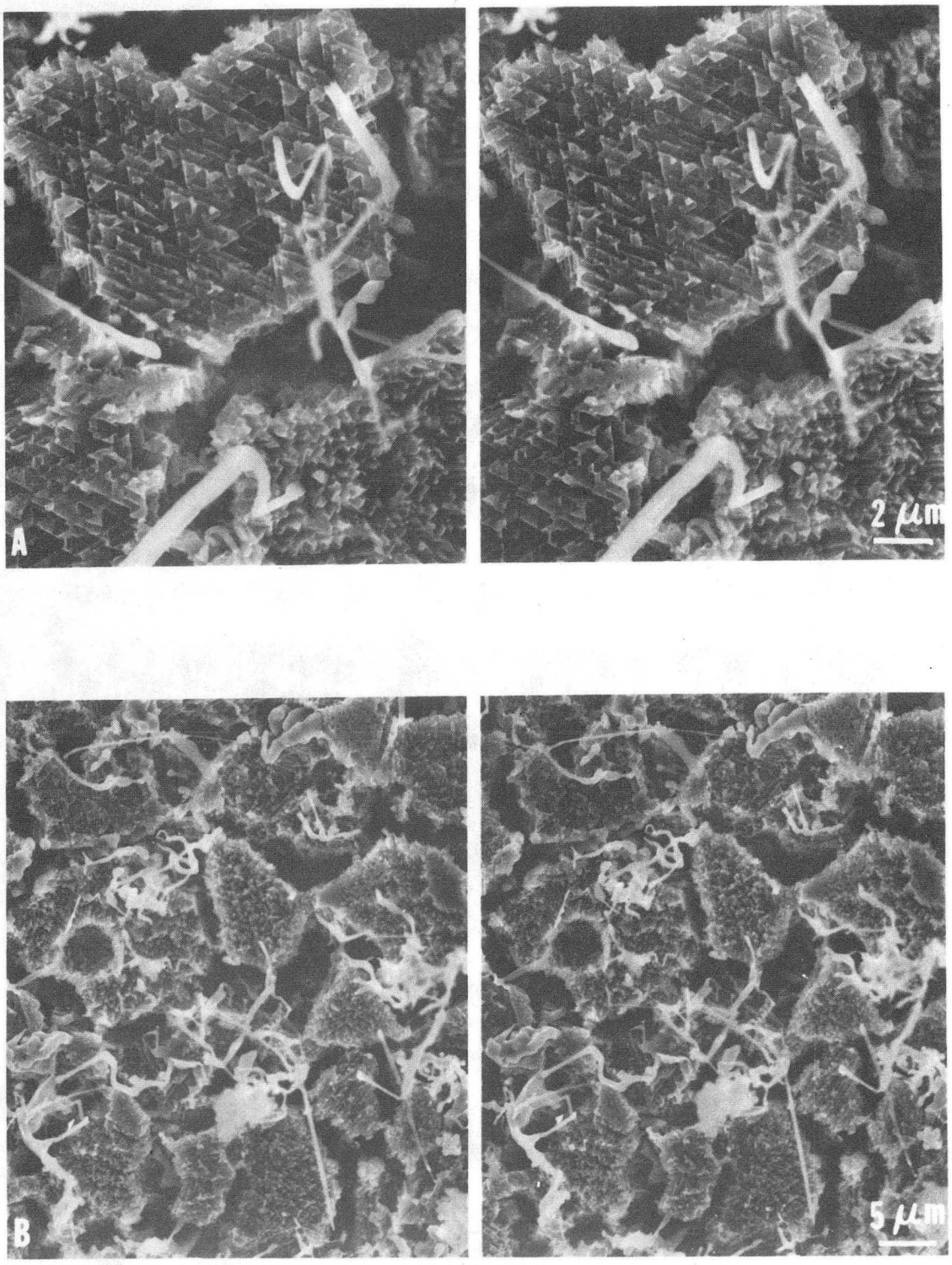

XBB 832-1110A

Figure 22.

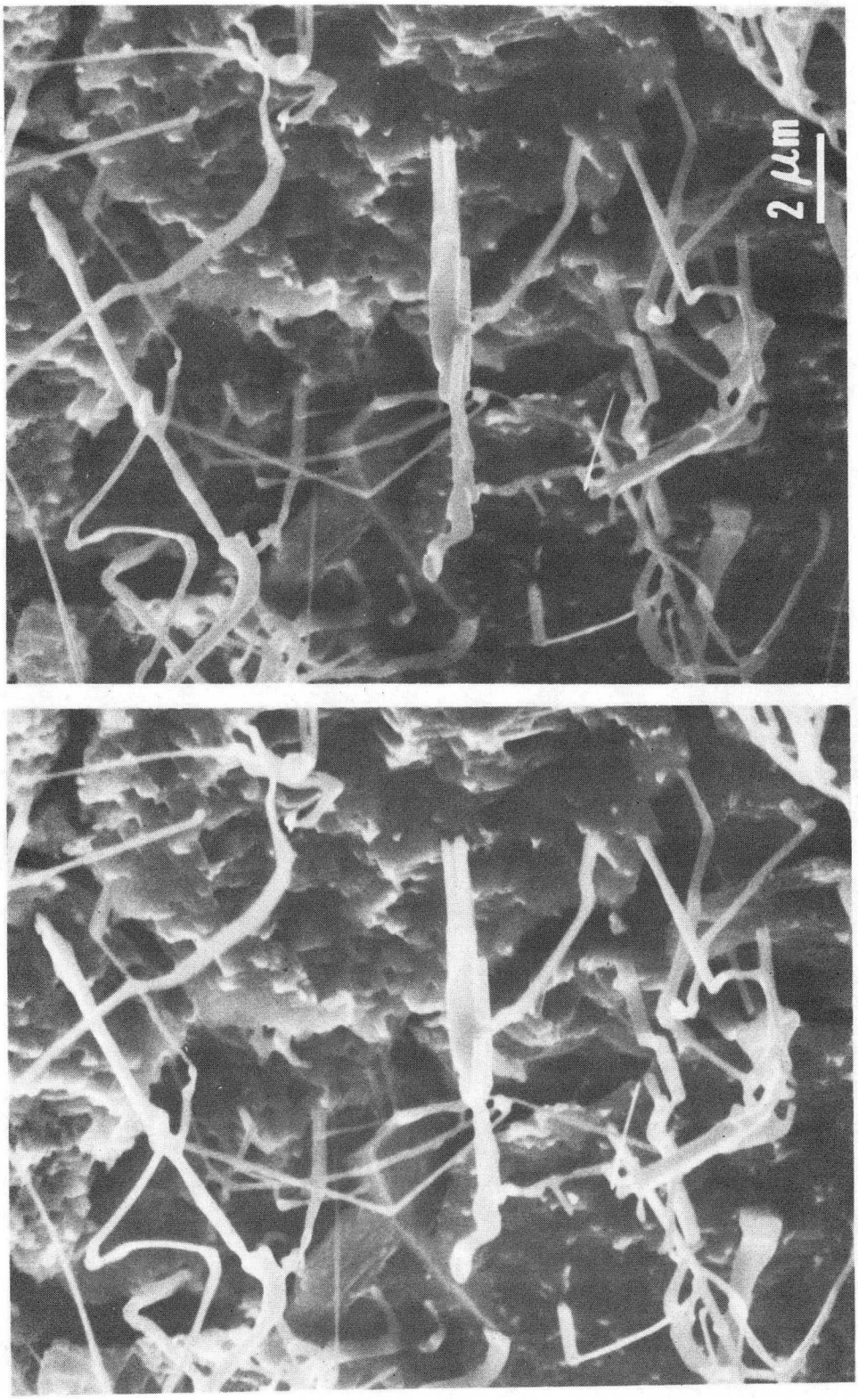

XBB 833-2628

Figure 23.

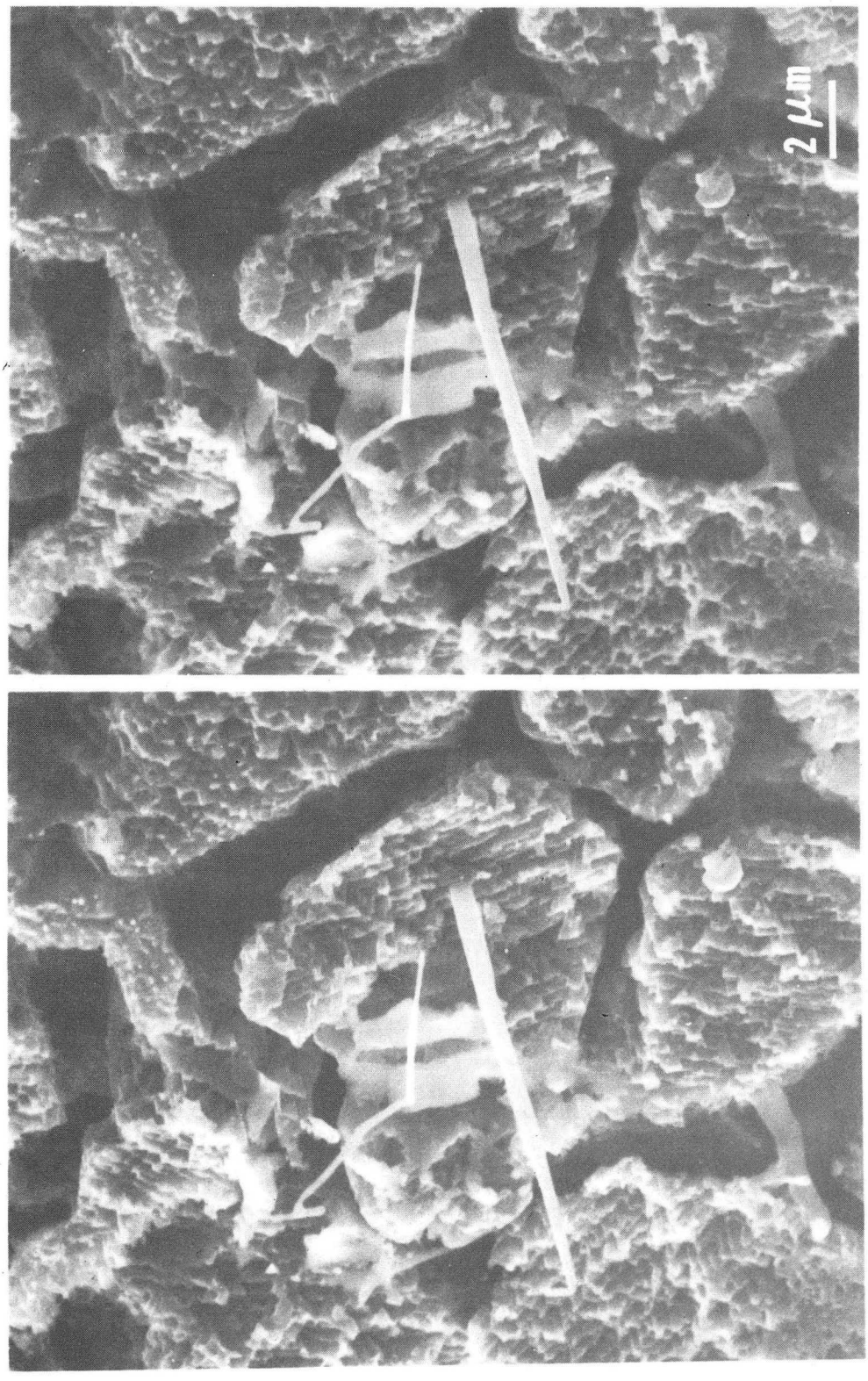

XBB 833-2629

Figure 24.

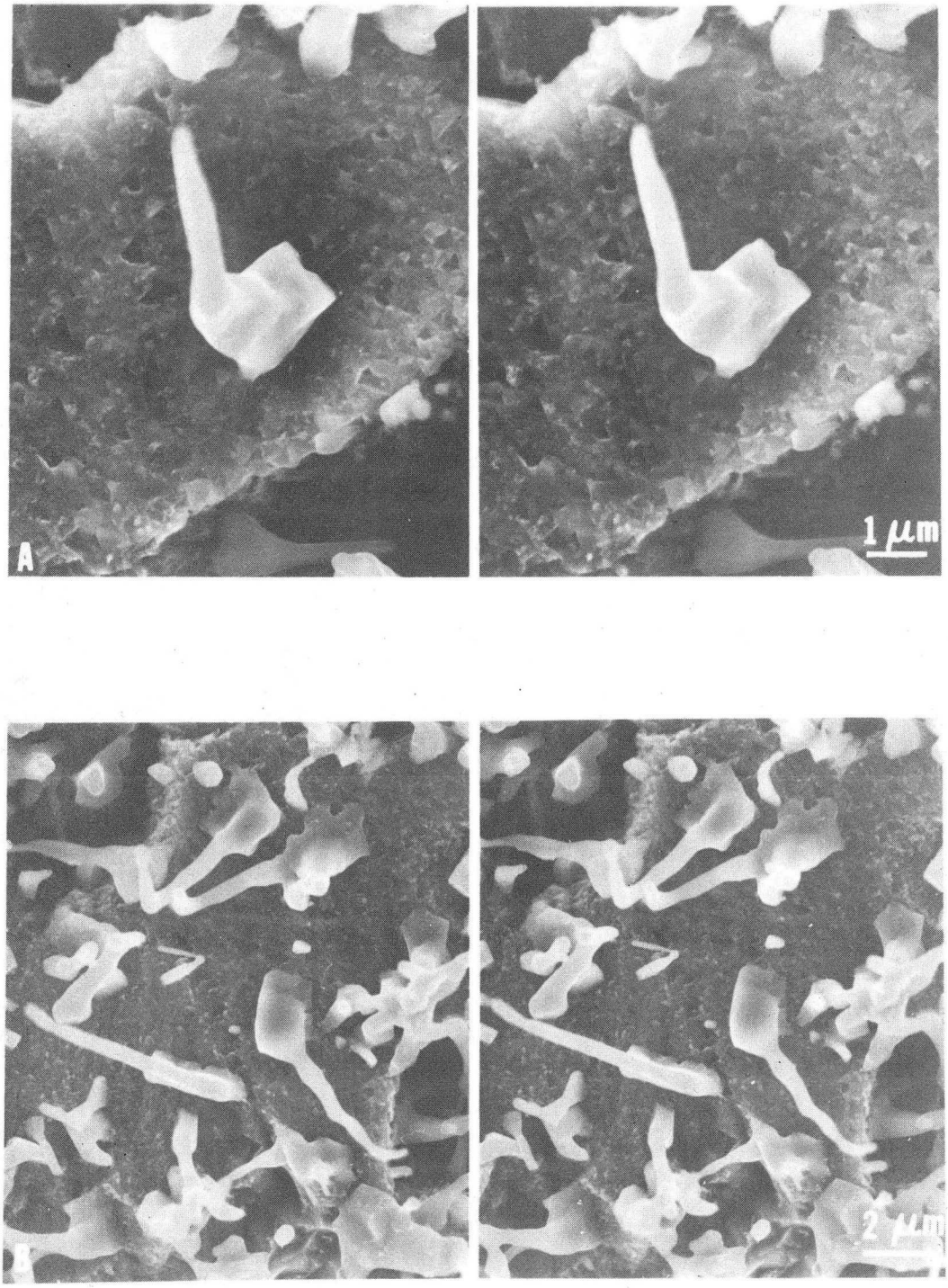

XBB 832-1108A

Figure 25.

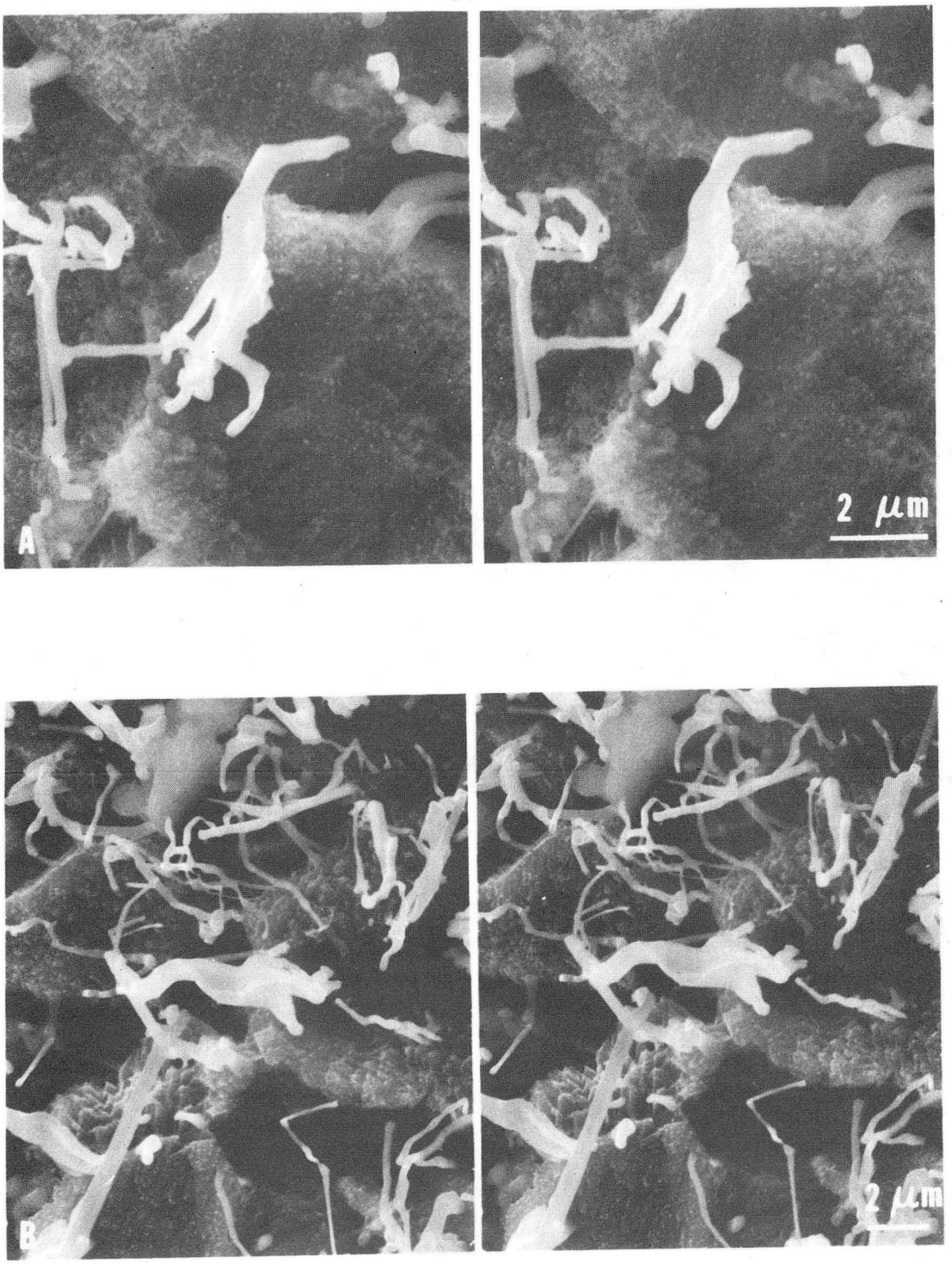

XBB 833-2630

Figure 26.

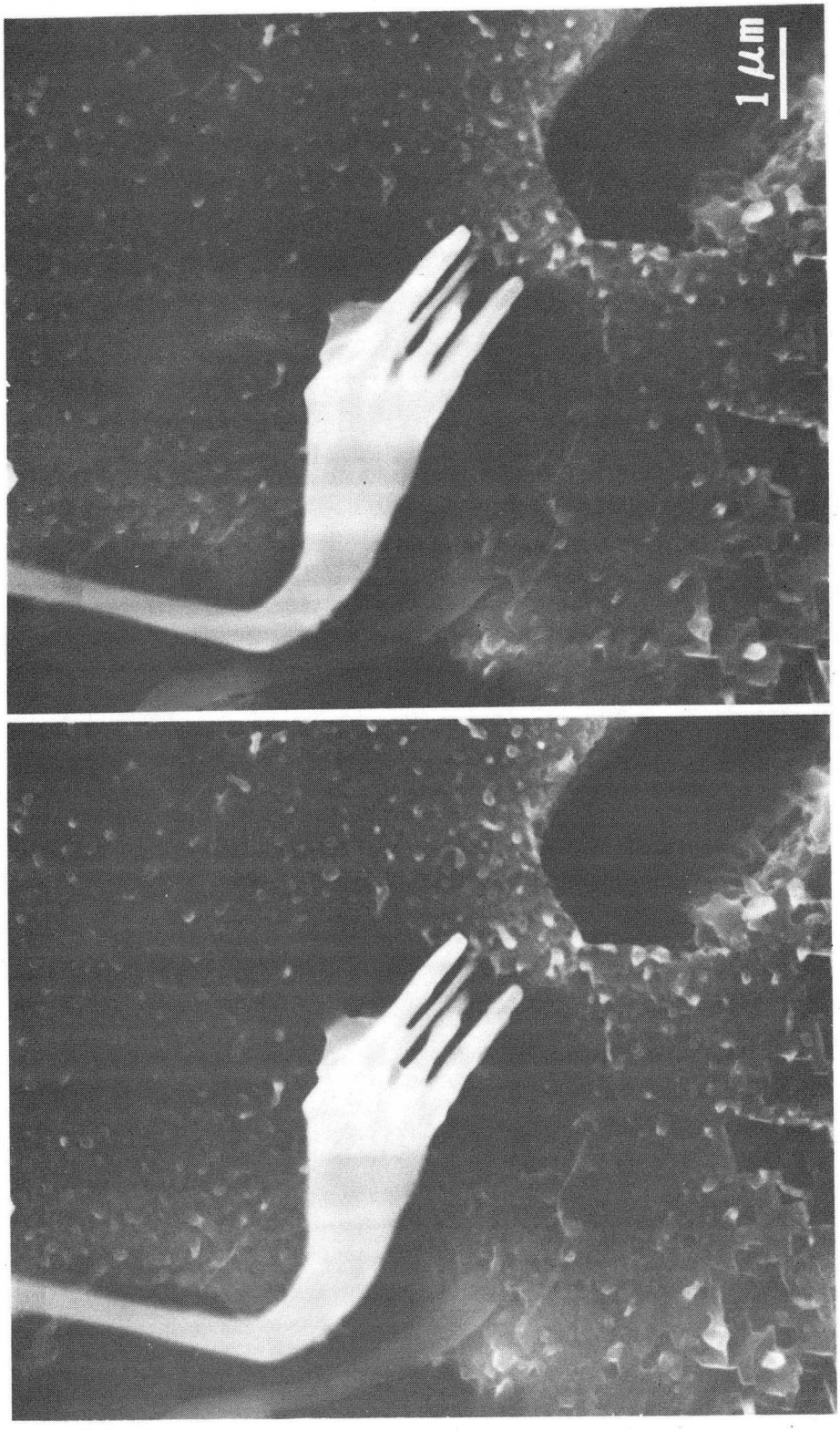

XBB 832-1115

Figure 27.

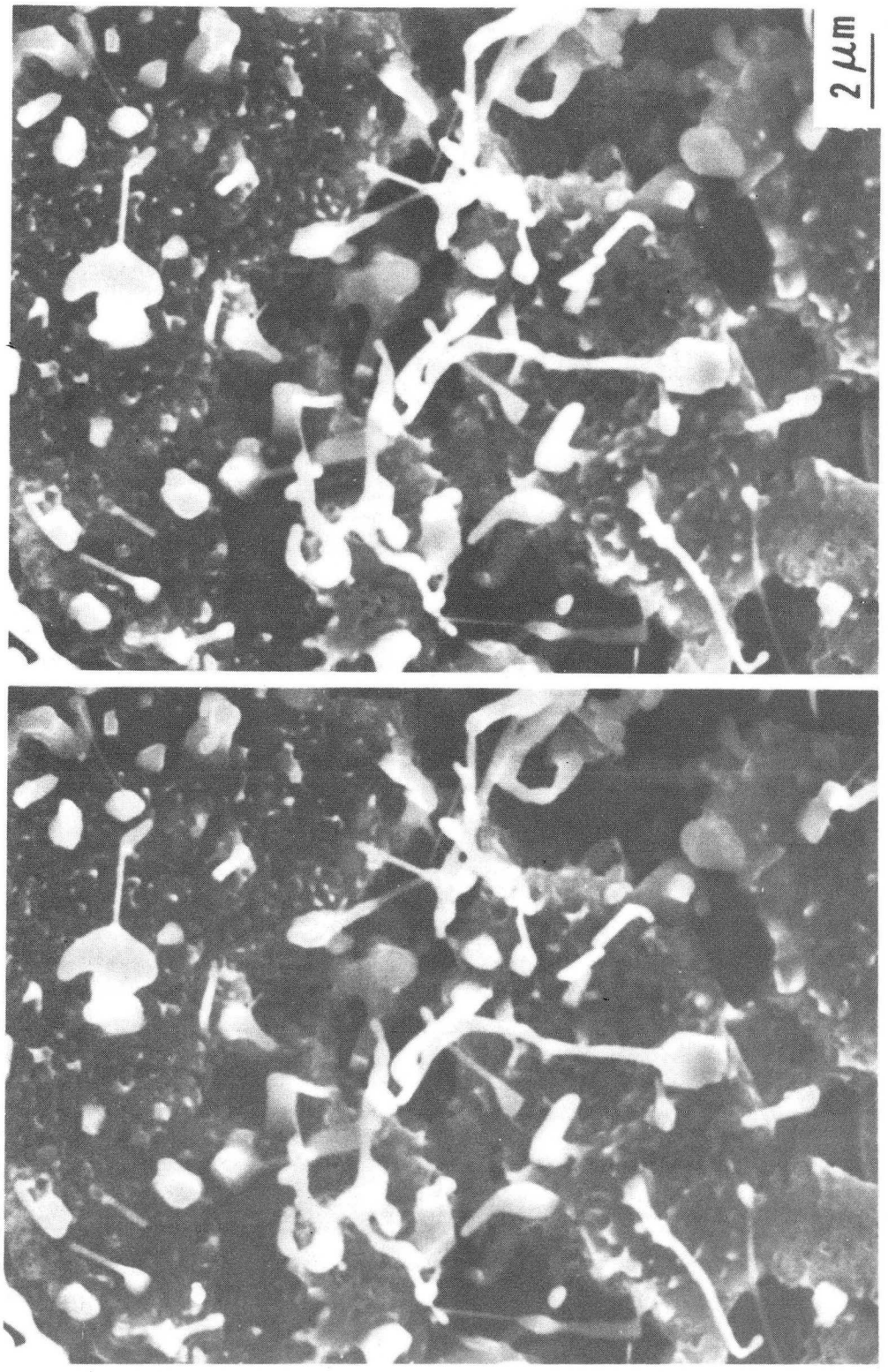

XBB 833-2631

Figure 28.

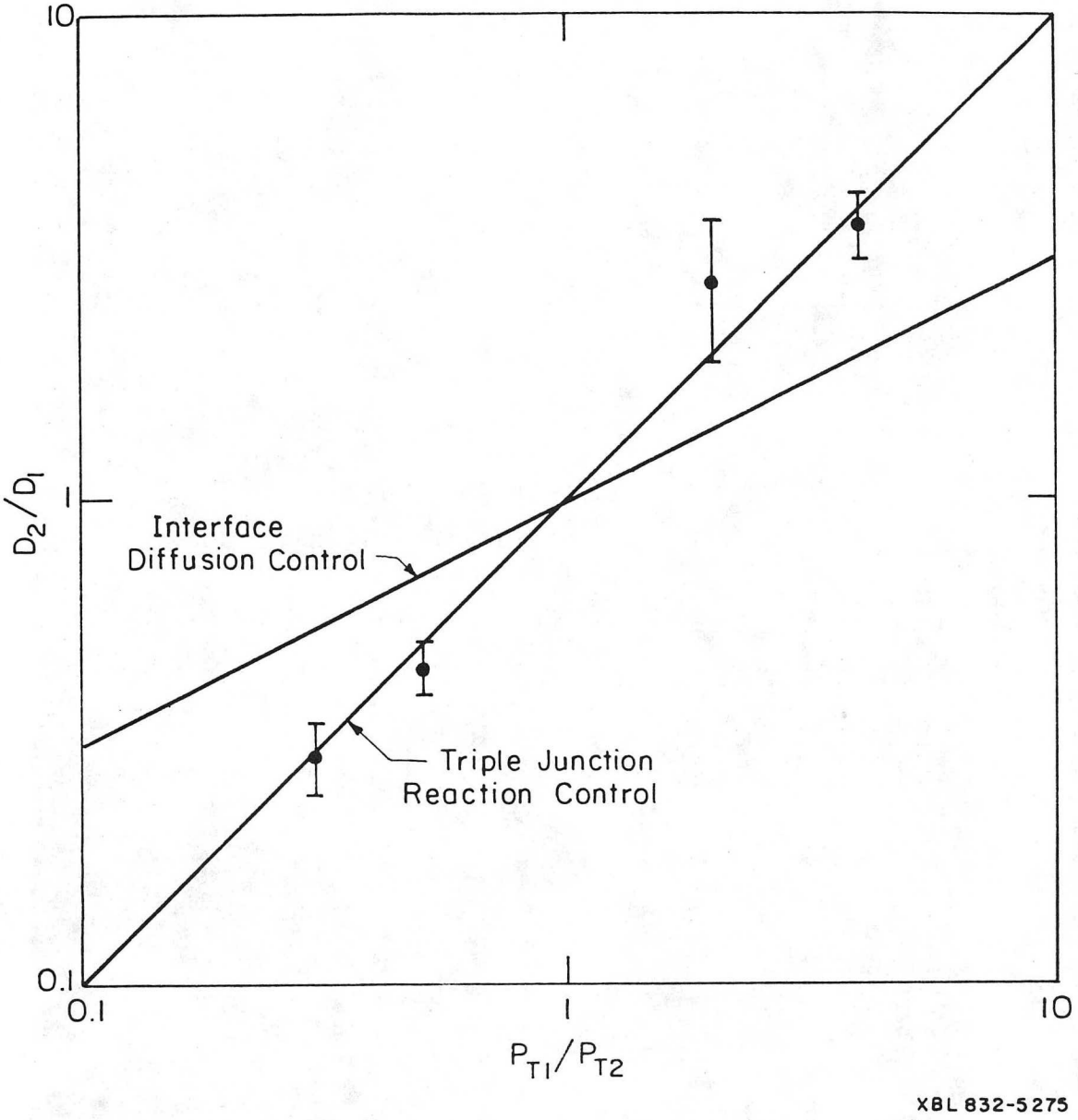
10
1
0.1
0.1
1
10
D_2/D_1
P_{T1}/P_{T2}
Interface
Diffusion Control
Triple Junction
Reaction Control
XBL 832-5275

Figure 29.

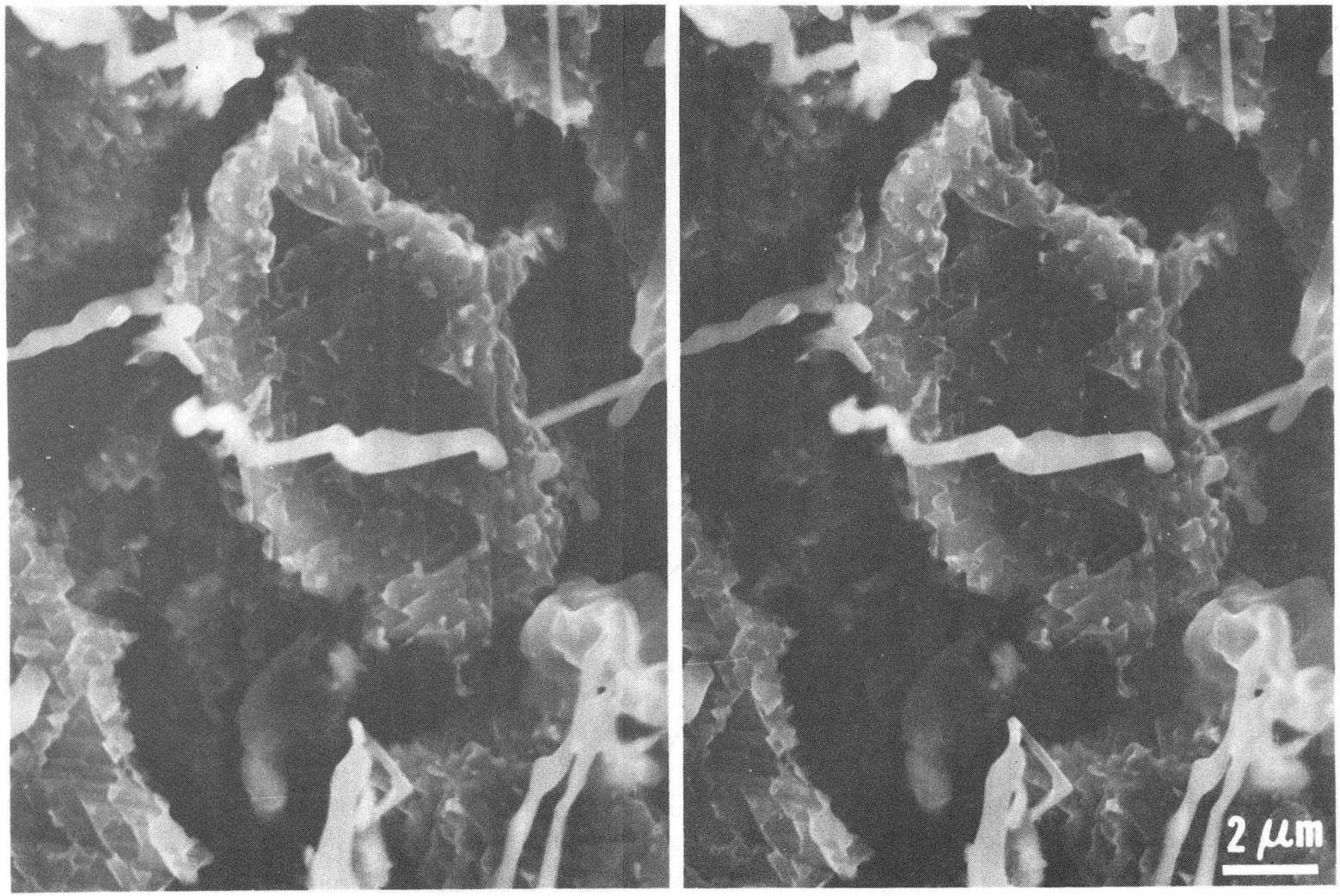

XBB 833-2632

Figure 30.

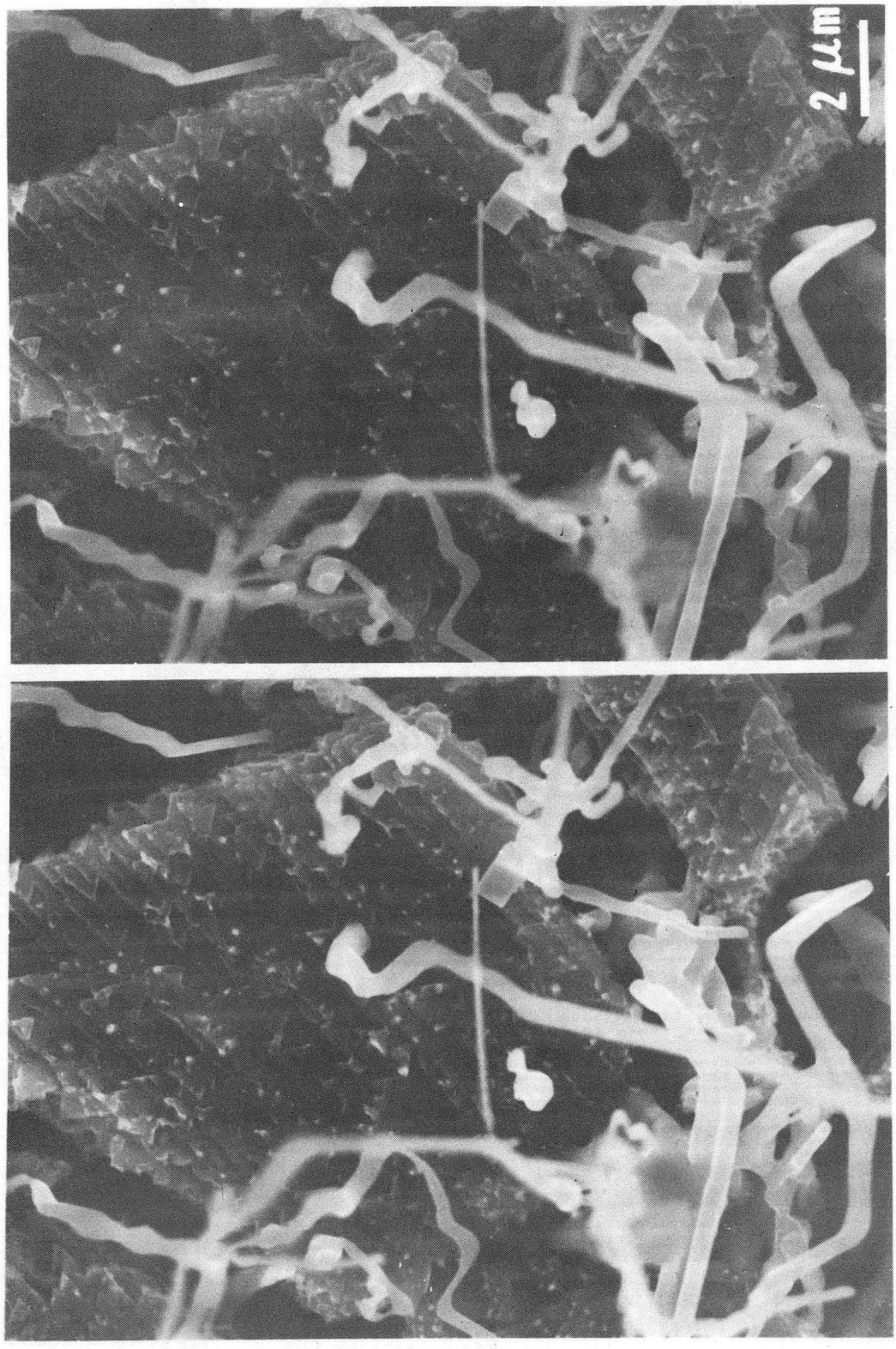

XBB 833-2633

Figure 31.

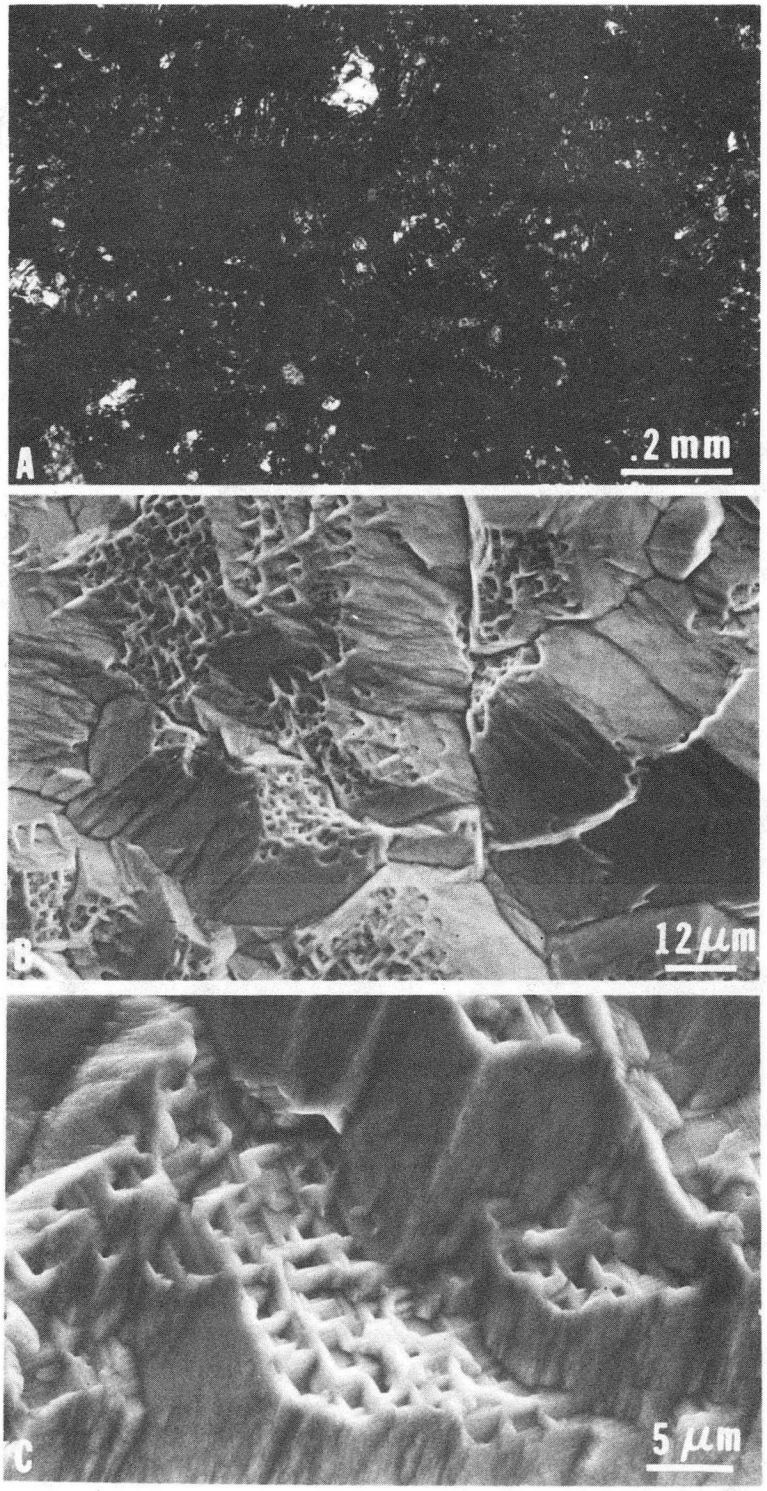

XBB 833-2634

Figure 32.

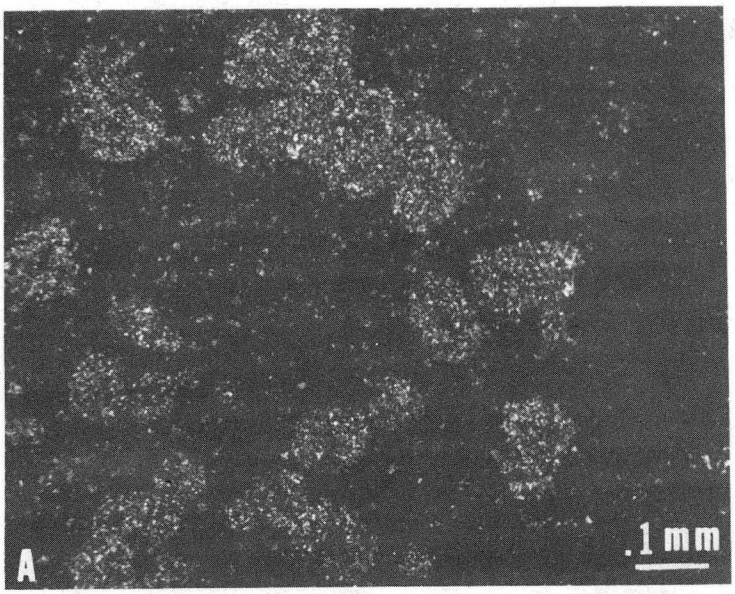

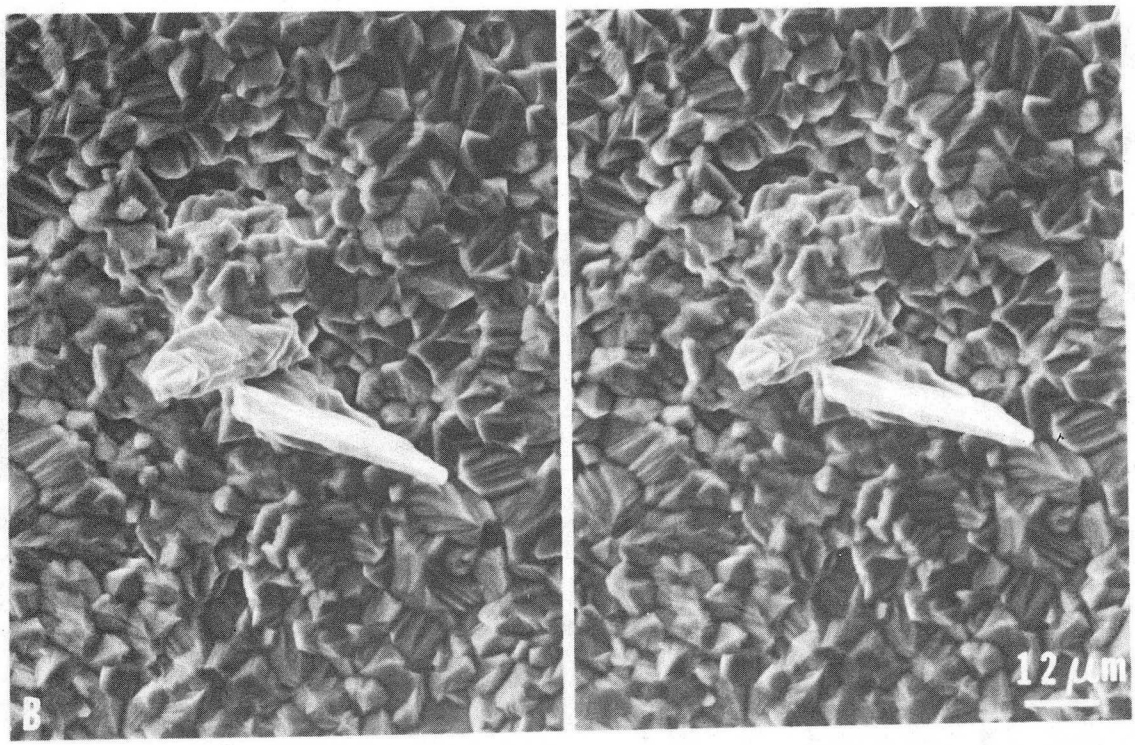

XBB 833-2635

Figure 33.

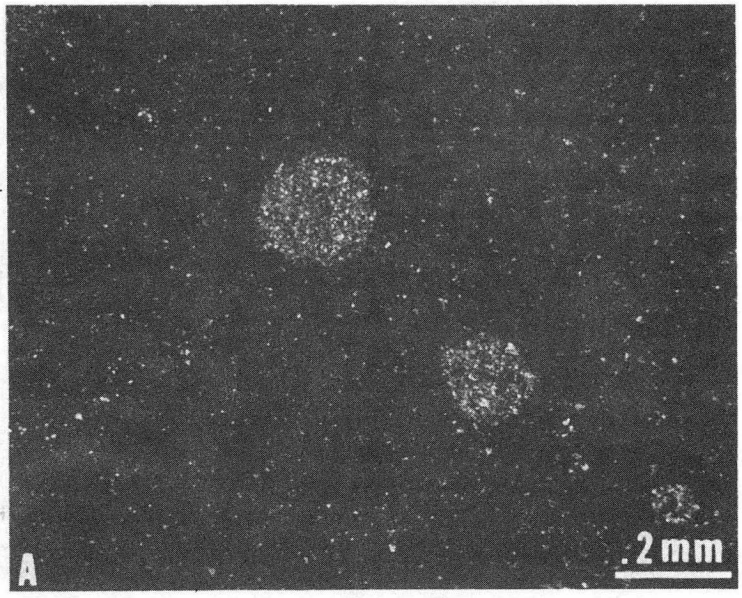

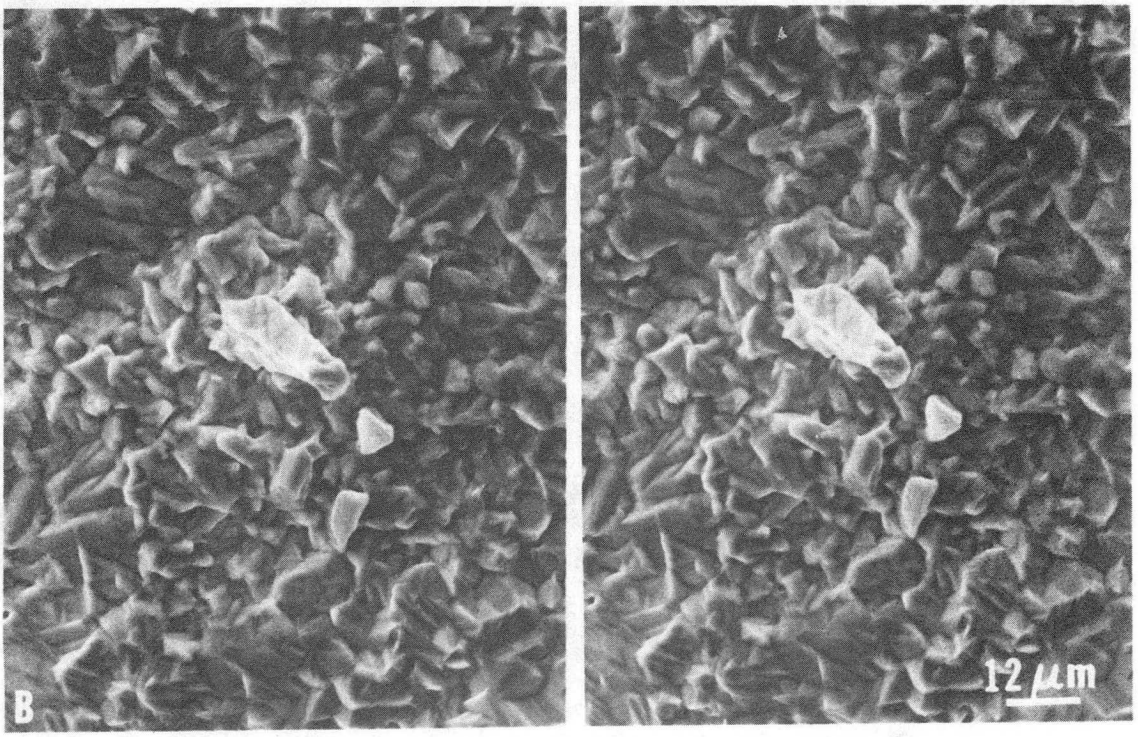

XBB 833-2636

Figure 34.

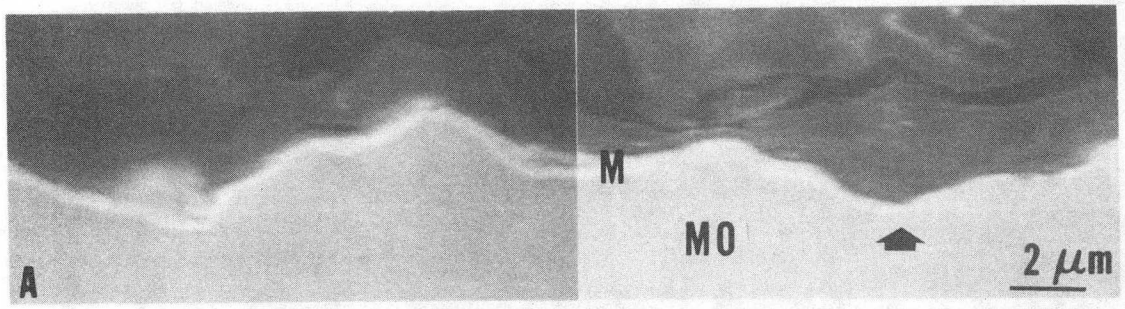

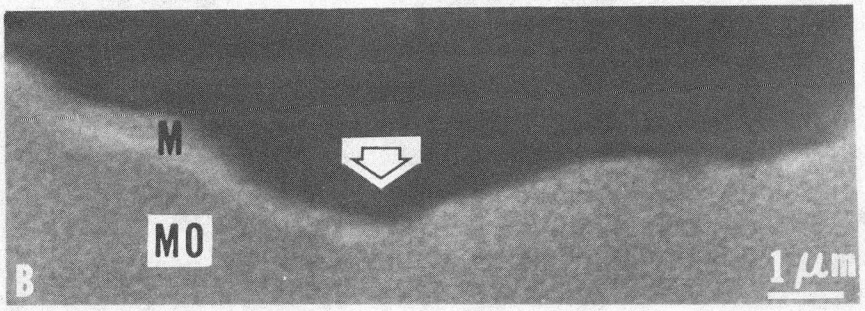

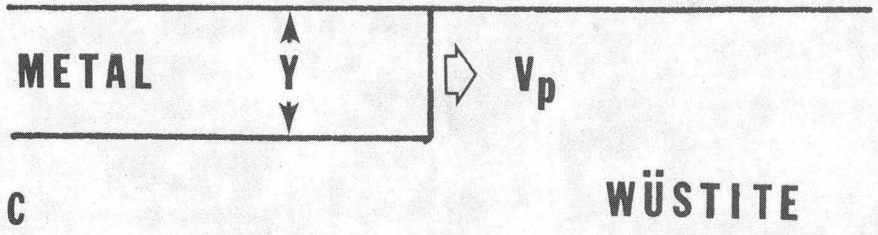

XBB 832-1366

Figure 35.

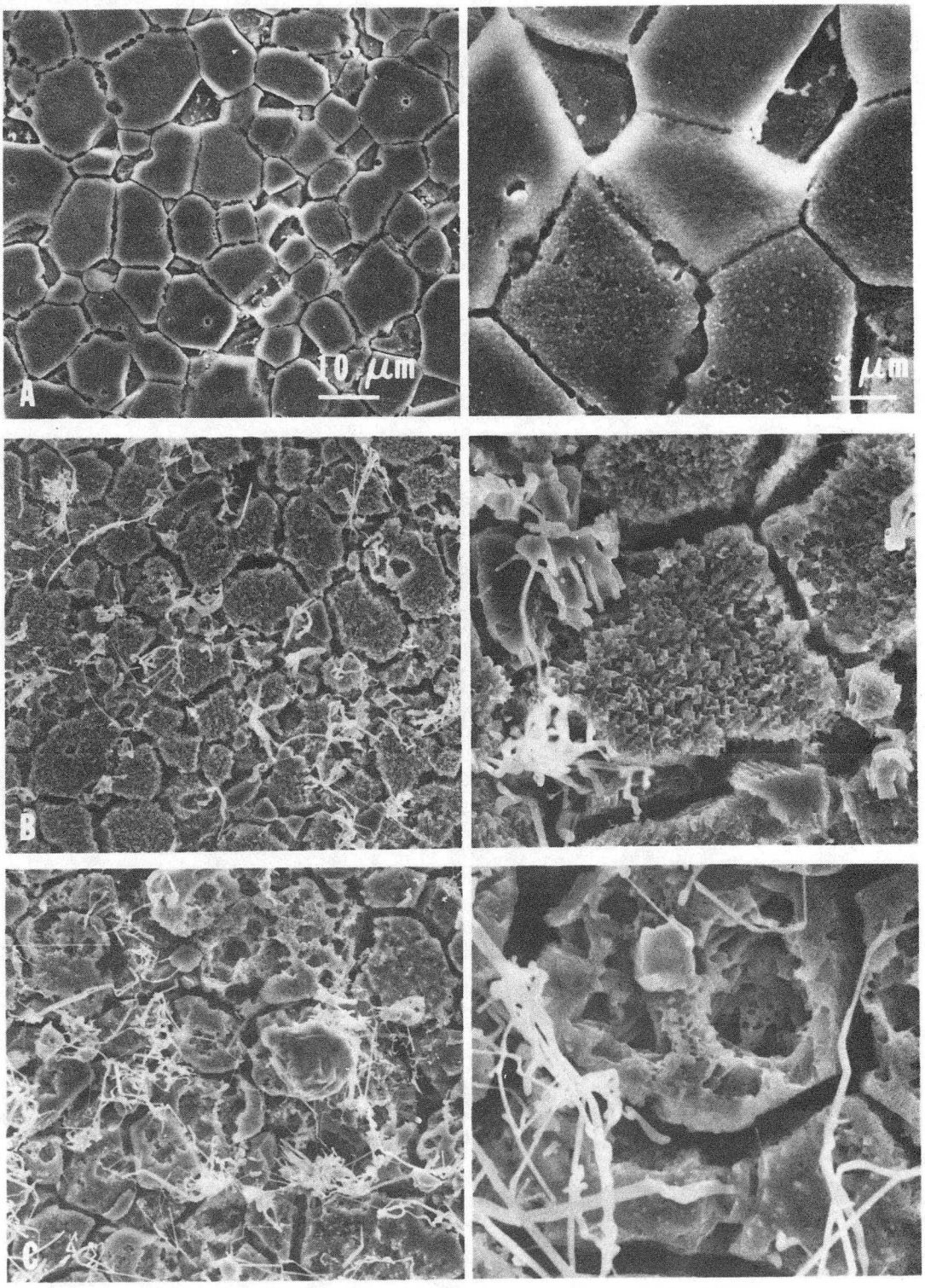

XBB 833-2637

Figure 36.

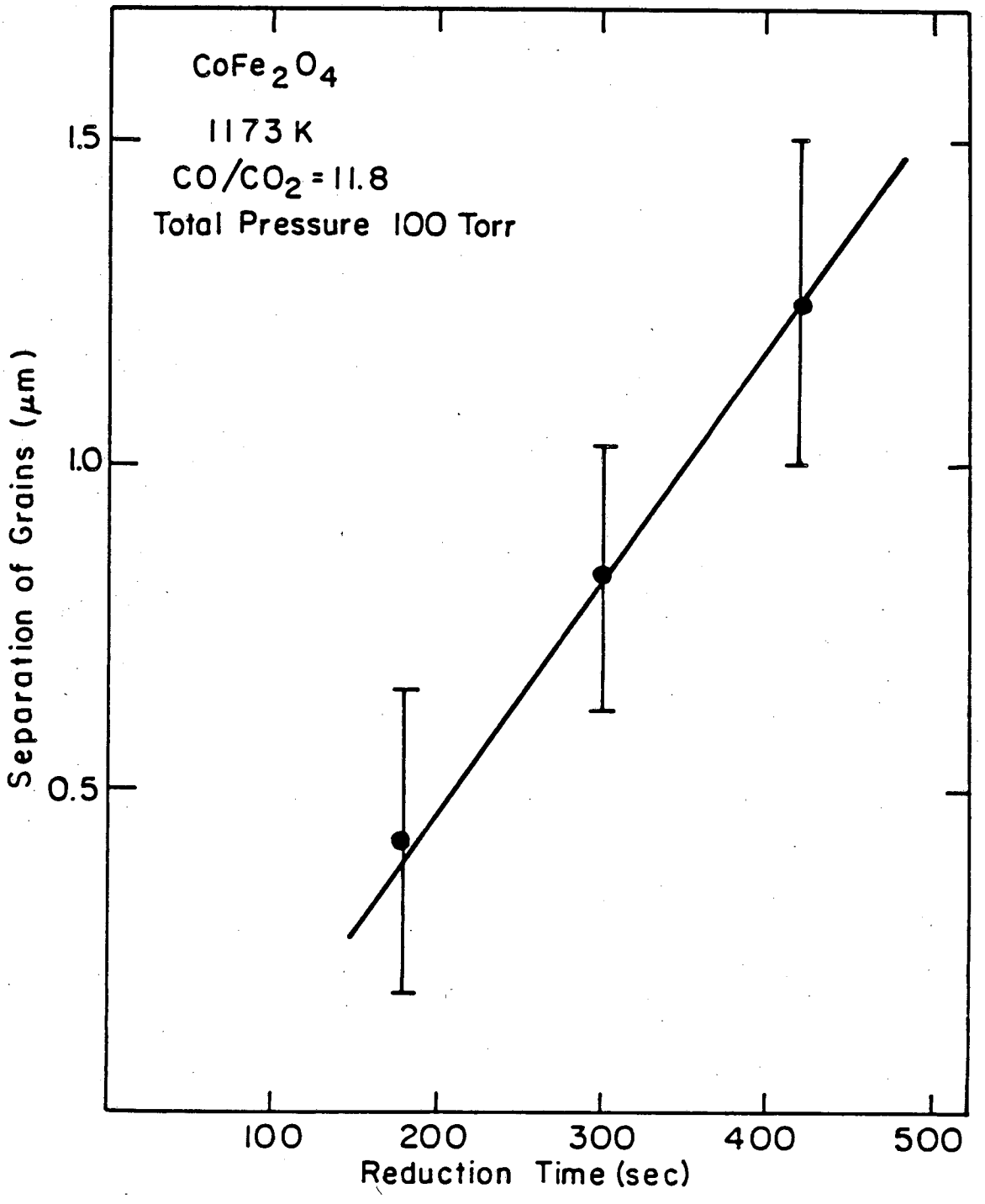
$CoFe_2O_4$
1173 K
$CO/CO_2 = 11.8$
Total Pressure 100 Torr
Separation of Grains (μm)
0.5
1.0
1.5
100
200
300
400
500
Reduction Time (sec)
XBL 832-5277

Figure 37.

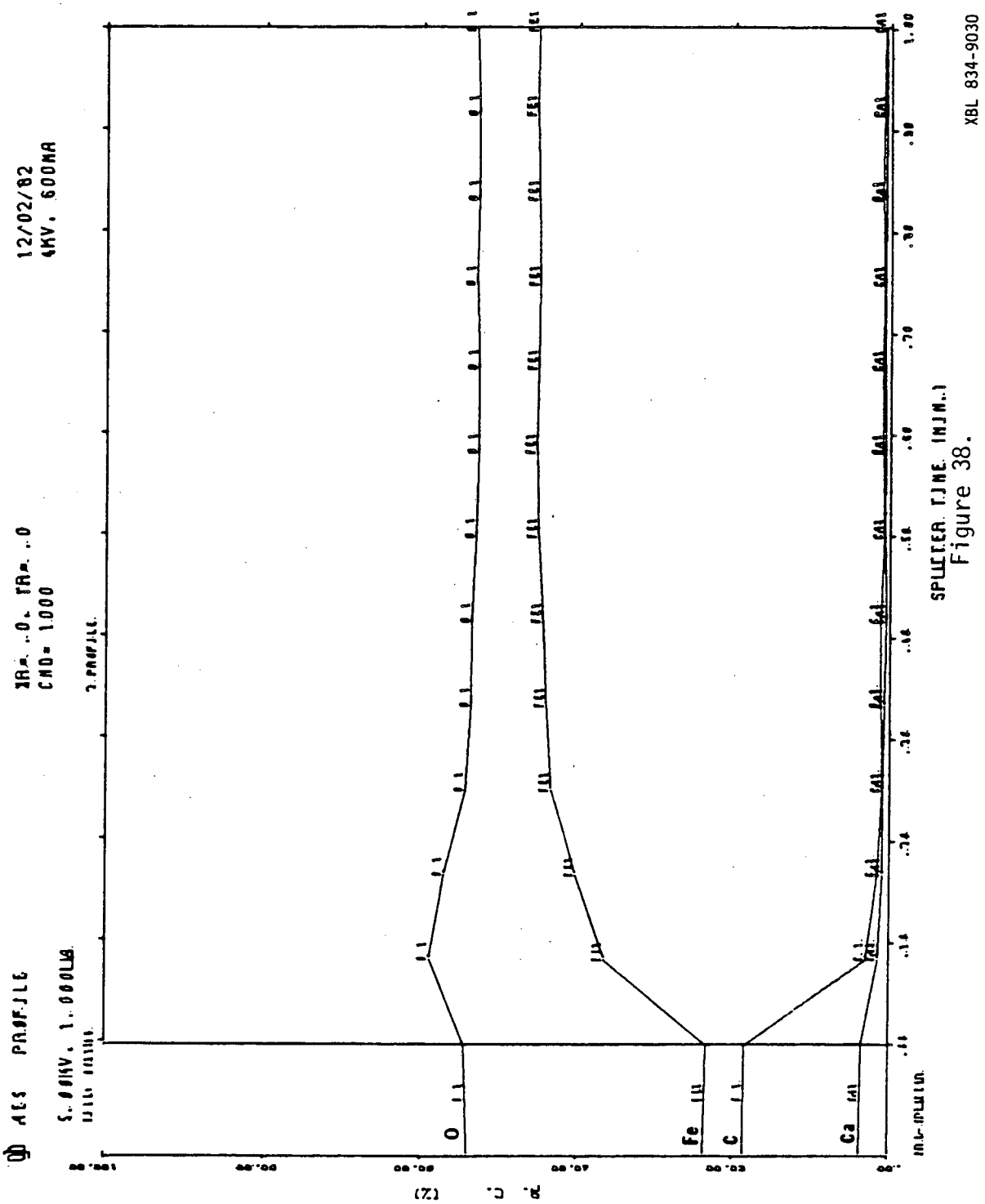
AES PROFILE
12/02/82
4KV, 600NA
CMD= 1.000
O
Fe
C
Ca
SPUTTER TIME (MIN.)
XBL 834-9030

Figure 38.

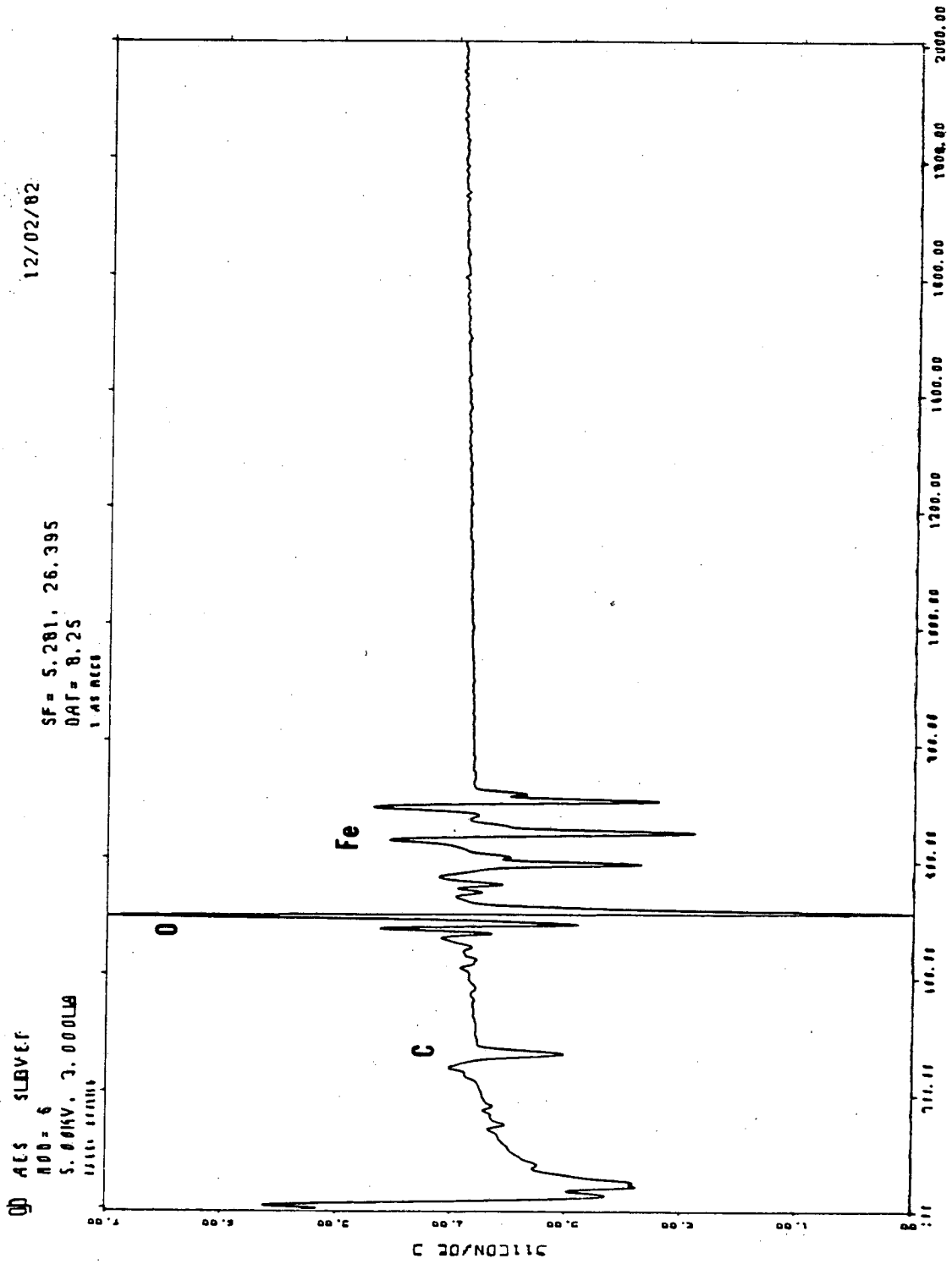

XBL 834-9029

Figure 39.

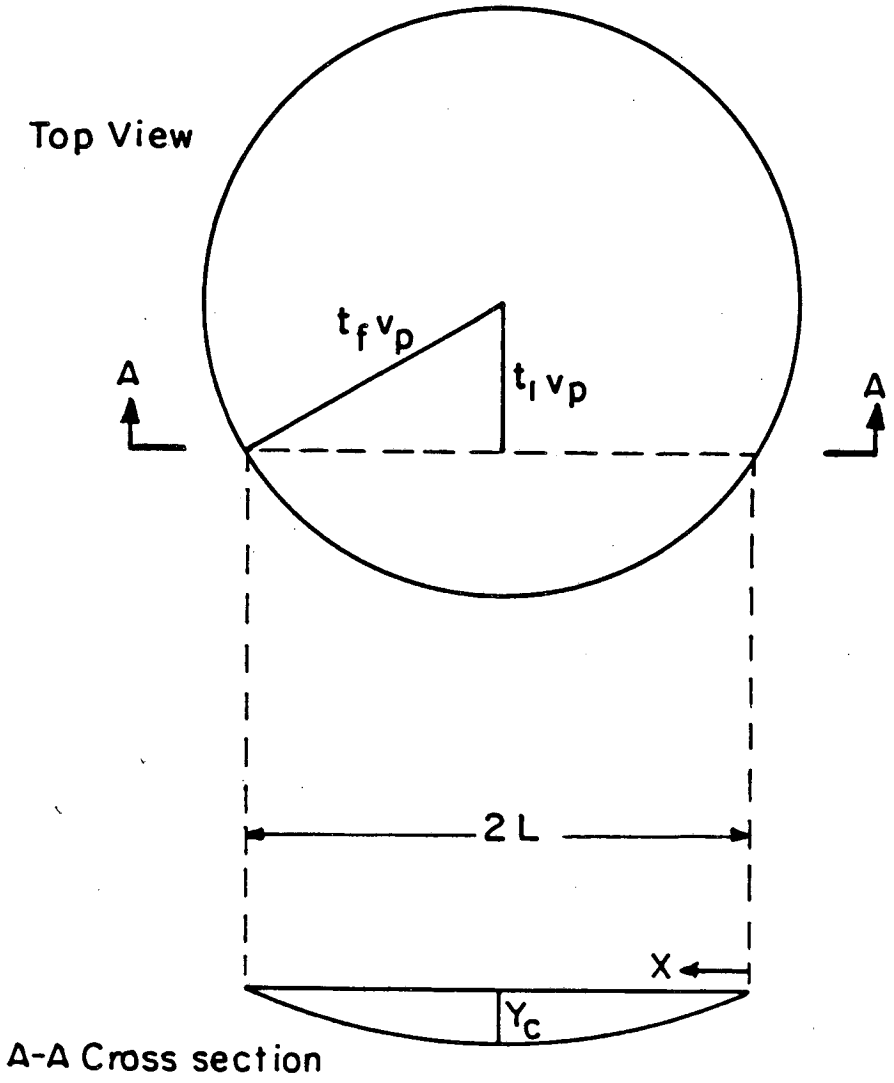

Figure 40.

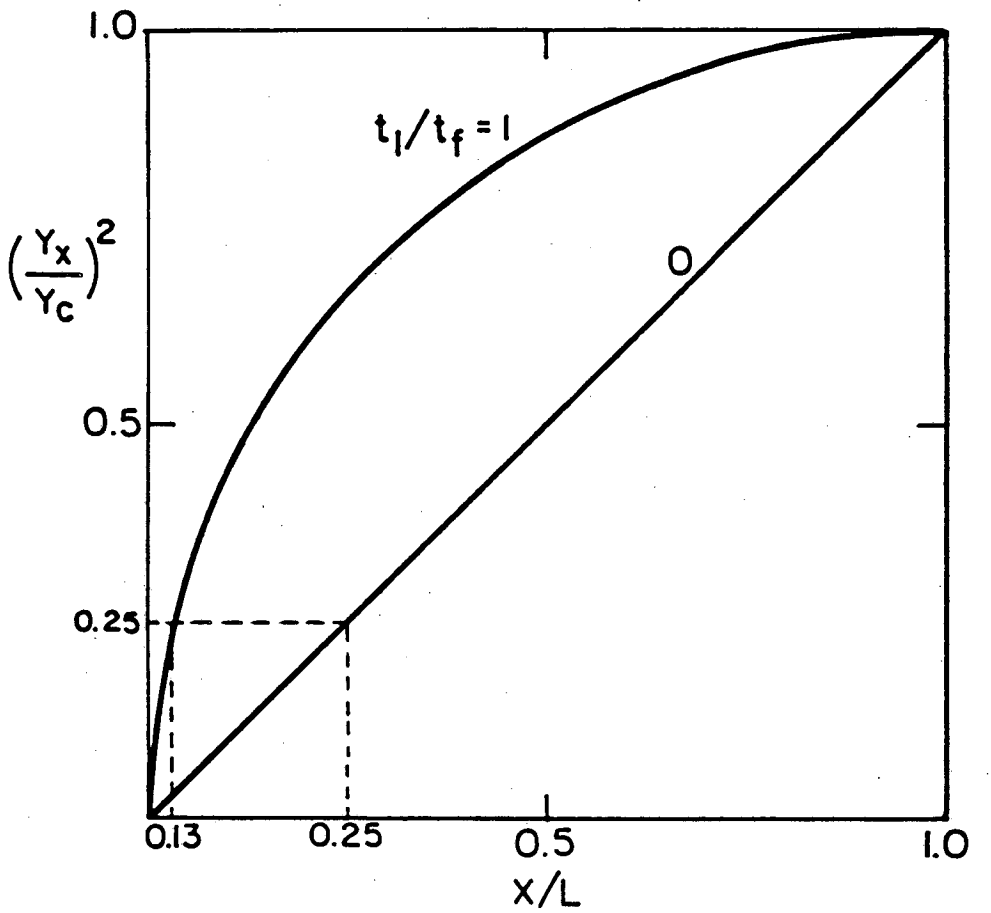

XBL832-5279

Figure 41.

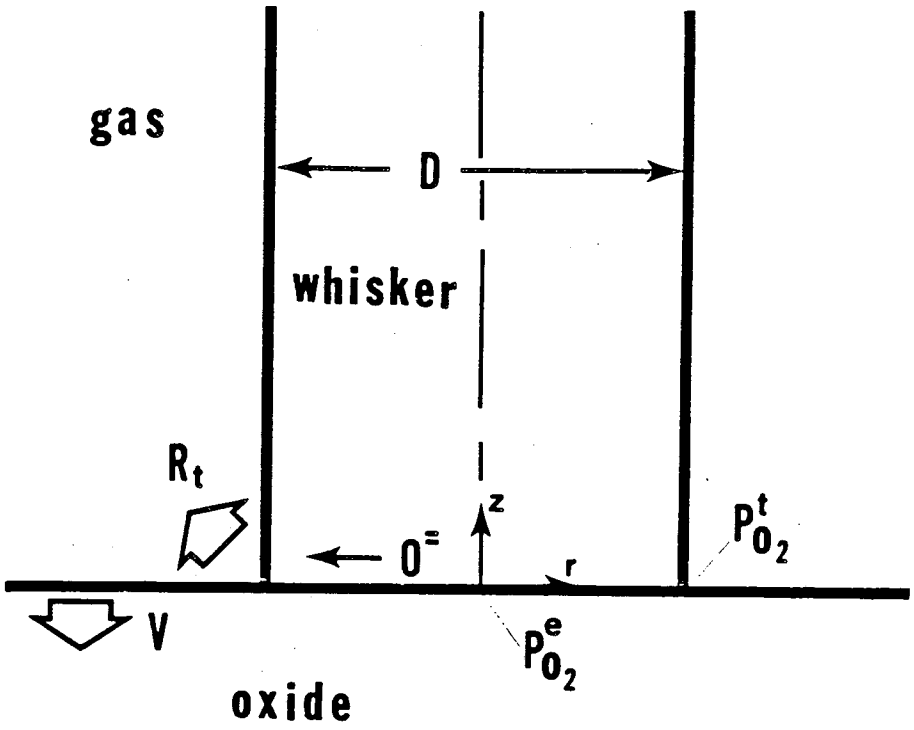

Figure 42.

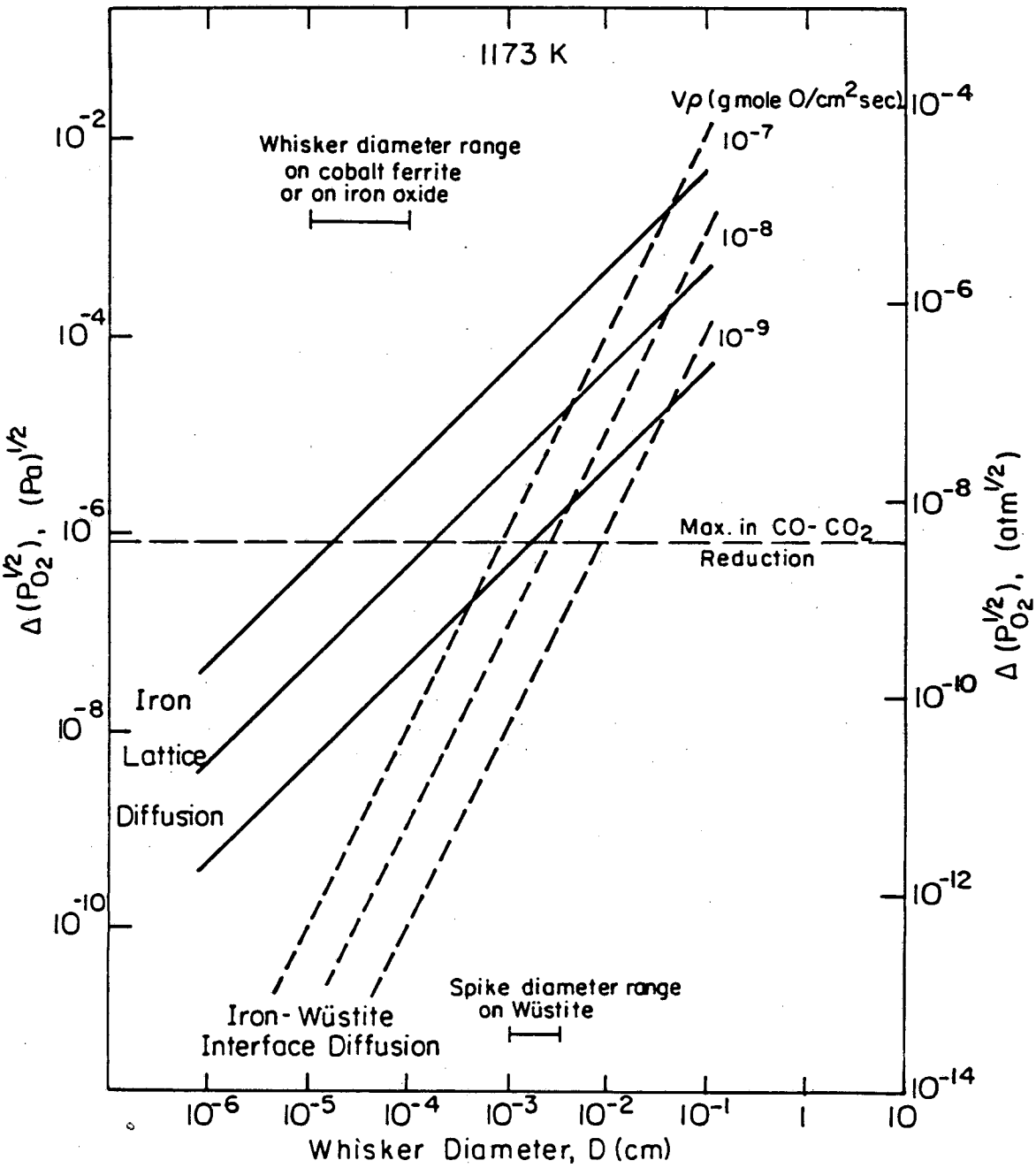

XBL 832-5276

Figure 43.

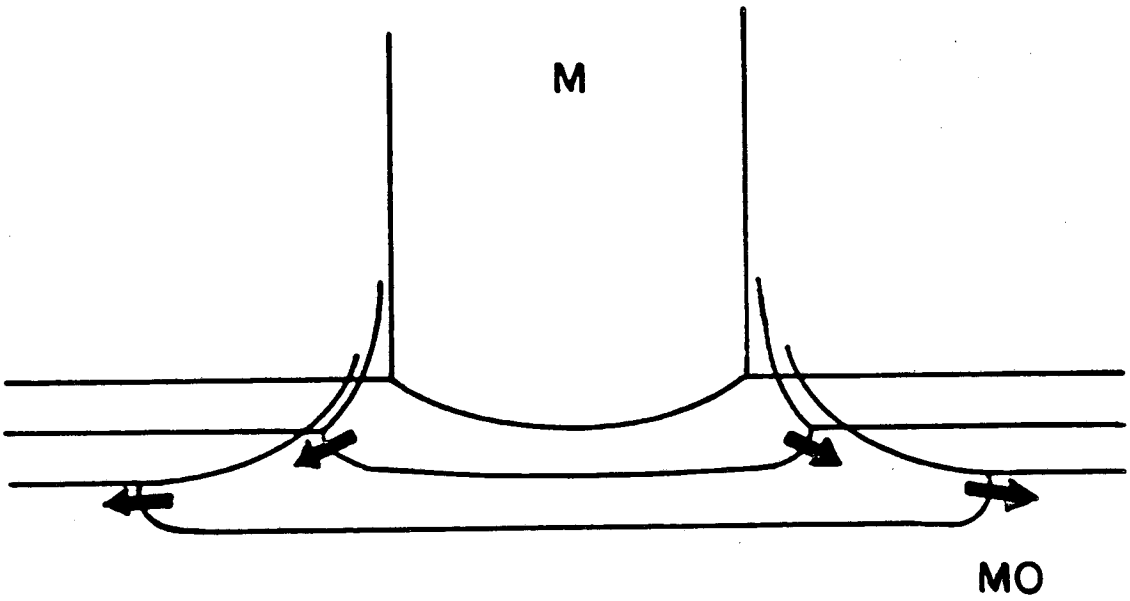

Figure 44.

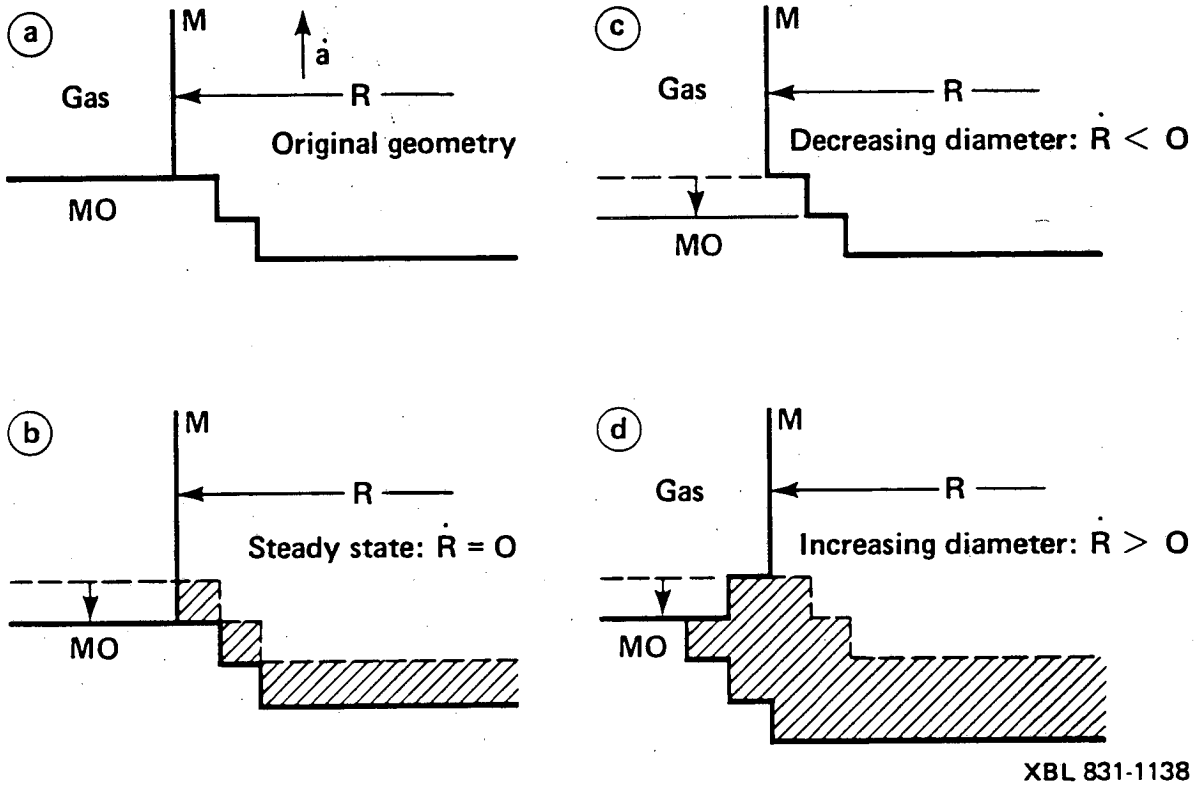
a
M
ȧ
Gas
R
Original geometry
MO
c
M
Gas
R
Decreasing diameter: Ṙ < O
MO
b
M
R
Steady state: Ṙ = O
MO
d
M
Gas
R
Increasing diameter: Ṙ > O
MO
XBL 831-1138

Figure 45.

TECHNICAL INFORMATION DEPARTMENT
LAWRENCE BERKELEY LABORATORY
UNIVERSITY OF CALIFORNIA
BERKELEY, CALIFORNIA 94720